

國立交通大學

電機學院光電工程研究所

博士論文

應用時序驅動之發光二極體背光源於
提升液晶顯示器之影像品質研究



Sequential Driving Light Emitting Diode Backlight for Image
Quality Enhancing on Liquid Crystal Display Applications

研究生：陳均合

指導教授：謝漢萍教授

中華民國九十八年一月

應用時序驅動之發光二極體背光源於
提升液晶顯示器之影像品質研究

Sequential Driving Light Emitting Diode Backlight for Image
Quality Enhancing on Liquid Crystal Display Applications

研究生：陳均合

Student : Chun-Ho Chen

指導教授：謝漢萍

Advisor : Han-Ping D. Shieh



A Thesis

Submitted to Institute of Electro-Optical Engineering

College of Electrical and Computer Engineering

National Chiao Tung University

in partial Fulfillment of the Requirements

for the Degree of

Doctor of Philosophy

in

Electro-Optical Engineering

2009

Hsinchu, Taiwan, Republic of China

中華民國 九十八 年 一 月

應用時序驅動之發光二極體背光源於 提升液晶顯示器之影像品質研究

博士研究生：陳均合 指導教授：謝漢萍 教授

國立交通大學 光電工程研究所

摘 要

隨著液晶顯示器的普及，顯示器規格也朝著高畫質與低功耗的方向發展。發光二極體(Light emitting diode, LED) 由於具有高色彩飽和度、局部控制的自由度與快速響應的特性等優勢，遂成為取代傳統冷陰極管(Cold cathode fluorescence light, CCFL)於液晶顯示器背光源的重要技術。採用發光二極體為背光源其優點為薄型化、重量輕及低耗電量，目前已被廣泛使用在攜帶式顯示器與高階監視器的產品上。在進一步降低耗電量的LED背光顯示系統之發展上，如不需使用彩色濾光片的色場序列法(field sequential color)，由視覺暫留原理可感知彩色影像，能大幅提昇提升系統效率與色域範圍。然而，因眼睛視點與所視物體的相對運動導致各色場於視網膜上非完美疊合時，造成的色彩分離(color break-up)現象需要被克服和抑制。

為了解決色分離問題，在中小尺寸的液晶顯示器，本論文提出了藉由規律變換色場的方式，使在視網膜上連續影像積分無色分離的結果，能有效的解決人眼追跡運動物體所造成的動態色分離現象。在液晶反應時間的限制內，我們也提出了分配影像強度到白色色場來解決靜態色分離現象，稱為 RGBW 方法。然而若是影像內容僅由兩個三原色為主要構成，其色彩重分配的效果會受影響。於是

們進而提出，依據影像內容調整第四個色場為青綠或黃色的 RGBC/RGBY 的交換色場序列方式，用以改善色彩重分配的程度。基於此方式，並更進一步發展決定最佳色場之演算法。藉由動態調整背光源顏色與搭配液晶同步處理，能集中影像強度於單一色場降低色分離現象，使其影像品質與顯示功能獲得提升。本論文並發展以視覺感受(visual perception)基礎上評估影像品質的條件和迴授控制(feedback control)的顯示電子電路，來實現動態即時的影像運算。由觀賞者感受與色分離指標，皆證明此方法是可以有效改善色分離現象，以及量產實現化的設計與技術。

針對大尺寸顯示器，應用局部控制的 LED 背光系統，針對局部影像調整的彩色背光對各區域來作色分離抑制的優化，具有提升顯示器動態範圍與影像的對比度，同時達到進一步降低功耗的優點。然而，此局部控制的背光源存在著區域範圍之光分佈最佳化議題，而本論文由分析人眼視覺對比敏感度，找出不可察覺邊界的背光分佈條件，以視角定義區塊的大小得到適當區塊數目設計通式。並且對邊界察覺度與對比增強度的交換考慮，推導出最佳的高斯分佈函數。符合此推薦值的光分佈設計，能有效提升對比，保持高均勻性，同時避免邊界察覺的現象以確保影像品質。

論文中展現了時序法驅動 LED 背光之光學和電路設計於液晶顯示器產業的重大應用潛力，提供技術上進一步設計與解決方案來開發高畫質低功耗的顯像技術。而結合光學模擬與電路實現的動態優化影像品質技術，也將在未來顯示器產業中具有益形的重要地位。

Sequential Driving Light Emitting Diode Backlight for Image Quality Enhancing on Liquid Crystal Display Applications

Doctoral Student: Chun-Ho Chen

Advisor: Dr. Han-Ping D. Shieh

**Institute of Electro-Optical Engineering
National Chiao Tung University**

Abstract

The popularity of liquid crystal displays (LCD) has encouraged designers to develop the LCD for high image quality and low power consumption. Light emitting diodes (LED), as LCD backlights has advantage in high color saturation, locally controlled ability, and fast on/off response, thus becomes major light sources to replace typical cold cathode fluorescence light (CCFL). Currently, LED backlighting is widely utilized in the mobile and high-level monitors because of its features such as thin format, light weight, and low power consumption. In the further development of LED backlighting, the field sequential color (FSC) mechanism, requiring no color filters to form color images, can greatly improve the light efficiency and the color gamut in perception. However, the color breakup (CBU) is essential to be suppressed while the color fields are not overlapped precisely in retina by the relative motion between viewing points and objects.

To resolve the CBU issue under the restriction of LC response time, on small and medium-sized LCDs we proposed a color field arrangement method to blur the integration of color fields in retina. The dynamic CBU induced by eye tracking objects can be eliminated. For the static CBU suppression, the RGBW method was described to redistribute the image intensity to a white field and discolor the primaries. The effectiveness of color redistribution depends on image content; therefore, we

proposed an exchange of color sequence RGBC/Y to modify the CBU artifact. Based on this dynamic control method, the optimized color field instead of yellow and cyan is determined by intelligently adapting the incoming video content. To concentrate image intensity into a single field, further reductions in CBU visibility can be achieved. We presented the index of CBU evaluation according to visual perception and the feedback control algorithm of color field optimization in real time application. After the implementation and observation, these proposed methods were confirmed as practical ways of CBU reductions in FSC applications.

For large-sized LCDs, the locally controlled LED backlight can be applied to adapt corresponding parts of image for local reduction of CBU visibility. Local adaptive backlighting also benefits the dynamic range, contrast, and power consumption. However, there is a design trade off on the light profile of each segment. Based on human contrast sensitivity function, we derived a threshold of insensible boundary and a general condition of segment number in angular unit. We evaluated the boundary visibility and contrast enhancement to identify the Gaussian light profile as a recommended one for contrast improvement, uniformity maintenance, and boundary imperceptions.

In this thesis, we presented the optical and circuit design of sequential driving LCD and provided technical solutions for upgrading the image quality and power consumption. Combining the optical model and circuit implementation for adaptive image optimization is anticipated to play a substantial role of the incoming display industry.

Acknowledgement

一晃眼五年多的光陰過去了，各種酸甜苦辣的往事仍歷歷在目。這一路上，對於指導我的師長同事們和曾經陪伴我的親朋好友們，在此以感激的心情來表達我滿滿誠摯的謝意。

首先要感謝指導教授謝漢萍老師，提供優質的環境使我順利地作研究。此外，謝老師嚴格且耐心的要求，更是砥礪我成長的一大動力。謝老師更提供了產學合作與國際交流的機會，大大地擴展我的視野。謝老師的學識與風範也是我心目中待人接物與自我實現的典範。同時謝謝黃乙白老師，有系統地引導大家思考，有效率地解決各式研究上的疑惑，也對大家的近況不吝付出關心。在荷蘭期間，感謝 Dr. Hugo Cornelissen 與 Dr. Fetze Pijlman 對我研究與生活上的照顧，讓我有幸一窺一流的設備規模及見識到各國頂尖人員、實習學生們如何的激發創意，通力合作以發展前瞻性的研究，更提醒我面對的是全球的競爭，要努力不懈，以期百尺竿頭更進一步，為學校及國家爭取榮譽。另外感謝陳科宏老師，田仲豪老師，陳皇銘老師，和口委們的提點指教，才能使論文更趨完備。此外，我還衷心感謝張瑋心老師與 Steve Wallace 老師不厭其煩地加強我英語寫作與口語的能力，豐富了這無形也是往後重要的資產。

在實驗室的研究與生活上，要謝謝一起努力的芳正、裕國、喬舜、柏儒、彥行、健翔、璧如、子翔、淇文、注宏及博濟，也感謝安琪學姐、企桓學長、仁宇學長、文奎學長、克偉學長、光裕學長、彥仲學長及豐旭學長在經驗上的傳承。對於玉棉、俊傑、俞文、耀中、哲仁、雅婷、振宇、秉宜、勝昌、建良、宛徵、景明、國振、仁杰、崑展、慶得、均均及已畢業的優秀學弟妹們，謝謝大家的幫忙。目前就讀的博文、靖堯、浩彤、宜如、宜伶、世勛、期竹及建宇，謝謝你們在研究上的參與。還要謝謝鄭榮安博士與助理小姐們，讓實驗室有組織有效率的運作。

此外我要感謝友達光電的劉軍廷副總、汪德美副理、許時嘉先生、杜昌隆先生、蔡博仁先生、中華映管的陳司芬處長、劉家麟經理、戴文智博士、施奕丞先生、徐名潭先生、蔡繼中先生、何明宗先生、飛利浦的工程師Stefan、Gilbert、Wim、Roberto、Giovanni、Eugen、Marcel及許許多多曾經幫助過我的人，謝謝你們。

對於我一路陪伴的好友，詠翔、金祺、聖萱、欣儀、正楓、中玓、崑健、旻昇、詠鈞、柔蓓、益豪、家恩、昱初及玉麟和室友佳煌、宜憲及龍毅和同為實習學生的 Laure、Jose、Johan、Lidia、Thomas、Fadi、Michael 及 Youbin，謝謝你們在相處時光中對我的鼓勵及關懷，帶給我許多美好的回憶與值得回味的點點滴滴。

最後，也是最重要的，要感謝我的爸媽、姊姊和奶奶，感謝您們的支持與鼓勵，讓我無後顧之憂的完成學業順利取得博士學位。往後的人生，我會好好的孝順您們，報答您們一直以來為我無怨無悔的付出。我由衷地、深深地感激。

Table of Contents

Abstract (Chinese)	i
Abstract (English)	iii
Acknowledgement	v
Table of Contents	vi
Figure Captions	viii
List of Tables	xiii
Chapter 1 Introduction	1
1.1 Liquid crystal displays (LCDs)	2
1.2 Light emitting diodes (LEDs)	5
1.3 LED backlight applications in LCDs	7
1.4 Motivation and objective of this thesis	8
1.5 Organization of this thesis	11
Chapter 2 CBU Mechanism and Driving Technologies	13
2.1 Physiology of eye movements	13
2.2 Mechanism of CBU	15
2.3 Color difference (delta E)	18
2.4 Hardware involved in sequential driving	23
2.5 Summary	30
Chapter 3 Proposed CBU Suppression Methods	31
3.1 Color fields arrangement.....	31
3.2 RGBW method.....	39
3.3 RGBC/RGBY method.....	43
3.4 Summary	48
Chapter 4 Adaptive LC/BL Feedback Control	49
4.1 The platform of FSC-LCD	49
4.2 RGBC/Y results	52
4.3 Concept of adaptive backlight	54
4.4 Feedback control for optimized BL determination method	57
4.5 Results.....	61
4.6 Summary	64

Chapter 5	Local Adaptation and Boundary Issue	65
5.1	Contrast sensitivity function considered.....	66
5.2	Verification using Lorentz distribution	68
5.3	Modified profile for 2D-dimming backlight.....	72
5.4	Proper light distribution formula	76
5.5	Summary	81
Chapter 6	Conclusion and Future Work	82
6.1	Conclusion	82
6.2	Future work.....	87
Reference.....		91
Appendix	Implementation of FPGA	98
A.1	Clock generation module	99
A.2	Input Buffer module.....	100
A.3	Image process module.....	101
A.4	Timing controller module.....	113
A.5	Summary	118
Publication List		119
Vita		122



Figure Captions

Fig. 1-1 The various kinds of LCDs.	2
Fig. 1-2 The cross-section view of an LCD.	2
Fig. 1-3 The ON-state, OFF-state, and gray-state of one pixel on an LCD.	3
Fig. 1-4 The edge-lit and direct-lit backlight systems.	4
Fig. 1-5 The white LED and colored LEDs.	6
Fig. 1-6 The comparison of spectrums between CCFL and RGB LED.	6
Fig. 1-7 The normal LCD with color filters and the FSC concept.	6
Fig. 1-8 The display mechanism of an FSC-LCD.	7
Fig. 1-9 (a) An original image and (b) a CBU image.	8
Fig. 1-10 The thesis architecture.	9
Fig. 2-1 Structure of human eye.	14
Fig. 2-2 (a) Perceived image and (b) saccade movement (black line).	14
Fig. 2-3 The scheme of CBU phenomenon in a conventional FSC-LCD.	16
Fig. 2-4 (a) The relationship between time and display position of a simulation scheme and (b) CBU image in a visual system.	17
Fig. 2-5 (a) Image in an FSC-LCD and path of a saccade. (b) Observed CBU during or just after the saccade.	18
Fig. 2-6 The CIE standard observer color-matching functions.	20
Fig. 2-7 (a) A 3D figure of visible colors and (b) the CIE xyz.	21
Fig. 2-8 The CIE $Lu'v'$	22
Fig. 2-9 The display electronic circuit.	24
Fig. 2-10 The transition between splay and bend states in an OCB mode LC.	24
Fig. 2-11 The transition curve from splay to bend state in OCB mode LC[82].	25
Fig. 2-12 The timing diagram of RSDS.	26
Fig. 2-13 Serial data input timing diagram of the LED controller.	28
Fig. 3-1 (a) Color fields of RGB, GBR, and BRG in three consecutive frames (b) the relation between time and location of motional image.	32
Fig. 3-2 (a) Mechanisms of the color breakup when eyes follow the motional image, (b) an integrated image in three consecutive frames with the CFA method.	33

Fig. 3-3 (a) Color fields of RGBR, GBRG, and BRGB in three consecutive frames, (b) the relation between time and location of motional white bar with width of 8 pixels and velocity of 6 pixels/frame, and (c) the simulation image on retina with the 4-CFA method when eyes follow the image.....	34
Fig. 3-4 The block diagram of the FSC controller.....	35
Fig. 3-5 The timing chart of the 4-CFA FSC-LCD.....	36
Fig. 3-6 The camera-tracking equipment.....	37
Fig. 3-7 Photos of a moving white bar, which were taken by a tracing camera, with bar widths of 15 and 30 pixels, velocities of 3 and 6 pixels/frame.	38
Fig. 3-8 Photos of moving cyan and yellow bars, which were taken by a tracing camera, with bar width of 15 pixels and velocity of 6 pixels/frame.....	38
Fig. 3-9 The flow chart of RGBW algorithm.....	40
Fig. 3-10 The CBU simulation images by using (a) RGB and (b) RGBW methods...	41
Fig. 3-11 The images displayed by a 5.6-inch FSC-LCD with (a) RGB and (b) RGBW methods.....	42
Fig. 3-12 The static CBU images for (a) RGB and (b) RGBW methods.	42
Fig. 3-13 The R, G, B, and W fields of an image.....	43
Fig. 3-14 The relation between time and location of moving image on (a) a conventional RGB 3-field and (b) the redistributed color FSC displays.....	44
Fig. 3-15 The gray levels in red and green/green and blue are redistributed to yellow/cyan field to form a full color image.	44
Fig. 3-16 The gamma function and an example of new gray level of one pixel in red field.....	45
Fig. 3-17 The flowchart of gray level redistribution and the following frame in (a)RGBY or (b)RGBC color sequence.	46
Fig. 3-18 The block diagram of system architecture.	47
Fig. 4-1 The display circuit of FSC-LCD.....	50
Fig. 4-2 The LC panel module of FSC-LCD.....	50
Fig. 4-3 The LED backlight of FSC-LCD.....	51
Fig. 4-4 The demonstration of a gradual change of color board.....	51
Fig. 4-5 Photos of (a) still images and (b) moving color bars taken by a tracing camera, with colors of white, yellow, cyan, and three specific colors. (c) The comparison between gray levels without and with modifications.....	53
Fig. 4-6 The comparison between Esum with conventional and the proposed method and the suppression ratio of this method to conventional one.....	54
Fig. 4-7 The color field sequences and simulated CBU images on (a) conventional	

RGB 3-field and (b) rearranged color FSC displays.	55
Fig. 4-8 The simulated CBU images of Lena in three conditions of (a) none, (b) c/y, and (c) proposed D-field.....	56
Fig. 4-9 The relation between color difference and backlight bit number.	58
Fig. 4-10 The relation between the error rate of color difference and sampling period.	58
Fig. 4-11 The concept of optimized BL determination and image processing in a real time application.	59
Fig. 4-12 (a) The flowchart and (b) an example of gray level determination of color backlight are according to the image content and color differences.....	60
Fig. 4-13 The variation of color difference E_{sum} with a scrolled speed of one image per second for these test images.....	61
Fig. 4-14 The E_{sum} comparison of test images with conventional, c/y, and dominated RGB methods and the ratio of E_{sum} of DRGB to conventional one.....	62
Fig. 4-15 The CBU images with (a) conventional RGB and (b) adaptive DRGB fields.	63
Fig. 5-1 The thesis architecture.....	65
Fig. 5-2 (a) Contrast sensitivity function and (b)with experimental values	66
Fig. 5-3 (a) Full-on backlight, (b) original of camera man, (c) 2D-dimming backlight, and (d) the gradient of 2D-dimming backlight.	69
Fig. 5-4 The selected images over different spatial scale. (a) Original image, (b) 2D-dimming backlight, and (c) the contour of gradient image (100x).....	71
Fig. 5-5 The backlight contrast ratio per images as a function of segment size. The solid line corresponds to the contrast ratio averaged over all the images.	72
Fig. 5-6 The percentage of pixel numbers below the threshold per gradient images as a function of segment size. The solid line corresponds to the average over all the images.	73
Fig. 5-7 The backlight contrast ratio and the percentage of pixel numbers below the threshold of gradient images as a function of segment and spatial filter size. The lines correspond to the average over 5 images.	74
Fig. 5-8 The segment numbers of screen as a function of segment size. The lines correspond to the viewing distances of factors of 1.5 to 6 longer than screen diagonal.....	75
Fig. 5-9 Three points in the model for light source contribution analysis.....	77
Fig. 5-10 Summation of differences and parameters in (a) 7x7 array (b) 15x15 and 31x31 array	78

Fig. 5-11 Summation of differences and parameters with sharp factor (a) $b=2$ (b) $b=3$	79
Fig. 5-12 Similarity between a, b, k model , Gaussian, and Lorentz distributions.....	80
Fig. 5-13 (a) 2D-dimming (b) full-on backlight image of Gaussian distribution.....	80
Fig. 6-1 The (a) original image and individual color fields of (b)global and (c)local adaptive backlights.	89
Fig. 6-2 The CBU images with (a) non-, (b) global, and (c) local adaptation.....	89
Fig. 6-3 The schematic of added white LEDs into the backlight module.....	89
Fig. A-1 The framework of controlled circuit.....	98
Fig. A-2 The block diagram of clock generation module.	99
Fig. A-3 The synthesis of clock generation module.....	100
Fig. A-4 The block diagram of input buffer module.....	100
Fig. A-5 The synthesis of input buffer module.	101
Fig. A-6 The block diagram of image process module.....	101
Fig. A-7 The synthesis of image process module.	102
Fig. A-8 The block diagram of timing generation logic.....	103
Fig. A-9 The synthesis of timing generation logic.....	104
Fig. A-10 The block diagram of write control logic.....	105
Fig. A-11 The synthesis of write control logic.....	105
Fig. A-12 The block diagram of write buffer controller.	106
Fig. A-13 The synthesis of write buffer controller.....	107
Fig. A-14 The block diagram of read control logic.	108
Fig. A-15 The synthesis of read control logic.....	108
Fig. A-16 The block diagram of read buffer controller.....	109
Fig. A-17 The synthesis of read buffer controller.	110
Fig. A-18 The block diagram of frame buffer interface.....	111
Fig. A-19 The synthesis of frame buffer interface.....	112
Fig. A-20 The block diagram of timing controller module.....	113
Fig. A-21 The synthesis of timing controller module.	114
Fig. A-22 The block diagram of source driver controller.	115
Fig. A-23 The synthesis of source driver controller.....	115

Fig. A-24 The block diagram of gate driver controller. 116

Fig. A-25 The synthesis of gate driver controller. 116

Fig. A-26 The block diagram of backlight driver controller. 117

Fig. A-27 The synthesis of backlight driver controller. 117



List of Tables

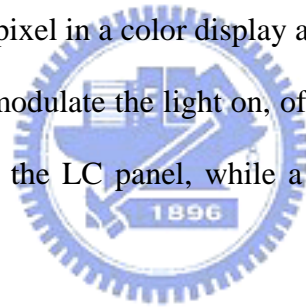
Tab. 2-1 The specifications of (a) the gate driver and (b) the source driver for the TFT LCD panel.....	27
Tab. 2-2 The specifications of LED driver	28
Tab. 3-1 The lowest field frequency that produces invisible flicker for each color	33
Tab. 4-1 Specifications.....	52
Tab. 5-1 The relation between pixel number and frequency in LCD TV and laptop...	67
Tab. 5-2 The relation between distance and contribution of light sources	77
Tab. 6-1 The comparison between normal RGB, 3 prior arts described in Chapter1, and the proposed adaptation method	83



Chapter 1

Introduction

Liquid Crystal Displays (LCDs) have become the dominant display technology for applications ranging from small mobile devices, notebooks, car navigation systems up to large-sized television sets as shown in Fig. 1-1[1]. This high penetration level can be attributed to a host of advantageous features, including high resolution, high brightness, light-weight and a thin form factor. Each individual pixel in a black and white LCD and each sub-pixel in a color display are created from a source of light and a light valve, which can modulate the light on, off, or to some intermediate level. Millions of light valves form the LC panel, while a source of light and optic films create the illumination.



Light Emitting Diodes (LEDs) are widely used as indicator lights on electronic devices and increasingly in illumination applications of backlighting for LCDs [2][3]. The LED backlight has the advantages such as small form factor, mercury-free, wide color gamut, quick light-up operation, long life time, etc. [4] Especially, the LED is very suitable for a local addressable [5][6] or a sequential driving backlight [7]-[9]. Among LCDs, the LED illumination becomes a popular technology for applications of high image quality and low power consumption.



Fig. 1-1 The various kinds of LCDs.

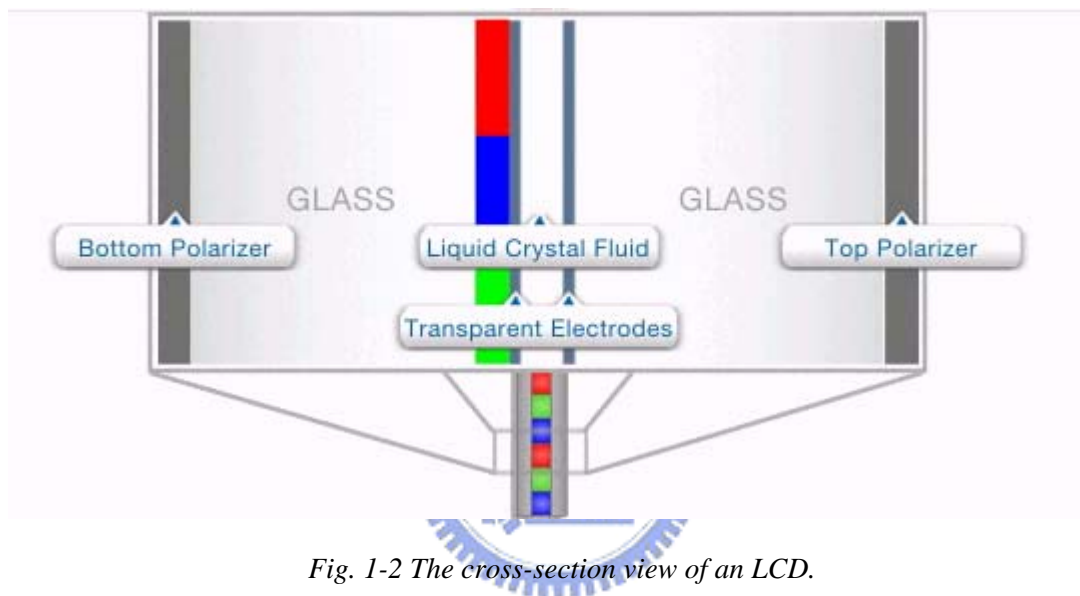


Fig. 1-2 The cross-section view of an LCD.

1.1 Liquid crystal displays (LCDs)

A cross-section of an LCD reveals its elements. The LCD panel is at the center of the display where the liquid crystal itself is located. Transparent electrodes patterned on each pane of glass encompass the liquid crystal as shown in Fig. 1-2. The orientation of the liquid crystal can be changed in subtle ways by applying a voltage to the electrodes in order to change the level of illumination displayed in each sub-pixel.

The LCD panel is the essential component in a display that controls the amount of light reaching the viewer. Light passes through a bottom polarizer that orients the

light to a single state of polarization by absorbing over 50% of the incoming unpolarized light. The polarized light then passes through the liquid crystal layer. The orientation of liquid crystal can be controlled by applying a voltage to the transparent electrode on the glass encompassing it. The degree of orientation of liquid crystal controls the degree of rotation of the incoming polarized light with a typical Twisted Nematic (TN) LCD. When there is no voltage applied to the electrodes, the liquid crystal is naturally oriented to rotate the light 90 degrees allowing it to pass freely through the top polarizer. However, if a voltage is applied, the liquid crystal aligns to the electric field and does not rotate the light, allowing the top polarizer to block it completely. By applying an intermediate voltage, the liquid crystal can be partially oriented to partially rotate the incoming light, creating shades of gray as shown in Fig. 1-3. Adding a color filter to the LCD panel creates color displays. In a color LCD, each red, green and blue sub-pixel is individually controlled, allowing varying amounts of red, green, and blue light through to the viewer for each pixel.

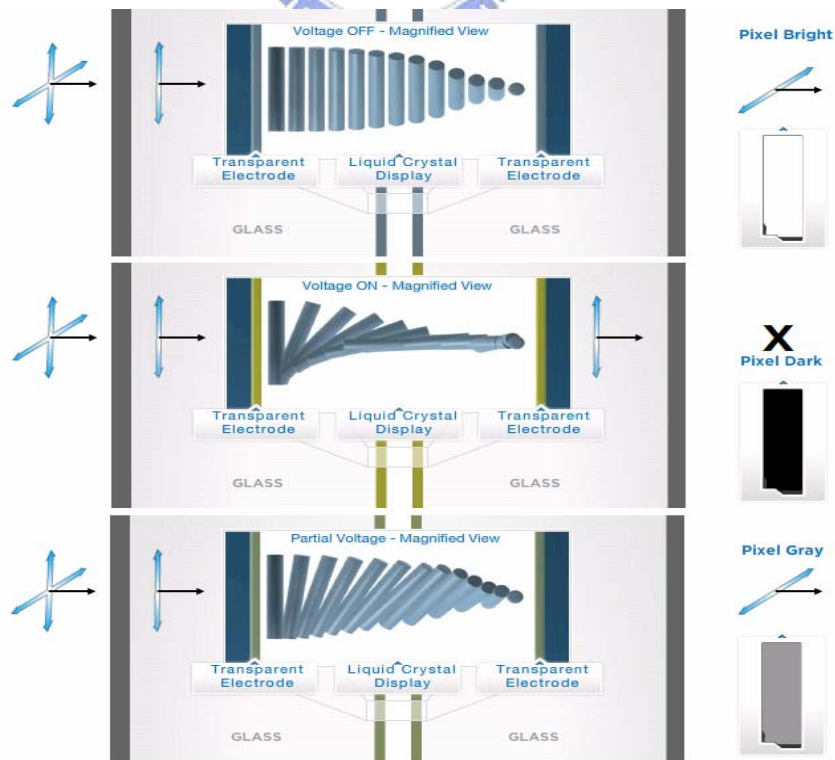


Fig. 1-3 The ON-state, OFF-state, and gray-state of one pixel on an LCD.

The uniform illumination of an LCD is achieved with either a lightguide in an edge lit system or a diffuser plate in a direct lit system as shown in Fig. 1-4 [10][11]. Edge lit backlights are typically used in handheld displays, notebook computers and computer monitors where display thickness is important. In the edge lit backlight, light from a row of LEDs or one or more fluorescent lamps enters a lightguide, which transports the light across the surface of the lightguide through total internal reflection [12]. The light is then extracted at specifically engineered points to uniformly illuminate the entire display. As the display area increases, multiple lamps can be placed at the edges of the lightguide to achieve sufficient brightness. There is a limit to the number of lamps that can be crowd at the edge of a lightguide. However, for larger area displays, such as most LCD TVs, direct-lit backlights are used [13][14]. In the direct lit backlight, LEDs or a set of fluorescent lamps are placed directly behind a thick white diffuser plate that spreads the light of the point sources or line sources uniformly [15][16].

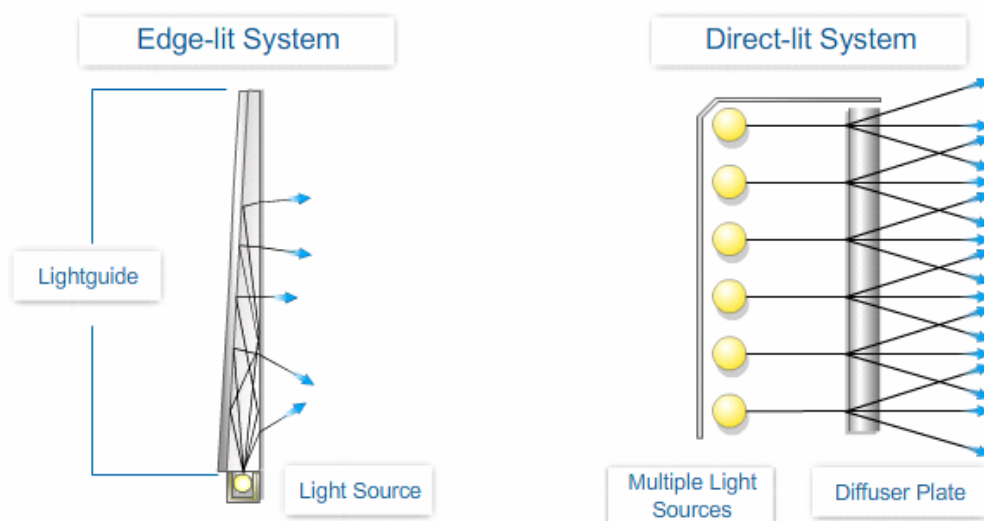
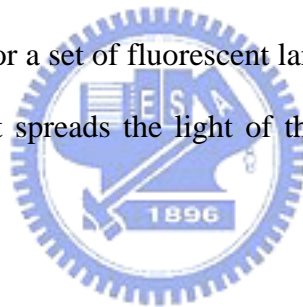


Fig. 1-4 The edge-lit and direct-lit backlight systems.

1.2 Light emitting diodes (LEDs)

All LCDs require a source of light to illuminate the LCD panel. The choice of a light source is critical in balancing the requirements of color gamut, power consumption, heat generation, size and cost. Each light source has a different spectral output that constrains the color gamut of the integrated display and each light source lends itself to different applications. Using sunlight or ambient room light works well for watches and cell phones with transfective displays. A Cold Cathode Fluorescent Lamp (CCFL) is typically used in laptop computers, LCD monitors and TVs, while the powerful light of an arc lamp is used in most LCD projectors. Light emitting diodes, or LEDs, are typically the source of light for LCDs in cell phones, PDAs, and other handheld applications. Some notebook and TV displays are also illuminated by LEDs [17][18]. These light sources are compact, efficient, and reliable. LEDs use low-voltage to produce colored or white light [19]-[21].

White LEDs in Fig. 1-5 first produce blue light, which is converted by a phosphor to white light, resulting in a broad spectrum accompanied by specific blue wavelength. Colored LEDs have a narrow wavelength spectrum such as red, green or blue light shown in Fig. 1-6 [1]. When mixed in a backlight, red, green and blue LEDs combine to produce a white light that covers nearly the entire NTSC color space. Color is normally provided in LCDs by color filters, one color per sub-pixel. Three sub-pixels, red, green, and blue, are required to cover the color range for each full pixel. The color filter limits the fraction of white light normally transmitted by the LCD to about 33%. One could eliminate the color filters and improve the display efficiency if each full pixel were sequentially illuminated by red, green and then blue light sources as shown in Fig. 1-7. If done quickly enough, the eye perceives that all three colors seem to be presented simultaneously. Colored LEDs are an ideal source

for this mode of illumination, known as Field Sequential Color [22]-[25]. This technique, while efficient, requires that the LCD respond at rates much faster than normal LCDs with color filters.

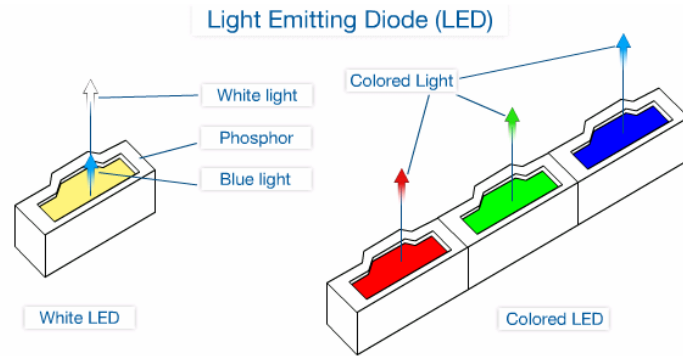


Fig. 1-5 The white LED and colored LEDs.

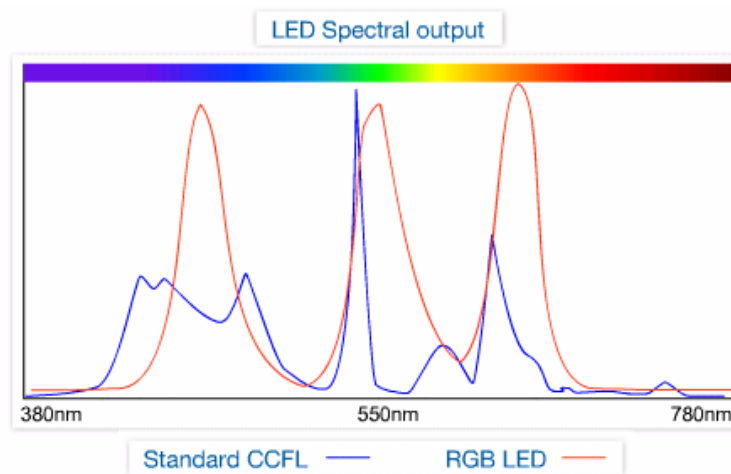


Fig. 1-6 The comparison of spectrums between CCFL and RGB LED.

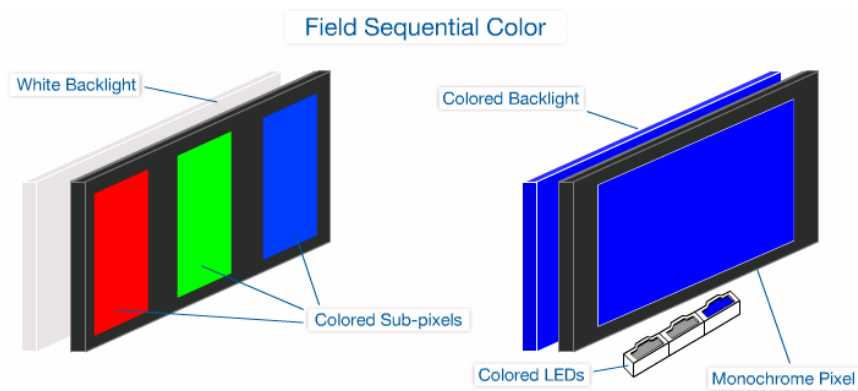


Fig. 1-7 The normal LCD with color filters and the FSC concept.

1.3 LED backlight applications in LCDs

An active-matrix LCD system is commonly illuminated by a constant full-on backlight consisting of conventional CCFLs. The generated light propagates through two sets of polarizers, color filters, diffusers and redirection foils, and in each of these components substantial proportions of light are scattered and absorbed. Overall, the efficiency of the above optical stack amounts to approximately 5-10%.

Most LCDs rely on spatial color synthesis to produce vivid saturated color images by juxtaposing micro color-filter (typically RGB) sub-pixels. However, color filters absorb roughly 70% of light and are therefore highly inefficient. To improve significantly LCD power efficiency, it is therefore appealing to remove the color filters and rely on temporal color synthesis to create full-color images. Such field-sequential color (FSC) displays rapidly flash the primaries time-sequentially, as illustrated in Fig. 1-8, such that the colors are mixed by means of temporal integration in the eye and all three colors seem present simultaneously [26]-[30]. Colored LEDs are an ideal source for this mode of illumination. To prevent luminance flicker, a three-primary system requires a minimum refresh rate of 180 Hz.

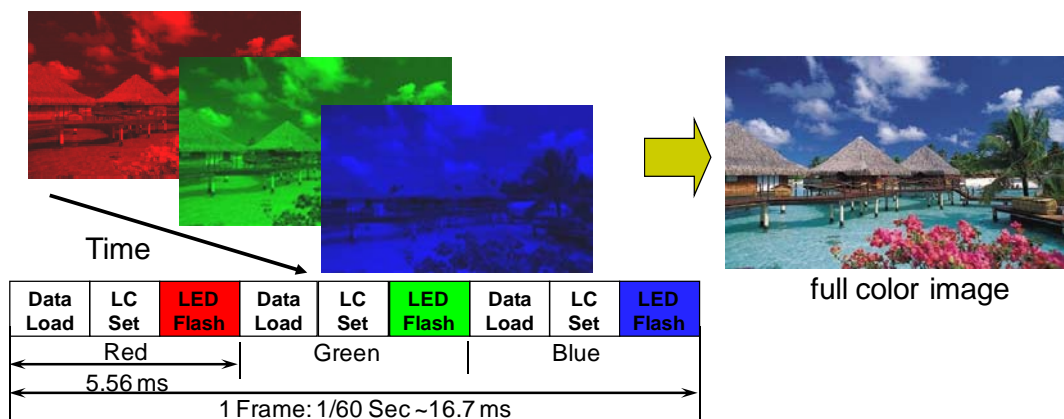


Fig. 1-8 The display mechanism of an FSC-LCD.

However, FSC-LCDs notoriously suffer from color breakup (CBU)[31]-[35],

which occurs when relative velocities between displayed objects and the eyes of the viewer exist. In that case, the constituent color components do not overlap perfectly at the retina and the individual color fields may become visible in the front-of-screen image (Fig. 1-9). This may occur during both smooth motion pursuit, and particularly saccadic eye movements which may result in high retinal color displacements [36]-[38]. CBU artifacts are highly annoying, causing some viewers severe viewing discomfort and in some cases even nausea [39].

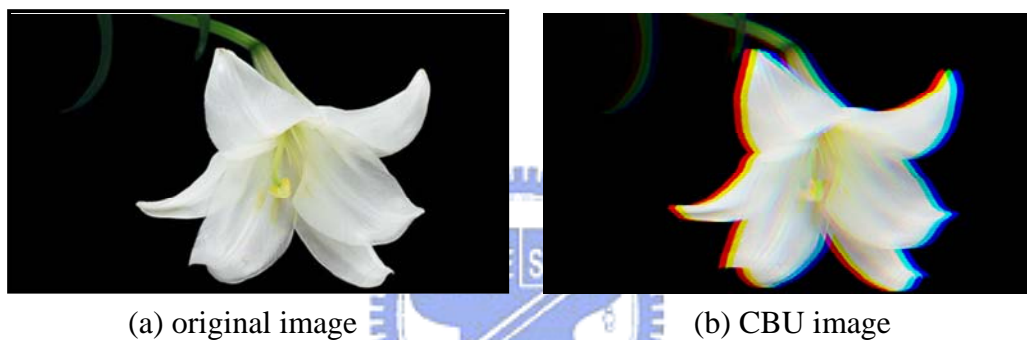


Fig. 1-9 (a) An original image and (b) a CBU image.

1.4 Motivation and objective of this thesis

In a world that is increasingly aware of its ecological footprint and the harm that is causing to our planet, there is a great incentive to reduce the power dissipation of state-of-the-art LCDs. LED backlight technologies are of advantageous of above requirements. However, these LED applications still exist several issues that need to be improved.

For the CBU issue, it has been widely studied in the context of digital light processing (DLP) projectors [40]-[42]. Since DLPs employ color wheels, most traditional solutions involve either straightforward field rate increases [43] or the inclusion of additional mono-color fields [44][45]. Although LED backlights can be

switched very rapidly, the response time of liquid crystal prevents the implementation of many of the above methods for large-screen FSC-LCDs. In spite of the emergence of new fast panel technologies, it is highly unlikely that affordable panels with frame rates higher than 240 Hz will be widely available in the foreseeable future. Cennini et al. [46] proposed a display solution based on spatio-temporal color synthesis that employs two color filters in combination with two color fields thus striking a compromise between conventional spatial color mixing and field-sequential technology. Although its benefits in terms of light efficiency and screen resolution are moderate compared to those achieved by full field-sequential displays, perception tests have confirmed that the visibility of CBU is drastically reduced.

To promote field sequential color technology by developing new processing algorithms to mitigate the effects of color breakup is the objective of this thesis. The performance of newly developed CBU reduction techniques will be evaluated and benchmarked against existing methods. The architecture of this thesis can be divided into three parts for CBU suppression on small- to large-sized LCDs as shown in Fig. 1-10. The methods have progressed from consistent color order to adaptive color field and the 2D-dimming control.

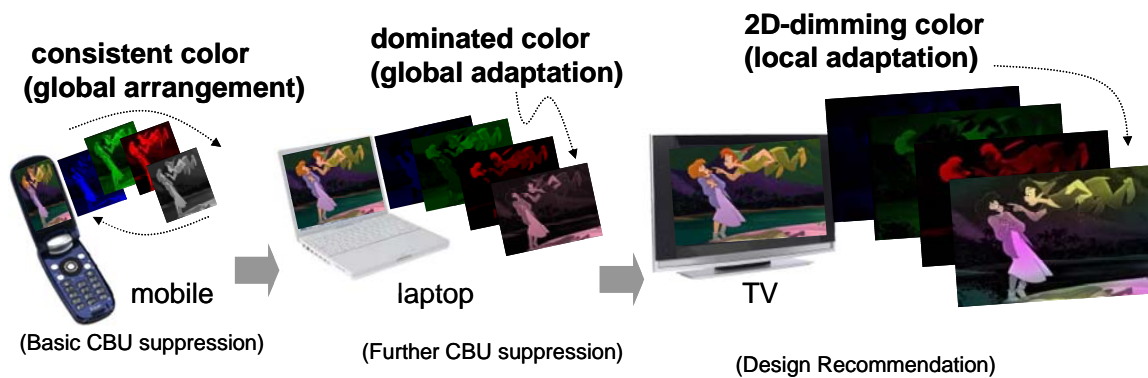


Fig. 1-10 The thesis architecture.

For mobile-sized one, we proposed an effective method, color field arrangement (CFA) [47]-[49], to reduce the CBU of FSC-LCDs. According to the relation between time and location of motional image, the adequate color field orders of three consecutive frames were found to compensate with each primary color. The CBU mechanism and perceived images on the retina were simulated when eyes followed the motional image. In addition, the flicker phenomenon, which occurs in both temporal variation of the luminance (brightness) and chromaticity (color) [50], has been considered and prevented. A 4-CFA method repeating on color fields was proposed to suppress the flicker phenomenon as well as the CBU.

To lighten the primary color fields by redistributing the LC gray levels to the fourth color field is also proposed [51]. The visibility of the CBU artifact is reduced while the intensity of color separation is decreased. We proposed the RGBW method, condensing the noticeable fields on a white field and reducing the intensities of R, G, and B fields [52][53]. However, the consistent color sequence is not suitable for all kinds of image contents. Therefore, we chose the cyan and yellow as the fourth color field in order to lighten the most sensitive green field. A full color image alternately consists of RGBC and RGBY color field sequences, adapted to image contents. It is obvious that the image intensities of primary colors are lightened. By redistributing gray levels, the noticeable fields are condensed to a primary and mix-colored one. The algorithm of arrangement the color field was studied for laptop-sized LCDs.

Further reductions in CBU visibility can be achieved by intelligently adapting the colors and intensities of the individual fields to the incoming video content [54]. This is generally achieved by focusing as much image energy in one temporal field. A common approach is to flash an adaptive image in one frame and use the remaining frames to display the color residuals. An effort was made in order to find the adaptive

color according to the image content in each frame. The algorithm of feedback determination of adaptive color and LC/BL signals was studied for the real time application, followed by the implementation and experimental results of CBU evaluation. With rearranging LC/BL signals dynamically to optimize color backlight, our results successfully demonstrate that the proposed method is a practical way to suppress the CBU in field sequence color LCD applications.

On large-sized LCDs, the local adaptation seems proper for the presentation of colorful images as local adaptation can concentrate more intensity to the adaptive field [55], a combination of locally controlled backlight and FSC concept. In each segment, the backlight can adjust for only a corresponding part of image. This backlight modulation is primarily determined by the number of addressable segments and the spatial extent of the optical profile of these segments [56]. We considered a boundary-free backlight pattern in this local adaptive backlight. In other words, the brightness variation at the boundary between segments should be indistinguishable. The threshold of boundary-free image was found according to human contrast sensitivity function. The criteria of insensible variations and the recommended profile and size of segment were determined [57].

1.5 Organization of this thesis

This thesis is organized as follows: the principle of color science and the introduction of driving hardware are presented in **Chapter 2**. The CBU mechanism, color standard such as CIE1931, CIE 1976, and the definition of color different are described in this chapter. Additionally, this chapter also presents the working principle of hardware components such as an OCB panel, LCD drivers, LED drivers, and an FPGA control board. In **Chapter 3**, using color field arrangement and RGBW method for suppressing CBU are demonstrated. The concepts of driving are distributed and

the experimental results are shown in this chapter. To suppress the issue of fixed driving principle, the exchange of color sequence RGBC/RGBY is proposed. The system architecture and the implementations of a timing controller are described in this chapter. In **Chapter 4**, the observations and the evaluation index of CBU are presented. With dynamically adjusting color sequence, the CBU is effectively reduced. The dynamic color backlight, an extended method, is proposed. This adaptive FSC-LCD is the first sequential driving display in the world adapted by image contents for further mitigating CBU. In **Chapter 5**, the large-sized FSC-LCD application and the local adaptation are discussed. The perceived threshold of boundary-free image and recommendation of the profile of local backlight are also presented. Finally, the summary of dissertation and future works are given in **Chapter**

6.



Chapter 2

CBU Mechanism and Driving Technologies

The sequential driving in the FSC-LCD is an effective mechanism without requirement of color filters in the conventional LCD. However, it faces a serious issue: color breakup (CBU). In order to suppress CBU, the basic concepts such as the eye movement response and the CBU phenomenon need to be understood. The color difference (ΔE) between the original and the CBU images is introduced and utilized to evaluate CBU phenomenon. In addition, the working principles of LC driving technologies such as the fast response LC, drivers, and circuits are introduced in this chapter.

2.1 Physiology of eye movements

Human eye is a complex visual system, and its structure is shown in Fig. 2-1. Light passes through the cornea and the pupil controlled by the iris to adjust the incident magnitude of light. Then the lens focuses the light on the retina, and there are two kinds of receptors to detect intensity and color of light. The rod cells are sensitive to light intensity; the cone cells are sensitive to color. The receptors detect light and convert it into electrochemical signals. Finally, the signals pass through the optic nerve to the brain, and humans can perceive images [58]. The CBU phenomenon in the FSC-LCD has strong dependence on perception.

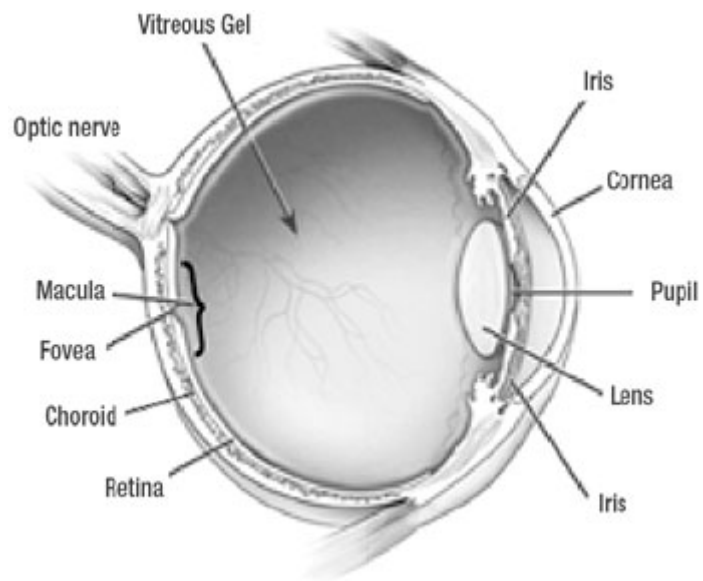


Fig. 2-1 Structure of human eye.

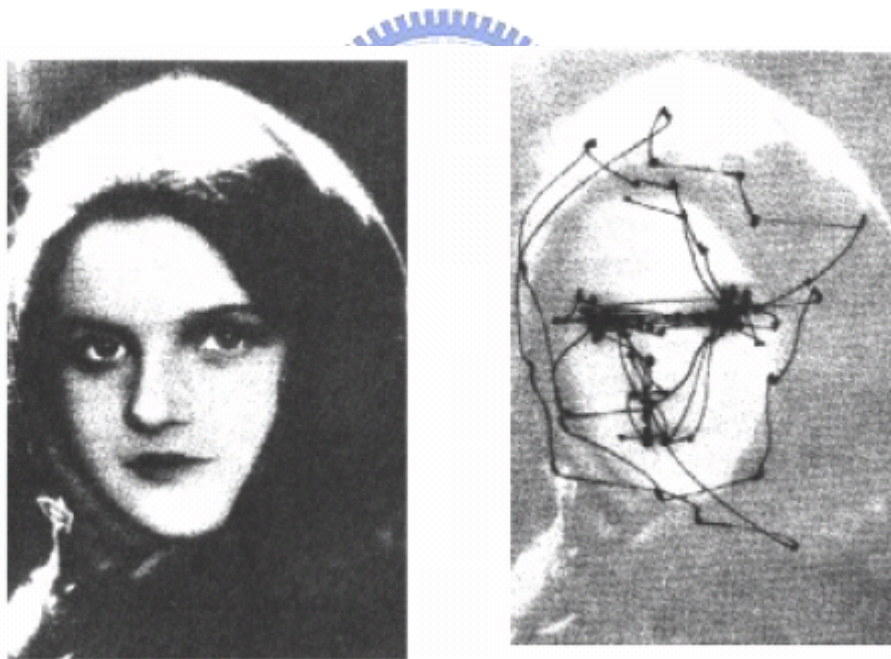


Fig. 2-2 (a) Perceived image and (b) saccade movement (black line)

The fovea lies near the projection point at the center of the retina. This region has the highest resolution and is 0.1% of retina area. In order to see objects clearly, humans need to move their eyes to focus on the fovea. In perception research, two major types of eye movements are mentioned: saccade and pursuit [59]. Saccade is a rapid, random movement while perceiving static objects. The movement moves around objects to focus on the fovea and gathers correct visual information [60]-[63]. The test image is shown in Fig. 2-2 (a), and the eye movement for the static image is lined with black in Fig. 2-2 (b). In order to recognize the woman, the observer's eye moves around her face to collect information. Generally, saccade is spontaneous, and the speed happens quickly at about 200 degree/sec [64].

The other type of eye movements is pursuit. Pursuit is a smooth and predictable movement when perceiving dynamic objects. When perceiving a moving object, the human eye will follow at the same velocity of the object to focus on the fovea and catch clear images. Compared to saccade, pursuit velocity is much slower, and some research proposes the velocity is about 90 degree/sec [65]. Moreover, pursuit movement (pursuit latency) means the delay in eye pursuit, which is defined as the difference in beginning motion time between the target and the eye. According to literatures, the pursuit latency is about 100 ms to 150 ms [66].

2.2 Mechanism of CBU

By displaying R, G, and B fields sequentially faster than the time resolution of the eye, a full color image can be observed. If there is a relative movement between human eyes and moving object, the field images will be integrated separately on the retina, resulting in perception of the rainbow effect or CBU on the margin of the image. The CBU mechanism will be described in the following section.

2.2.1 Dynamic CBU

The dynamic CBU phenomenon always occurs at the edge of moving image on an FSC display. The mechanism of dynamic CBU is related to “Smooth Pursuit Eye Movement (SPEM)” of the visual system. Smooth pursuit is an eye movement that smoothly tracks a moving object in the visual system. The purpose of smooth pursuit is to perceive a moving object. Therefore, dynamic CBU can be perceived when three fields, R, G, and B, alternate slower than the SPEM.

A white image moves from left to right on an FSC-LCD and human eyes pursue this moving image as shown in Fig. 2-3. While the FSC-LCD displays a moving image from an initial pixel to the next one, R, G, and B fields are shown at the initial pixel, then these fields are presented at the next pixel. However, human eyes shift while displaying the individual field. Thus, R, G, and B fields separately project on the retina. After integrating color fields in the brain, the dynamic CBU is perceived.

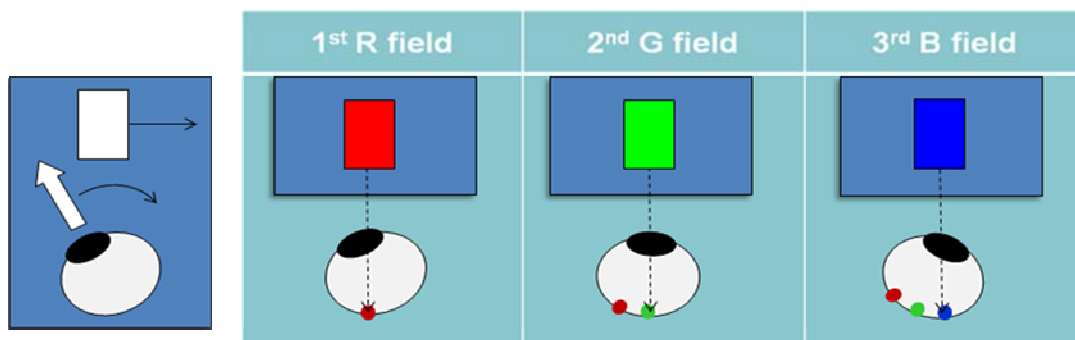
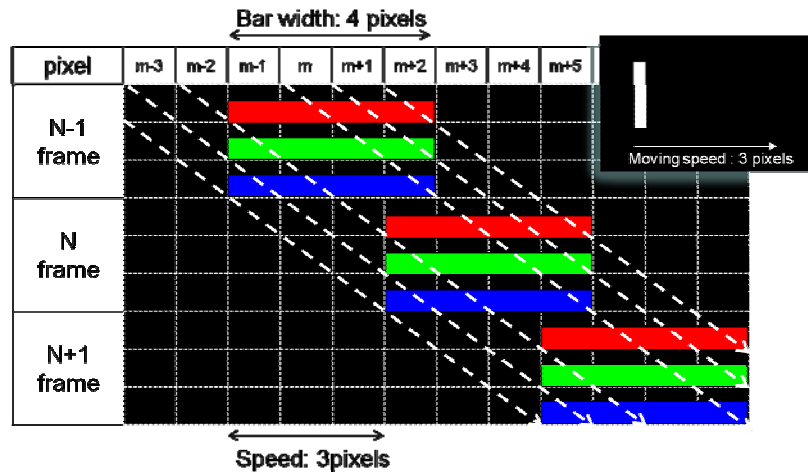
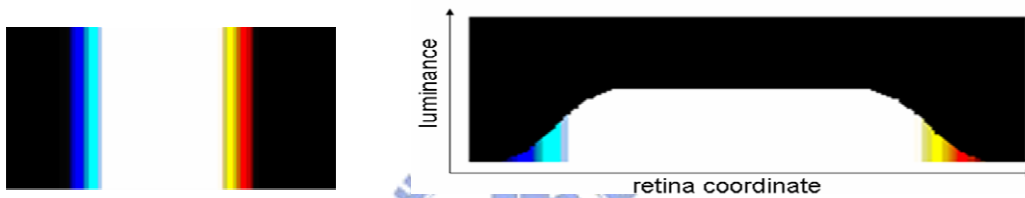


Fig. 2-3 The scheme of CBU phenomenon in a conventional FSC-LCD.



(a)



(b)

Fig. 2-4 (a) The relationship between time and display position of a simulation scheme and (b) CBU image in a visual system.

We can simulate the integration of the visual system by using Matlab software, as shown in Fig. 2-4(a), the relationship between time and display location (horizontal direction). A white bar moves from left to right and the dotted lines represent the observer's viewpoint shift. When the observer watches a moving image, observer will shift the viewpoint to trace the moving image. Consequently, the observer will recognize an image as shown in Fig. 2-4(b) [67].

2.2.2 Static CBU

For a stationary image, CBU is observed during or after a saccadic eyes movement. Saccade is an eye movement that randomly and rapidly moves to scan and perceive a target image. If there are several white images as shown in Fig. 2-5 eye will perceive part of the image that attracts the interest [68]. Human's visual system will be sensitive to white bars in this case, as shown in Fig. 2-5(a), where line-A represents the eye saccade movement. Saccade eye movement is much faster than SPEM, the stationary image seems to break up into several field colors, as shown in Fig. 2-5(b).

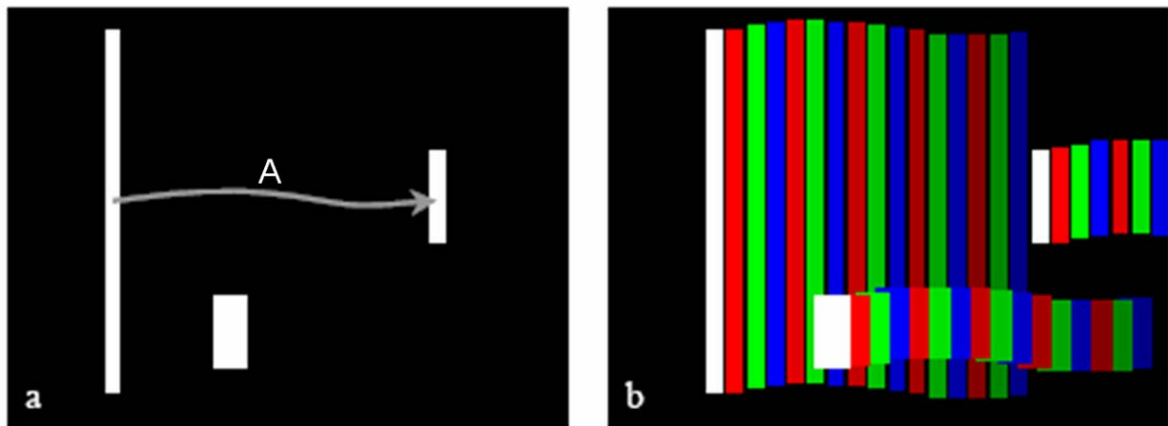


Fig. 2-5 (a) Image in an FSC-LCD and path of a saccade. (b) Observed CBU during or just after the saccade.

2.3 Color difference (ΔE)

In the study of the perception of color, one of the first mathematically defined color spaces was the CIE 1931 XYZ color space (also known as CIE 1931 color space), created by the International Commission on Illumination (CIE) in 1931 [69]. The CIE XYZ color space was derived from a series of experiments done in the late 1920s by W. David Wright [70] and John Guild [71]. The human eye has receptors (called cone cells) for short (S), middle (M), and long (L) wavelengths. Thus in principle, three parameters describe a color sensation. The tri-stimulus values of a

color are the amounts of the three primary colors in a three-component additive color model needed to match that test color. The tri-stimulus values are most often given in the CIE 1931 color space, in which they are denoted X, Y, and Z [72]. CIE XYZ is based on direct measurements of human visual perception, and serves as the basis from which many other color spaces are defined.

In the CIEXYZ color space, the tri-stimulus values are not the S, M, and L responses of the human eye, but rather a set of tri-stimulus values called X, Y, and Z, which are roughly red, green and blue, respectively. Two light sources, made up of different mixtures of various wavelengths, may appear to be the same color; this effect is called metamerism. Two light sources have the same apparent color to an observer when they have the same tri-stimulus values, no matter what spectral distributions of light were used to produce them.

Due to the nature of the distribution of cones in the eye, the tri-stimulus values depend on the observer's field of view. To eliminate this variable, the CIE defined the standard (colorimetric) observer. Originally this was taken to be the chromatic response of the average human viewing through a 2° angle, due to the belief that the color-sensitive cones resided within a 2° arc of the fovea. Thus the CIE 1931 standard observer is also known as the CIE 1931 2° standard observer.

The color matching functions are the numerical description of the chromatic response of the observer. The CIE has defined a set of three color-matching functions, called $\bar{x}(\lambda)$, $\bar{y}(\lambda)$ and $\bar{z}(\lambda)$, which can be thought of as the spectral sensitivity curves of three linear light detectors that yield the CIEXYZ tri-stimulus values X, Y, and Z. The tabulated numerical values of these functions are known collectively as the CIE standard observer (Fig. 2-6) [73]. The tri-stimulus values for a color with a spectral power distribution are given in terms of the standard observer by:

$$X = \int_0^{\infty} I(\lambda)\bar{x}(\lambda)d\lambda \quad (\text{Eq. 2 - 1})$$

$$Y = \int_0^{\infty} I(\lambda)\bar{y}(\lambda)d\lambda \quad (\text{Eq. 2 - 2})$$

$$Z = \int_0^{\infty} I(\lambda)\bar{z}(\lambda)d\lambda \quad (\text{Eq. 2 - 3})$$

where λ is the wavelength of the equivalent monochromatic light (measured in nanometers).

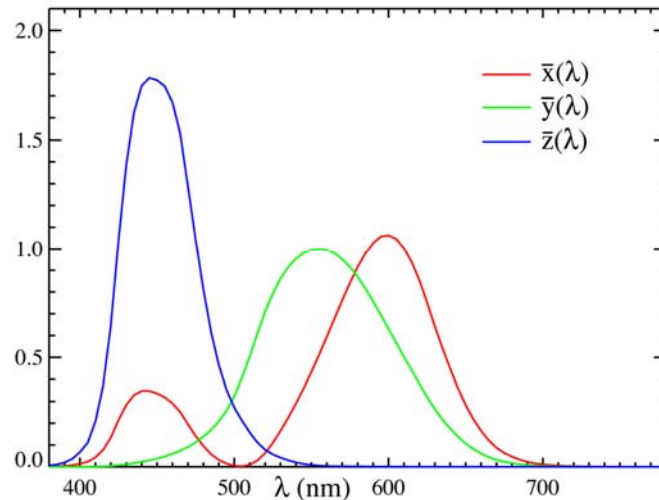


Fig. 2-6 The CIE standard observer color-matching functions

Since the human eye has three types of color sensors that respond to different ranges of wavelengths, a three-dimensional plot of all visible colors is shown in Fig. 2-7(a). However, the concept of color can be divided into two parts: brightness and chromaticity. For example, the color white is a bright color, while the color grey is considered to be a less bright version of that same white. In other words, the chromaticity of white and grey are the same while their brightness differs.

The CIE XYZ color space was deliberately designed so that the Y parameter was a measure of the brightness or luminance of a color. The chromaticity of a color was then specified by the two derived parameters x and y, two of the three normalized values which are functions of all three tri-stimulus values X, Y, and Z:

$$x = \frac{X}{X + Y + Z} \quad (\text{Eq. 2-4})$$

$$y = \frac{Y}{X + Y + Z} \quad (\text{Eq. 2-5})$$

$$z = \frac{Z}{X + Y + Z} = 1 - x - y \quad (\text{Eq. 2-6})$$

The derived color space specified by x , y , and Z is known as the CIE xyZ color space and is widely used to specify colors in practice. The diagram represents all of the chromaticities visible to the average person. These are shown in color and this region is called the gamut of human vision. The gamut of all visible chromaticities on the CIE plot is tongue-shaped or horseshoe-shaped as shown in Fig. 2-7(b). The curved edge of the gamut is called the spectral locus and corresponds to monochromatic light, with wavelengths listed in nanometers. The straight edge on the lower part of the gamut is called the line of purples. These colors, although they are on the border of the gamut, have no counterpart in monochromatic light. Less saturated colors appear in the interior of Fig. 2-7(b) with white at the center.

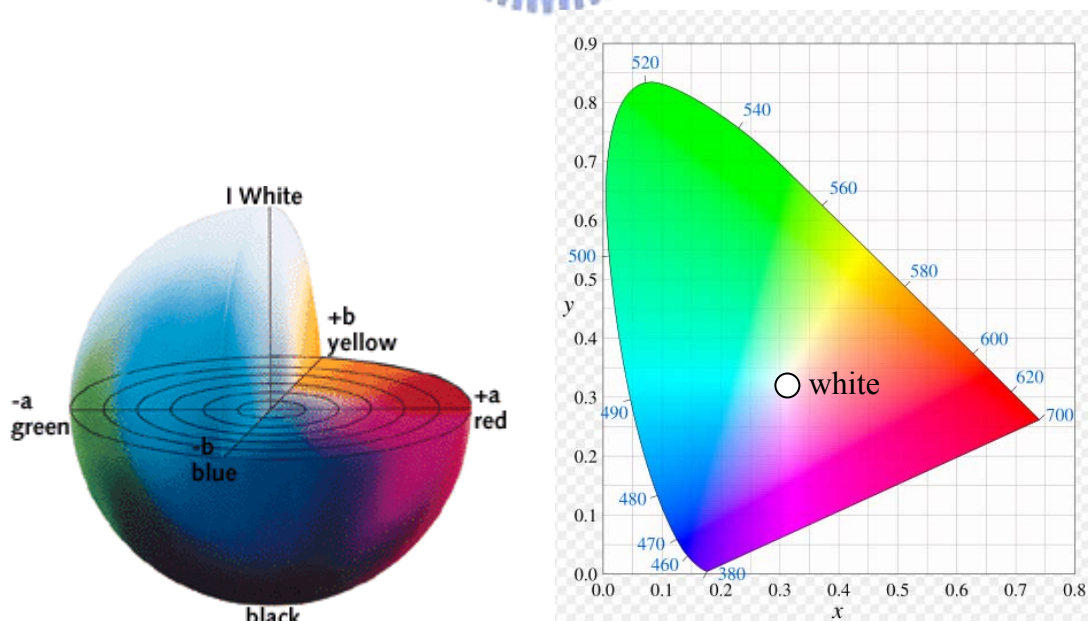


Fig. 2-7 (a) A 3D figure of visible colors and (b) the CIE xyZ .

In colorimetry, the CIELUV color space (Fig. 2-8) is a color space adopted by CIE in 1976, as a simple-to-compute transformation of the 1931 CIE XYZ color space, which is an attempt at perceptual uniformity [74][75]. It is extensively used for applications such as computer graphics which deal with colored lights. The non-linear relations are given below: [76]

$$L = \begin{cases} 116 \left(\frac{Y}{Y_n} \right)^{\frac{1}{3}} - 16, & \frac{Y}{Y_n} > \left(\frac{6}{29} \right)^3 \\ \left(\frac{29}{3} \right)^3 \left(\frac{Y}{Y_n} \right), & \frac{Y}{Y_n} \leq \left(\frac{6}{29} \right)^3 \end{cases} \quad (\text{Eq. 2 - 7})$$

$$u' = \frac{4X}{X + 15Y + 3Z} \quad (\text{Eq. 2 - 8})$$

$$v' = \frac{9Y}{X + 15Y + 3Z} \quad (\text{Eq. 2 - 9})$$

where Y_n is equal to 100 as the tri-stimulus of reference white [77].

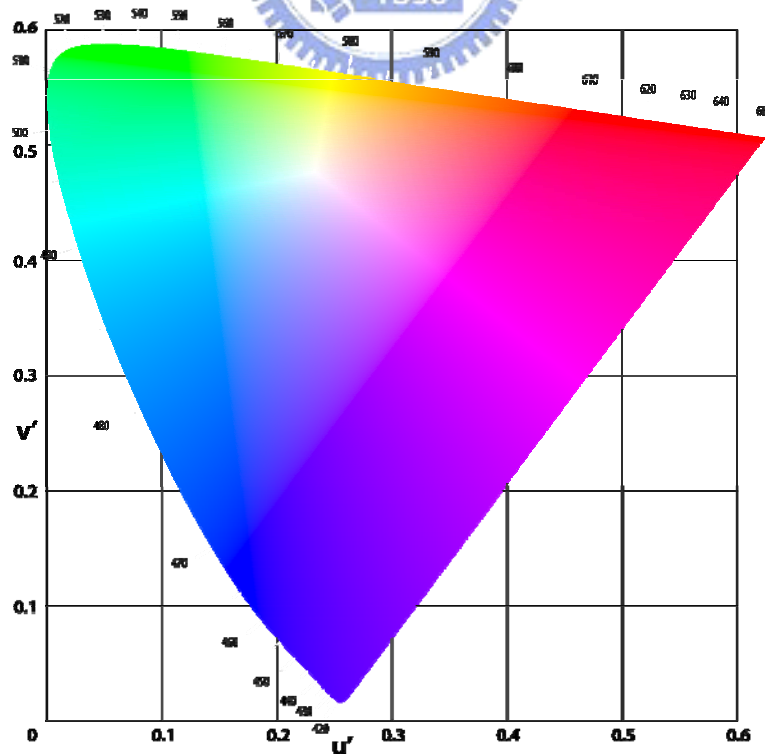


Fig. 2-8 The CIE $Lu'v'$.

By utilizing CIE1976, a more uniform chromaticity diagram can be established. Therefore, the color difference is defined by ΔE in the CIELUV chromaticity diagram. Consequently, the CBU phenomenon will be evaluated by the ΔE index between the CBU image and the original image to verify the proposed method [78]-[80]. We sum up the color difference between modified and original image pixel by pixel as an index, ΔE_{sum} , for the evaluation of color separation.

$$\Delta E_{sum} = \sum_{total\ pixel} \sqrt{(L_{CBU} - L_0)^2 + (u'_{CBU} - u'_0)^2 + (v'_{CBU} - v'_0)^2}. \quad (\text{Eq. 2-10})$$

where $Lu'v'_{CBU}$ and $Lu'v'_0$ are color values of CBU and original image in the $Lu'v'$ color space.

2.4 Hardware involved in sequential driving

The fast response LC and display electronic circuit are key components in FSC-LCDs. The LC response time is essential for one temporal field with the rate higher than 180 Hz [22]. Otherwise, the display electronics should be capable of synchronic driving with the LCD panel and LEDs. An FPGA as a timing controller is designed to process the incoming video content into each color field data, as show in Fig. 2-9. The features of the hardware are described in this section.

2.4.1 OCB mode

The optically compensated bend (OCB) mode LC, owning a feature of high speed response, is used for LCDs, especially highlighting motion images [81]. In OCB mode, the pre-tilt angles in the top and bottom substrates are in opposite directions. The opposed pre-tilt angles have two important properties. First, the optical self-phase compensation effect is induced on LC directors. As a result, the viewing angle is wide and symmetric. Second, the bend directors in an on-state voltage eliminate the back-flow effect, resulting in a faster response time. As the

applied voltage increases, the LC directors change from splay to bend deformation, as illustrated in Fig. 2-10. Below the critical voltage ($V_c \approx 1.8V$), splay state is more stable than bend state. On the contrary, above V_c , bend state is more stable as shown in Fig. 2-11. The OCB mode LC will be maintained in bend state by applying a bias voltage [82][83].

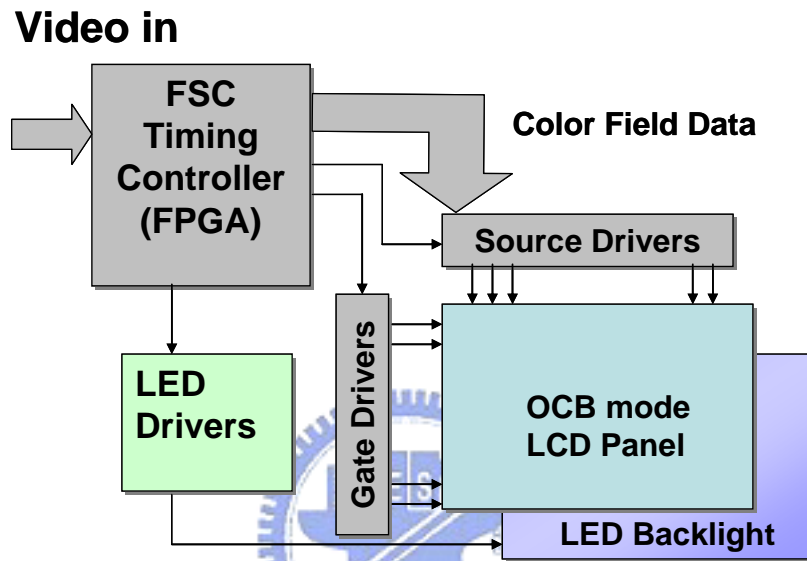


Fig. 2-9 The display electronic circuit

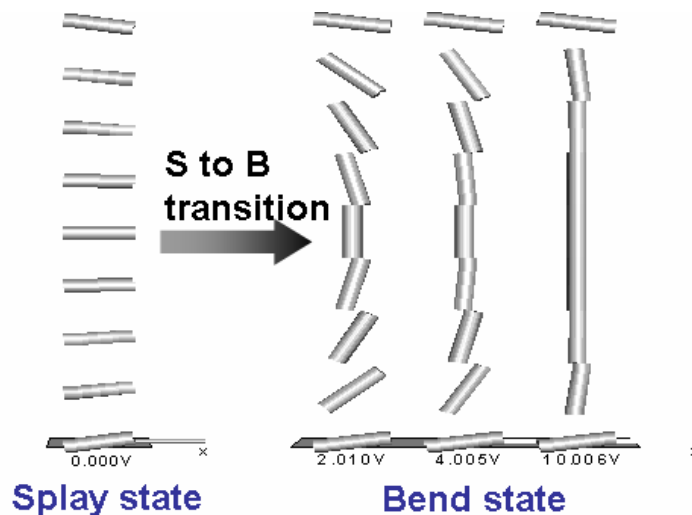


Fig. 2-10 The transition between splay and bend states in an OCB mode LC

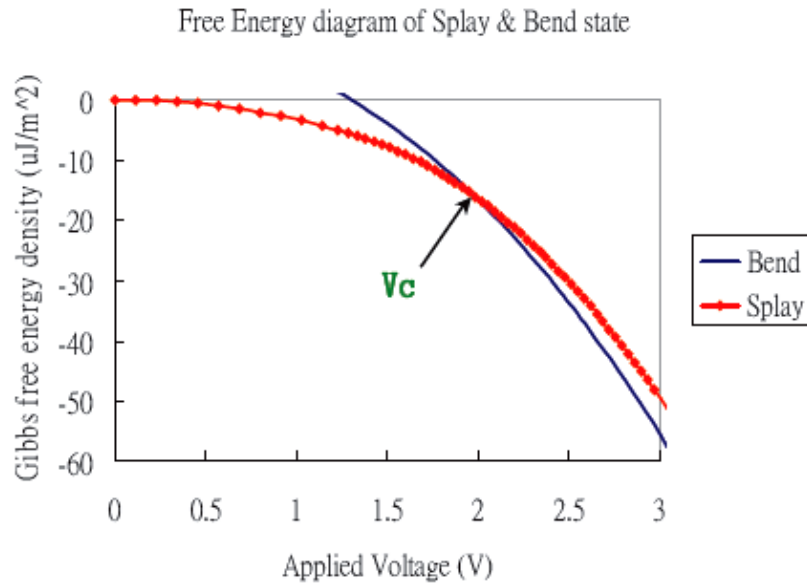


Fig. 2-11 The transition curve from splay to bend state in OCB mode LC[82]

2.4.2 Source and gate drivers

LCD source driver ICs with RSDS (Reduced Swing Differential Signaling) interface and single 12-bit differential bus for 24-bit data are utilized in the driving system. The source driver can receive 12-bit differential data from timing controller and can output 480-channel LCD driving voltage. The specifications are shown in Tab. 2-1 (a). There are some advantages of the RSDS interface, as shown below.

- Reduced bus width – enables smaller and thinner column driver boards
- Low power dissipation – extends system run time
- Low Electromagnetic Interference (EMI) generation – eliminates EMI suppression components and shielding
- High noise rejection – maintains signal image
- High throughput – enables high resolution displays

The timing diagram of RSDS data transition is shown in Fig. 2-12. We can see the differential signals are received at the rising edge of clock-P and clock-N. The 24 bit data can be received by using a 12 bit differential bus during one clock-P/N cycle.

Then the source driver can transform the received data, and control the LC by applying voltage to 480 output channels.

After the source driver output an electric signal in one line of the frame, the gate driver applies voltage to turn the thin film transistor (TFT) on. Thus, the source driver's signal can store into each pixel in one line of the frame. In this way, the LC of each pixel can be controlled individually. In order to turn TFTs on, a start pulse signal is necessary to drive the gate driver output a high voltage. After a start pulse is triggered, output pins of gate driver will sequentially produce high-driving voltage pulses for the LCD panel. This gate driver can produce voltage through 240 channels to the LCD panel, The max clock frequency is 200 KHz, as shown in Tab. 2-1 (b).

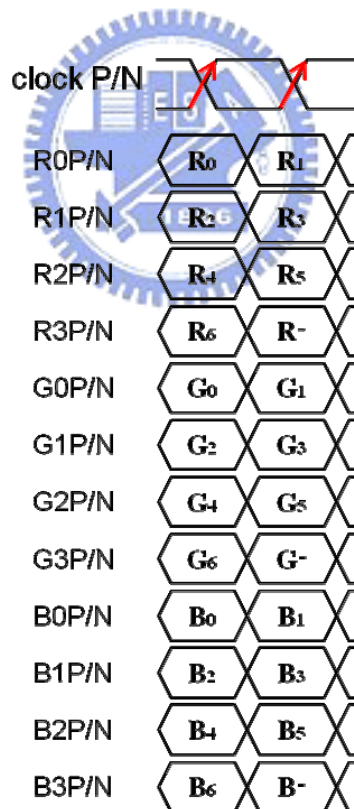


Fig. 2-12 The timing diagram of RSDS.

Tab. 2-1 The specifications of (a) the gate driver and (b) the source driver for the TFT LCD panel

(a)

Source driver	
Output	480 output channels
Input	RSDS input interface for low EMI
Resolution	8-bit resolution / 256 gray scale

(b)

Gate driver	
Output	240 output channels
input clock	< 200 KHz

2.4.3 LED driver

The LED backlight system consists of LED drivers and 3-in-1 LEDs (R, G, and B). Each LED driver is a 16-channel constant-current sink driver. Each channel has an individually adjustable 4096-step grayscale by Pulse-Width Modulation (PWM) operation and 64-step constant-current sink (dot correction). The dot correction adjusts the brightness variations between LED channels and other LED drivers.

This LED driver has the capability of adjusting the output current for each channel (OUT0 to OUT15) independently. The driven method, called Dot Correction mode (DC mode), is used to adjust LED brightness. Each of the 16 channels can be programmed with a 6-bit word. Thus the channel output can be adjusted in 64 steps from 0% to 100% of the maximum output current. Dot correction data are entered for all channels at the same time. The complete dot correction data format consists of 16 x 6-bit, which forms a 96-bit wide serial output data to control the current of 16

channels independently. This LED driver also can adjust the brightness of each channel by using a PWM control scheme. It uses the 12-bit width digital signal per channel to result in 4096 (2^{12}) different brightness steps, which is called grayscale mode (GS mode). The total grayscale data of 16 channels is 16 x 12 bit width, which forms a 192-bit wide data packet. Consequently, each LED current is controlled by the LED driver with DC mode operation. Each LED lighting period is controlled by a LED driver with GS mode operation. The serial data input timing diagram with DC and GS mode is shown in Fig. 2-13 and Tab. 2-2.

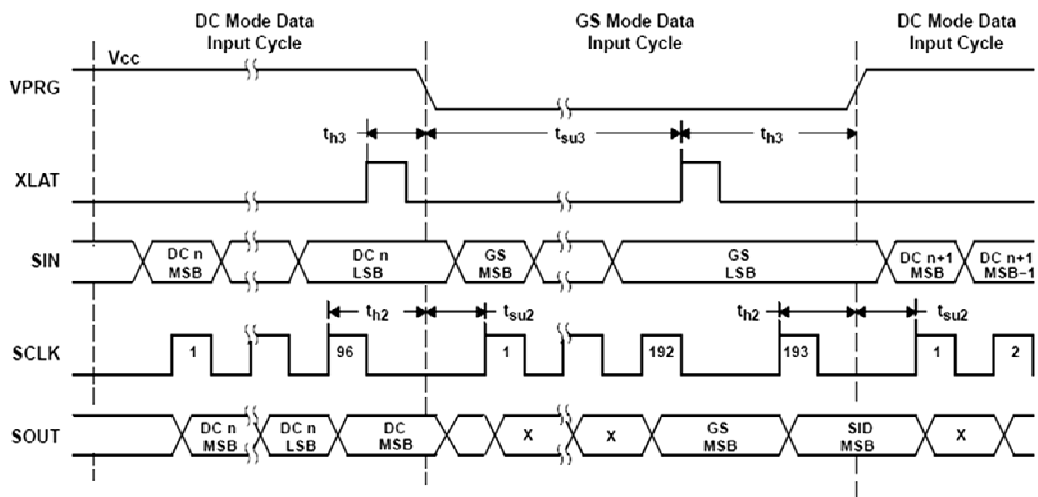


Fig. 2-13 Serial data input timing diagram of the LED controller.

Tab. 2-2 The specifications of LED driver

Input frequency	30 MHz (max)
Output channels	16 output channels
Dot correction (DC mode)	6-bit (64 steps) for LED current
Grayscale PWM mode (GS mode)	12-bit (4096 steps) for LED grayscale

2.4.4 FPGA

A field-programmable gate array is a semiconductor device containing programmable logic components called "logic blocks". Logic blocks can be programmed to perform the function of basic logic gates such as AND, and XOR, or more complex combinational functions such as decoders or mathematical functions. In most FPGAs, the logic blocks also include memory elements, which may be simple flip-flops or Static Random Access Memory (SRAM). In this thesis, the memory elements used in FPGA are Static Random Access Memory (SRAM) and Synchronous Dynamic Random Access Memory (SDRAM), which were used as data buffers and the frame buffers, respectively.

In order to define the behavior of the FPGA, the user provides a hardware description language (HDL), the Common HDLs are VHDL and Verilog. Then, the user uses an electronic design automation tool; a technology-mapped net-list is generated. This net-list can be fitted to the actual FPGA architecture by using a process called place-and-route. The user will validate the map, place and route results via timing analysis, simulation, and other verification methodologies. Once the design and validation process is complete, the binary file is generated to configure the FPGA.

2.5 Summary

The physiology of eye movement and CBU phenomenon have briefly discussed in this chapter. In order to recognize the stationary image, the observer's eye moves around the object to collect information during eye saccadic motion. For a moving object, the human eye will follow at the same velocity of the object to catch clear images, which is called the pursuit. The relative movement between human eyes and the object results in perception of CBU. The saccade and pursuit are related to static and dynamic CBU in perception while color field images are integrated separately on the retina.

To evaluate the CBU effect, we began as the color standard CIE 1976 to calculate the color difference for the evaluation index. The CIE 1976 is more uniform color space than CIE 1931 and suitable for the evaluation of color difference. We summed up the color difference between the original and CBU images at each pixel as an index, showing the factors of the color separation in CBU images. This index will be used to verify the proposed methods to suppress CBU.

In addition, the key components including OCB LC and display driving technologies such as drivers and control circuit are introduced in this chapter. The bend state of OCB enables the fast response light valve, which is essential for one temporal field with the rate higher than 180 Hz. The display electronics is capable of driving this panel with synchronic design of LCD and LED drivers. The control signals are implemented in an FPGA as a timing controller to process the incoming video content into individual field stream of data.

Chapter 3

Proposed CBU Suppression Methods

A novel CBU suppression method, color fields arrangement (CFA), was proposed to eliminate the artifacts for FSC-LCDs. The modified order of consecutive color fields results in superimposed color images on a retina without CBU. To suppress the static CBU effectively, the RGBW method was introduced to concentrate image intensity to a white field and discolor the primary color fields. The visibility of CBU artifacts can be reduced as the evaluation of dynamic and static models. For images with cyan, yellow, and magenta color, the exchange of color sequence of RGBC and RGBY was used to dynamically mitigate the CBU effects based on image contents.



3.1 Color fields arrangement

The FSC-LCD is desirable for its high optical efficiency, low power consumption, and low cost. However, the color breakup is significantly observed on FSC-LCDs. We have proposed a 4-color field arrangement (4-CFA) method to suppress the artifacts for FSC-LCDs.

3.1.1 Concept

The two dimension time and location diagram was analyzed in order to determine an integration image of consecutive frames on FSC-LCDs. The fields of primary colors are respectively displayed in Fig. 3-1. When the observer views a moving image, the viewpoint follows the shift of the image, as indicates by the arrow A. Consequently, the observer recognizes a CBU image as rainbow color in Fig. 3-2

(a). The outline portion of image is determined by the order arrangement of color fields. Two other frame images with the color fields arrangement (CFA) were obtained. The integration of three consecutive frames is shown in Fig. 3-2 (b). The image on a retina will be compensated as a gray level image because of the viewpoint through the same ratio of each primary color. Consequently, the observer recognizes a non-CBU image with these color fields.

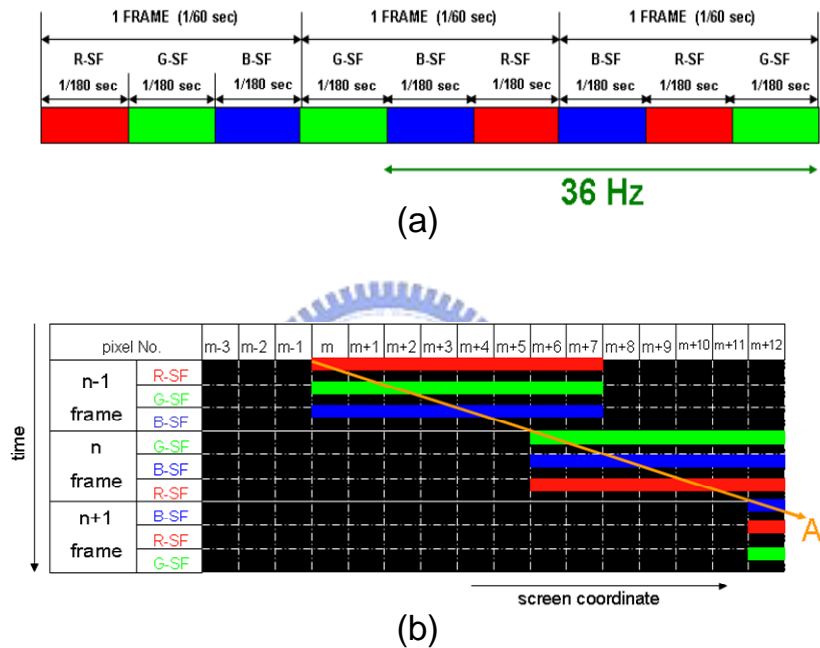
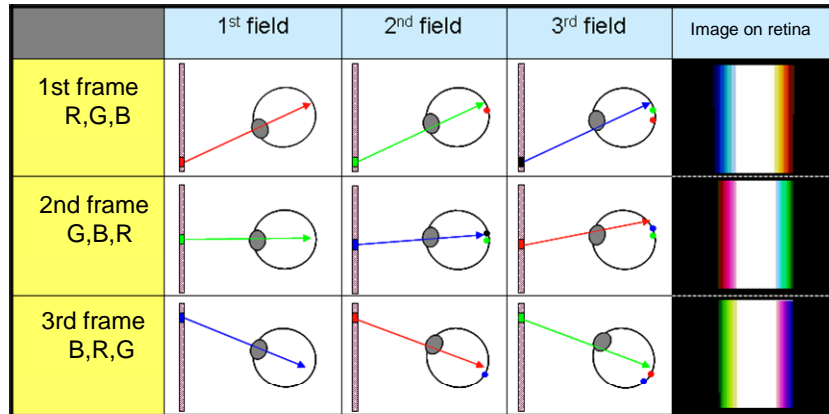


Fig. 3-1 (a) Color fields of RGB, GBR, and BRG in three consecutive frames (b) the relation between time and location of motional image.



(a)



(b)

Fig. 3-2 (a) Mechanisms of the color breakup when eyes follow the motional image, (b) an integrated image in three consecutive frames with the CFA method.

Although the CFA method can avoid the CBU of dynamic images, a flicker phenomenon will be an issue for the CFA method [84]. Because the human eye is more sensitive to green color, the lowest field frequency for green color to perceive invisible flicker is 50 Hz as shown in Tab. 3-1 [85]. However, the green field appeared at the first and third field in straight two frames. The green field frequency of 36 Hz in this worst case would be lower than the invisible condition. In order to suppress the flicker phenomenon, we proposed to insert a fourth color field to speed up the field frequency.

Tab. 3-1 The lowest field frequency that produces invisible flicker for each color

	R	G	B
Frequency (Hz)	30	50	35

3.1.2 4-CFA method with repeating color orders

The color fields with orders of RGBR, GRBG, and BRGB in three consecutive frames were proposed in the 4-CFA method. The color of the fourth field repeated the one of the first field as shown in Fig. 3-3(a). The motional image and simulation result of a moving image of white bar are shown in Figs. 3-3(b) and (c). The margin of perceived image is blurred due to differences in brightness but without color separations. In addition, the flicker phenomenon should be suppressed because of the color field frequency of 80 Hz, higher than the invisible condition of 50 Hz.

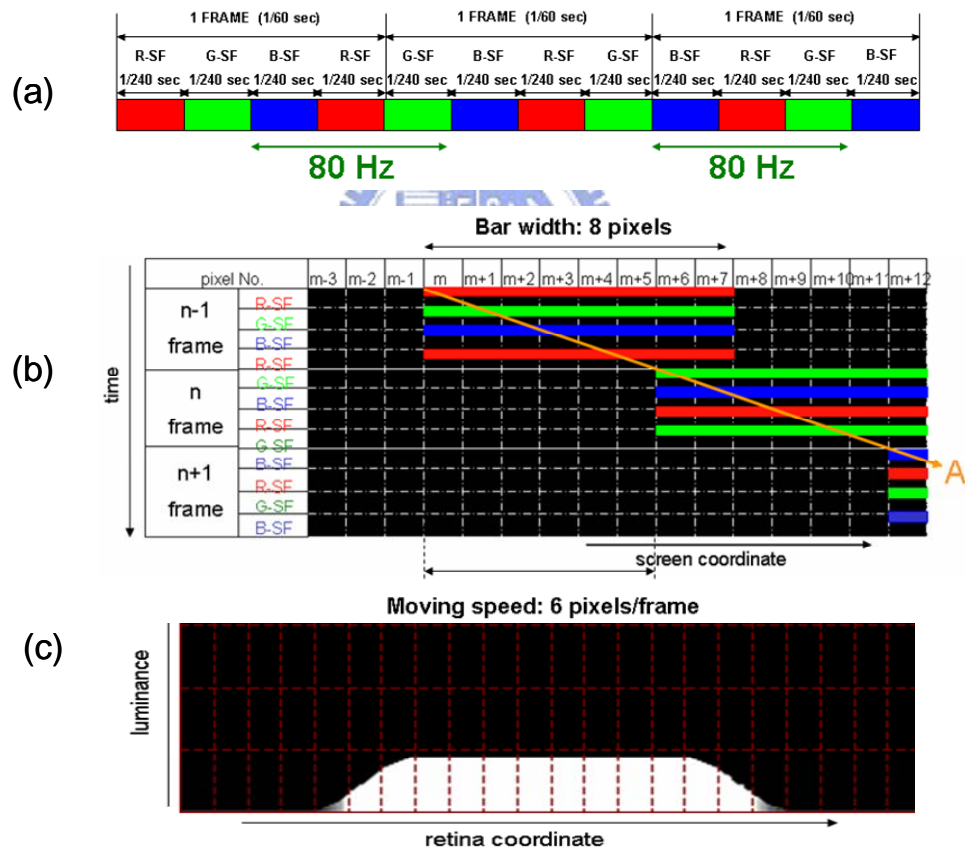


Fig. 3-3 (a) Color fields of RGBR, GRBG, and BRGB in three consecutive frames, (b) the relation between time and location of motional white bar with width of 8 pixels and velocity of 6 pixels/frame, and (c) the simulation image on retina with the 4-CFA method when eyes follow the image.

3.1.3 Implementation of FSC controller

A timing controller, which is designed to convert the image data to a desired format in response to the timing signal, is a key component in an FSC system. The block diagram of the controller is shown in Fig. 3-4. This controller consists of the data convert, frame buffer, memory switch, and LED lighting unit. A graphic card is used to convert the input video rate to 60 Hz in advance. These 24-bit RGB input signals are stored into monochromatic red, green, blue data separately in the data convert unit. The function of the memory switch unit is to access the consecutive frame data alternately between two banks of SDRAM. As one is on reading operation, the other one is on writing operation. To avoid conflicts of the consecutive frame data during the operation, a frame buffer is as a register to translate the data into LCD drivers. At the same time, an LED timing unit determines the enable signals for LED drivers to switch corresponding LEDs on.

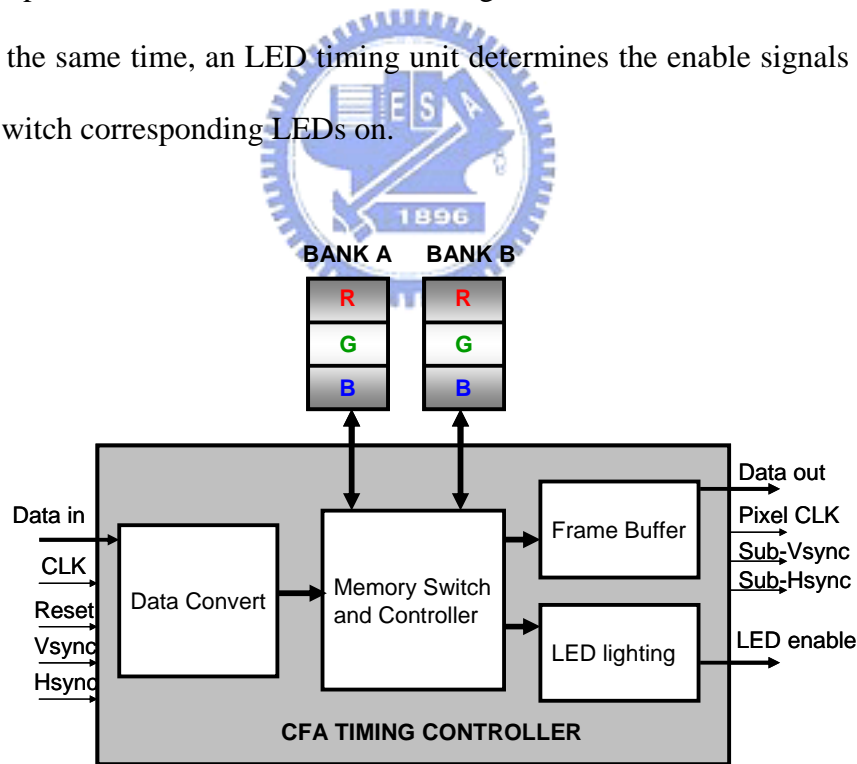


Fig. 3-4 The block diagram of the FSC controller.

A 5.6-inch OCB-LCD with QVGA resolution was used as a prototype to evaluate the properties of CBU and flicker phenomenon. The response time of OCB mode LC cell (t_{LC}) and the data addressing time (t_{TFT}) were about 1.0 and 1.2 ms in this study. For a field frequency of 240 Hz, the illumination time of LEDs (t_{LED}) about 1.9 ms was obtained as shown in Fig. 3-5. The backlight intensity of first and fourth fields was modified to meet the criterion of white balance. From the observation, there was no flicker as we predicted.

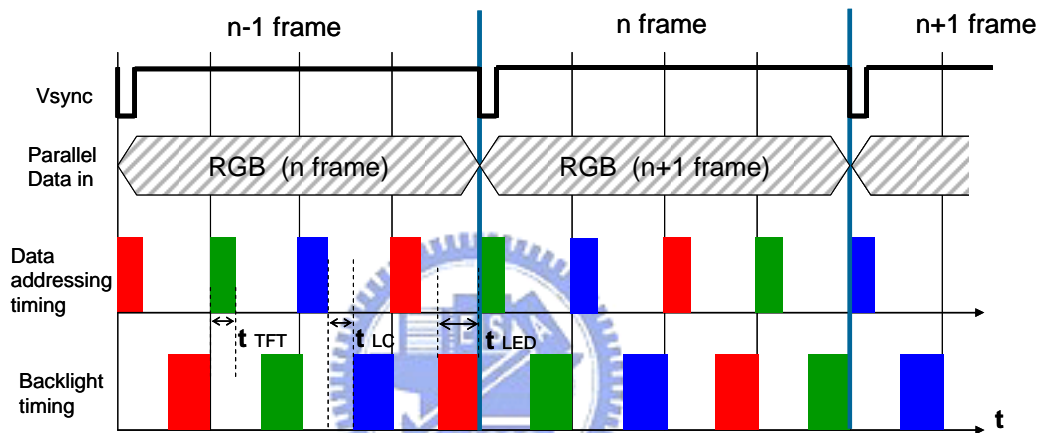


Fig. 3-5 The timing chart of the 4-CFA FSC-LCD.

3.1.4 Physical evaluation of CBU

The evaluation of CBU was carried out by a camera-tracking experiment. The perception of CBU was evaluated to verify the proposed CBU reduction method. The motion image was used as a test pattern to compare the image quality with the conventional and proposed methods. A stage with a high-speed camera, Phantom V5.1 by Vision Research, Inc.[86], was set up on a track and adjusted the velocity by a computer interface. In order to simulate the shift of the observer's viewpoint, we synchronized the moving velocity of the bar on the image and the camera on the track, as shown in Fig. 3-6. The exposure time of camera was set to 1/20 second to integrate three consecutive frames while a frame frequency was 60 Hz. The experimental

results of perceived images are agreed with the observation, as shown in Fig. 3-7. The CBU is eliminated in the 4-CFA method with a blurring margin as predicted in Fig. 3-3(c). On the contrary, the conventional CBU was obvious for multicolor. Considering the moving velocities, the CBU widths are proportional to the velocities of objects on a motional image. Similarly, the blurring margin of fast-motional image became wider in the 4-CFA method. Fig. 3-7 shows the comparison results with bar widths of 15 and 30 pixels. The widths of CBU and blurring margin were independent to bar widths in both driving methods. Moreover, cyan and yellow bars were tested in the 4-CFA method as shown in Fig. 3-8. Images with narrower and blurring margins were obtained simultaneously. Comparatively, field rate increasing [43], one of previous CBU reducing methods, could narrow the CBU width but not blur the margin at the same time. On the contrary, the intensity of color separation could be lightened but the CBU width could not be narrowed by multi-primary-color insertion method [44]. From the experimental results, the 4-CFA method is concluded as the practical method to eliminate the dynamic CBU phenomenon.

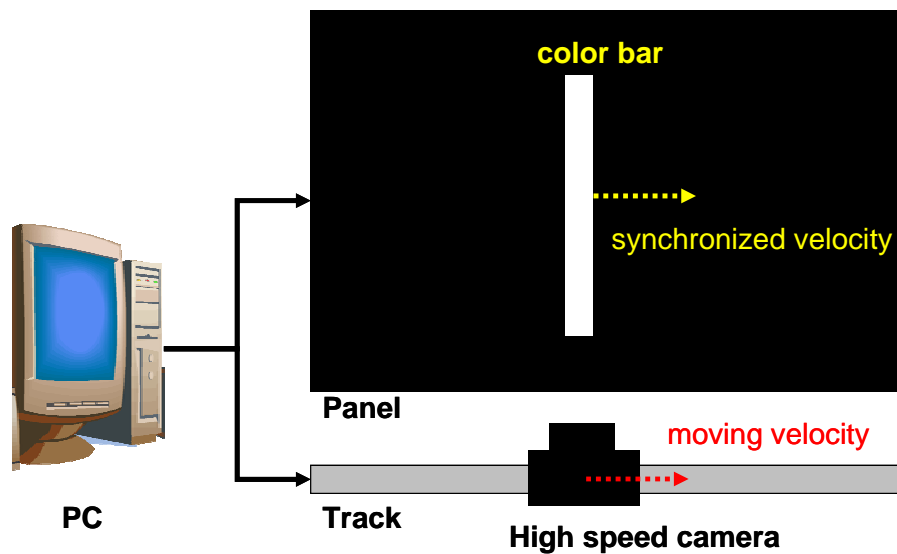


Fig. 3-6 The camera-tracking equipment

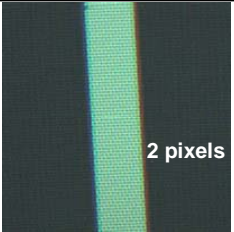
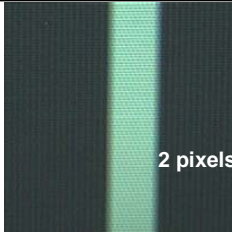
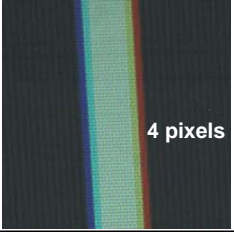
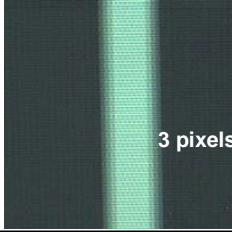
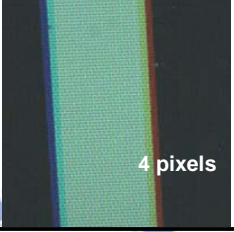
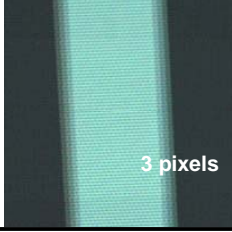
White bar	3-RGB	4-CFA
Width 15 pixels Velocity 3 pixels / frame	 2 pixels	 2 pixels
Width 15 pixels Velocity 6 pixels / frame	 4 pixels	 3 pixels
Width 30 pixels Velocity 6 pixels / frame	 4 pixels	 3 pixels

Fig. 3-7 Photos of a moving white bar, which were taken by a tracing camera, with bar widths of 15 and 30 pixels, velocities of 3 and 6 pixels/frame.

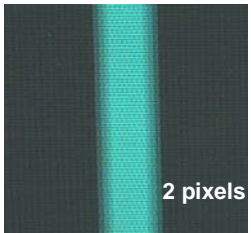
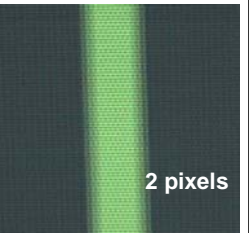
4-CFA	Cyan bar	Yellow bar
Width 15 pixels Velocity 6 pixels / frame	 2 pixels	 2 pixels

Fig. 3-8 Photos of moving cyan and yellow bars, which were taken by a tracing camera, with bar width of 15 pixels and velocity of 6 pixels/frame.

In addition to the dynamic CBU, the static CBU should be considered for evaluating the image qualities. The static CBU occurs when abrupt perturbation produces the saccadic movement. This movement gives a retina broken color sequence which is easily experienced while rotating the head or eyes. Therefore, the effective way to reduce this artifact is to increase the sequential frequency. For the still image, the field frequency of 4-CFA in three consecutive frames is 240 Hz. Comparing the static CBU with the conventional and 4-CFA methods, the field frequency of 4-CFA is 1.3 times faster than that of the conventional one, resulting the slighter static CBU width. The results of our evaluation supported that the proposed 4-CFA method can reduce the visibility of CBU artifacts.

3.2 RGBW method

In order to further mitigate the static CBU during the saccadic motion, we proposed the RGBW method, redistributing gray levels to condense the noticeable fields on a white field and reduce the intensities of R, G, and B fields. This concept contains the redistribution algorithm, followed by experimental results demonstrating the performance of gray level redistributions and the CBU evaluation on an LC panel.

3.2.1 Concept and simulation

With the RGBW method, one frame is divided into four fields, R, G, B, and white (W). In W field, RGB LEDs turn on simultaneously. The gray level of each pixel in W field depends on the minimum gray level of corresponding pixel in R, G, and B field. The algorithm of RGBW method is shown in Fig. 3-9. The gray levels (GL) of R, G, B, and W field images are represented by GL_R , GL_G , GL_B , and GL_W , respectively.

$$\text{gray level} = 255 \times T^{1/4} \quad (\text{Eq. 3-1})$$

The relationship between gray level and transmittance is shown in Eq. 3-1, where T is the transmittance of LC and γ is the gamma value of LCD. In RGBW algorithm, we assume the gamma value is one. The first step of RGBW algorithm is to sort the RGB gray levels of one pixel in an image for the minimum one of these gray levels. Then subtract the minimum one from original RGB gray levels in this pixel to new gray levels in RGB fields. Finally, the minimum is assigned as white gray level for W field. This process is repeated for each pixel of the image. For a pure white image, only the W field is displayed, thus CBU can be totally eliminated by using RGBW method. For other colors, at least one gray level of color fields will be zero.

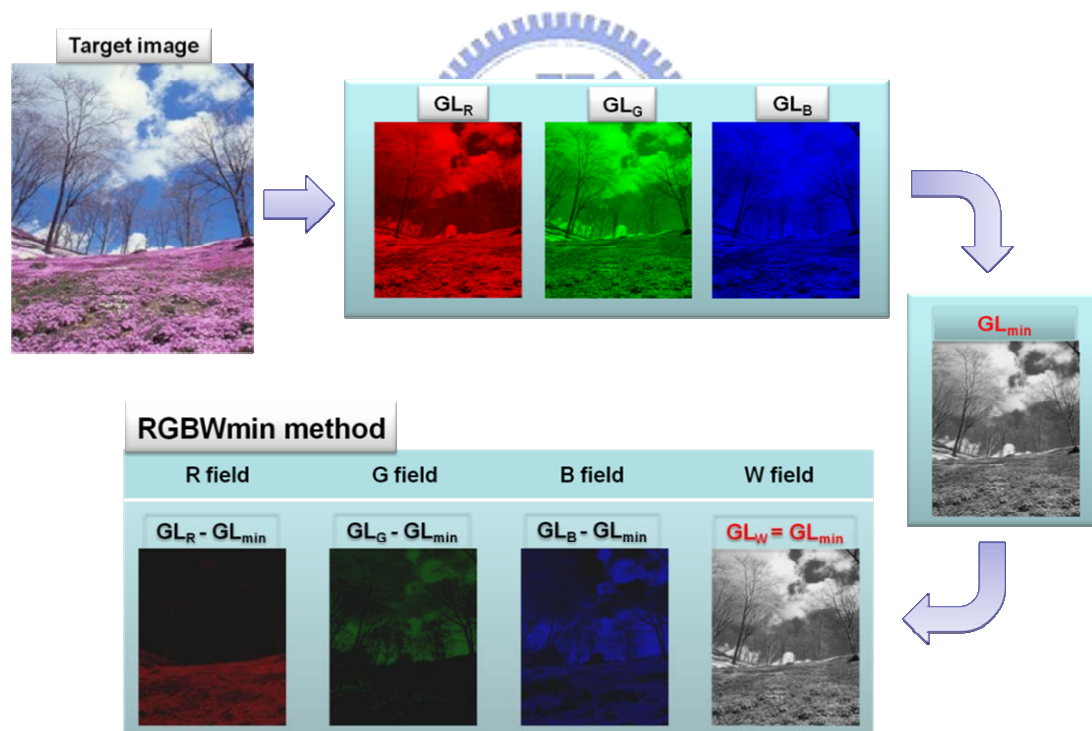


Fig. 3-9 The flow chart of RGBW algorithm.

We have simulated an image with conventional RGB and proposed RGBW methods. These images were shifted per field to simulate CBU. The image quality can be improved by RGBW, as shown in the area of Fig. 3-10 circled by the solid line. The reduced intensities of R, G, and B fields can suppress CBU with inserting a white field.

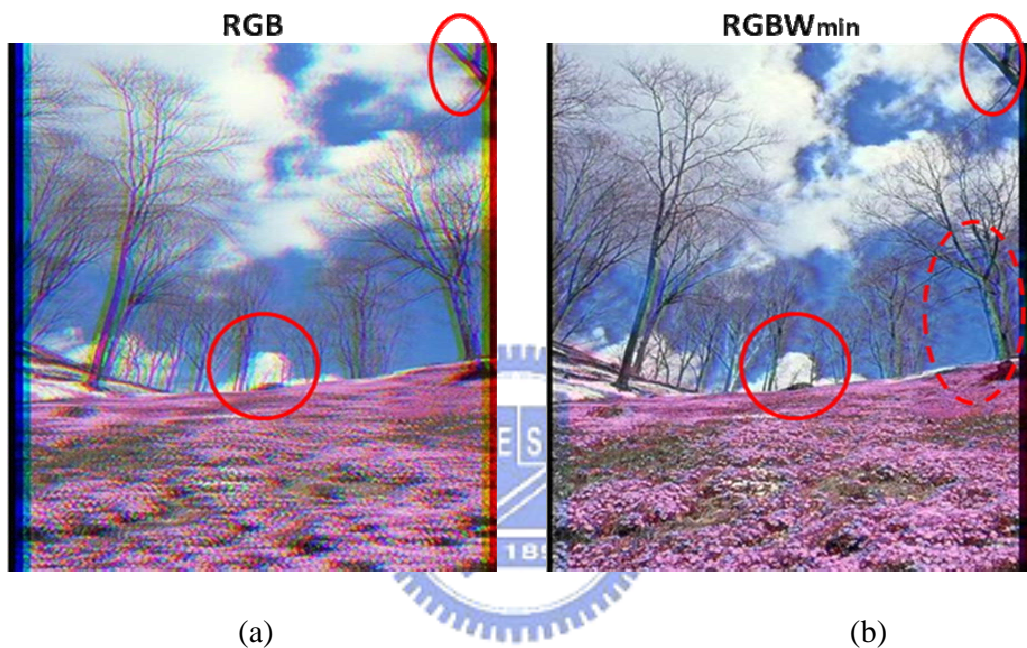


Fig. 3-10 The CBU simulation images by using (a) RGB and (b) RGBW methods.

3.2.2 Experimental results

We displayed an image on a 5.6-inch FSC-LCD with RGB and RGBW methods as shown in Fig. 3-11. The images composed of specific color bars such as strong red, grass green, sky blue, and white. We used a slit to shake in front of the display, thus caused static CBU as shown in Fig. 3-12. In the RGB method, stationary image seemed to break up into R, G, and B color fields on the edge of the slit, especially for a white image. However, in proposed RGBW method, the white image did not cause static CBU. Even for other colors, the stationary image only broke up into one color field on the edge of the slit. Consequently, static CBU can be suppressed by the RGBW method.

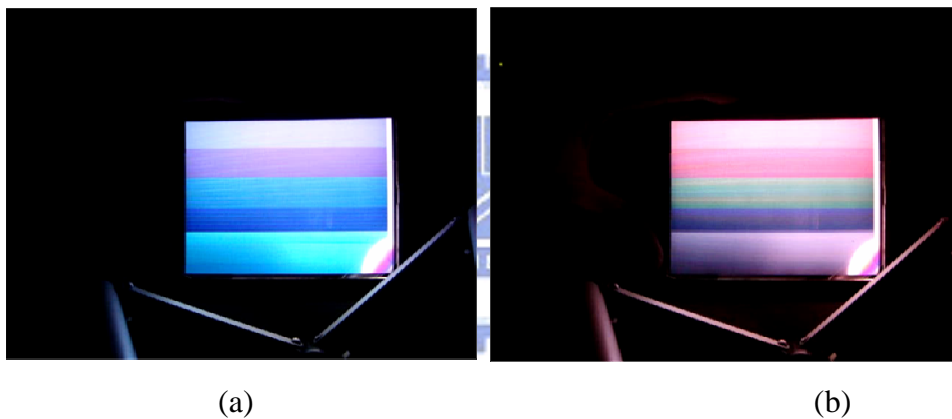


Fig. 3-11 The images displayed by a 5.6-inch FSC-LCD with (a) RGB and (b) RGBW methods.

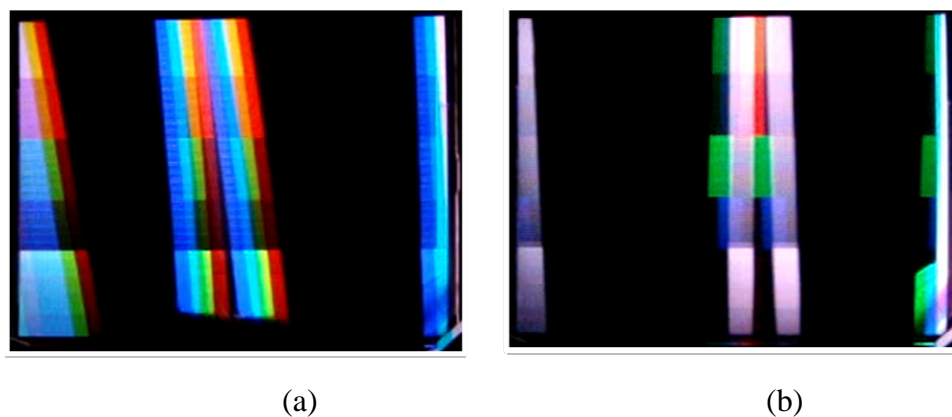


Fig. 3-12 The static CBU images for (a) RGB and (b) RGBW methods.

3.3 RGBC/RGBY method

If the major colors of an image are composed of cyan, yellow, and magenta, the method will not be useful for static CBU reduction. For example, the major color is yellow in Fig. 3-13, resulting in the intensities of R and G non-reduced even by inserting a white field. Therefore, static CBU cannot be effectively suppressed. Another example of perceived CBU is shown in Fig. 3-10(b) cycled by a dot line.

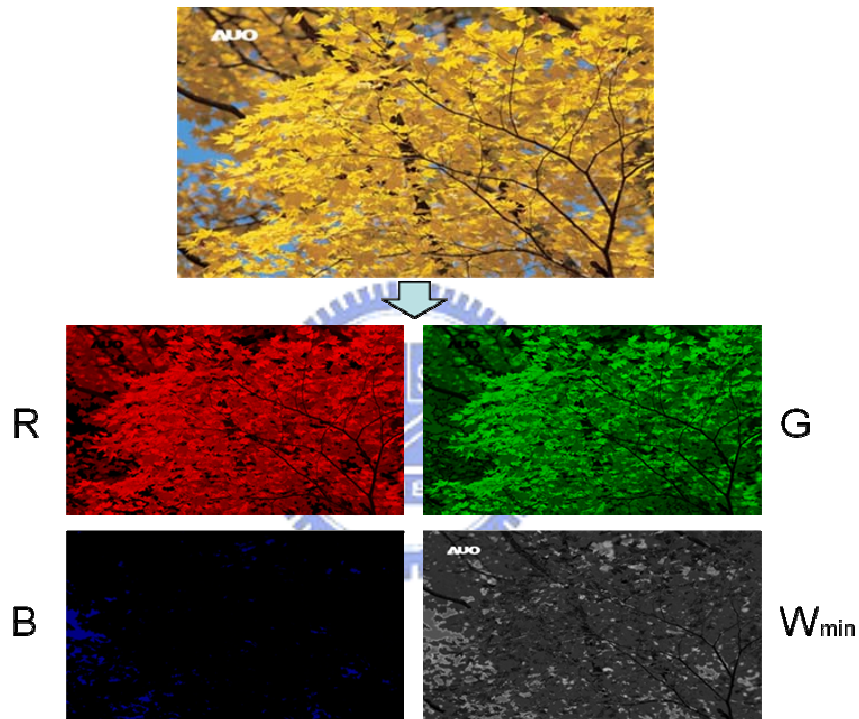


Fig. 3-13 The R, G, B, and W fields of an image.

3.3.1 Concept

In order to suppress the CBU artifact for a wider range of image contents, we proposed to lighten the primary color fields by redistributing the LC gray levels to the fourth color field as shown in Fig. 3-14(b). The visibility of the CBU artifact is reduced while the intensity of color separation is decreased. We chose the cyan and yellow as the fourth color field in order to lighten the most sensitive green field. This 4-field operation was determined by the response time of available LC in large-sized

applications. Fig. 3-15 shows that a full color image alternately consists of RGBC and RGBY color field sequences. It is obvious that the image intensities of primary colors are lightened.

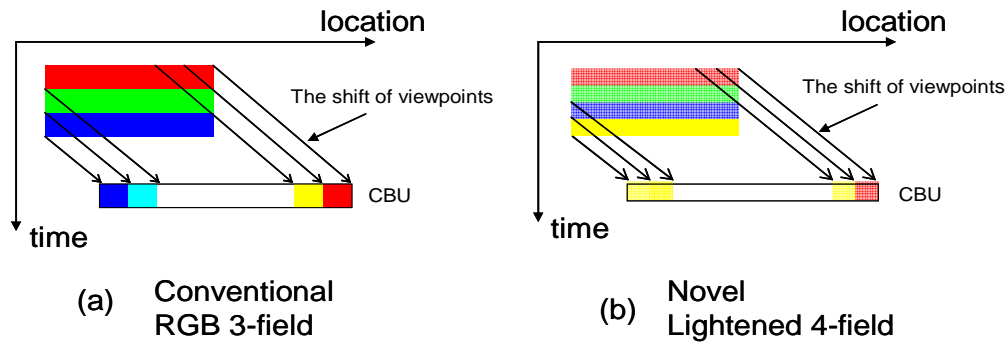


Fig. 3-14 The relation between time and location of moving image on (a) a conventional RGB 3-field and (b) the redistributed color FSC displays.

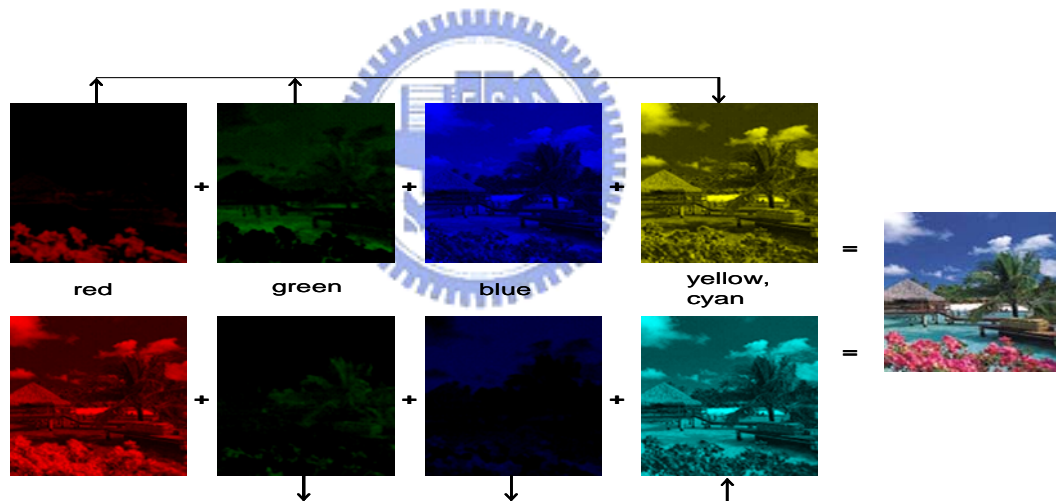


Fig. 3-15 The gray levels in red and green/green and blue are redistributed to yellow/cyan field to form a full color image.

3.3.2 CY exchange algorithm

The redistributions of LC gray levels on the color sequence of RGBC and RGBY are determined by the image content. For example, when the green gray level in a pixel is lower than the red one, the gray level of yellow field is set as the lower gray level, the green one. The new gray level of this pixel in the green field is set to zero because the gray level is redistributed to the yellow field. In order to maintain the

white balance, the gamma curve between gray levels and transmittances should be considered. Therefore, the new gray level in the red field r' is represented as

$$r' = T^{-1}(T(r) - T(g)), \quad (\text{Eq. 3-2})$$

where $T(i)$ are the transfer function from gray level i to a transmittance. T^{-1} is the inverse function of $T(i)$, as shown in Fig. 3-16.

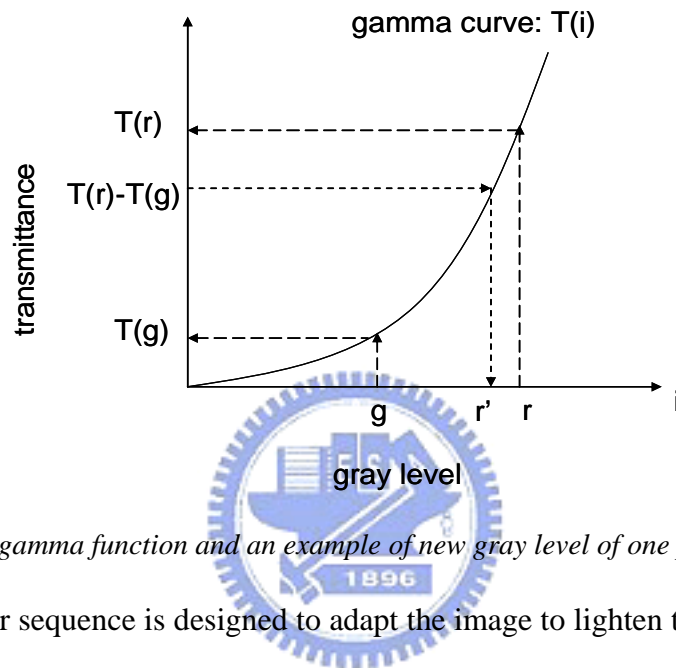
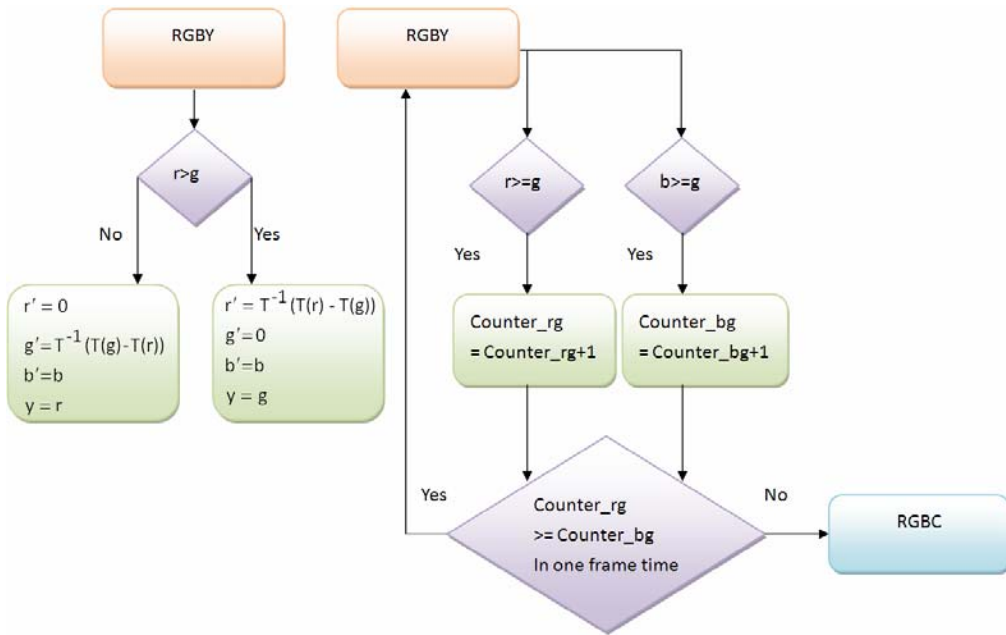
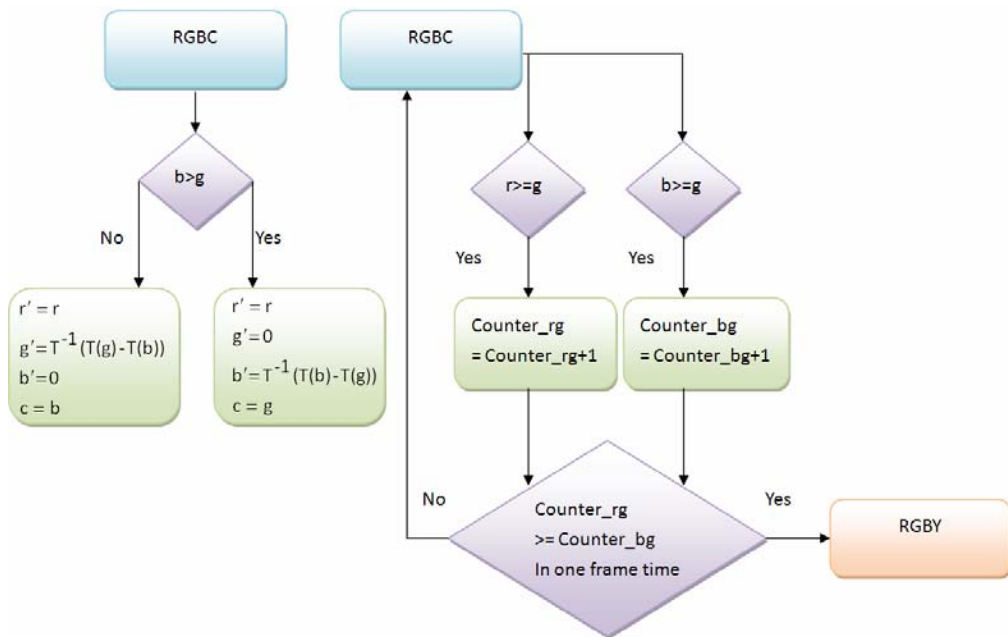


Fig. 3-16 The gamma function and an example of new gray level of one pixel in red field.

The color sequence is designed to adapt the image to lighten the primary colors. Fig. 3-17 shows the flowchart to determinate the new gray levels of color sequence. The counter_bg adds one when the gray level of blue is equal or larger than that of green for individual pixel of image. So does the counter_rg when the red gray level is equal or larger than the green one. The larger one of these two counters implies the image consisting of higher gray levels. In order to discolor the primary color fields, these higher blue/red gray levels are redistributed into the cyan/yellow color. Therefore, the color sequence will be switched to RGBC/RGBY in the following frame. Moreover, the comparison between red/green or blue/green original data determines the new gray levels of red, green, blue, yellow, and cyan fields. These new LC signals and backlight fields are synchronized by a frame buffer, a signal register for the gray levels of LC and backlight sequential order in each frame.



(a) RGBY



(b)RGBC

Fig. 3-17 The flowchart of gray level redistribution and the following frame in (a)RGBY or (b)RGBC color sequence.

3.3.3 System architecture

The display system can be divided into three parts: input video source transfer interface circuit, FPGA controlled circuit, and output display circuit. The function of transfer interface circuit is to transfer the input digital visual interface (DVI) signals into low-voltage differential signalling (LVDS). Then LVDS type signal can be processed in a FPGA. In the FPGA controlled circuit, its main function is to generate control and data signals for enabling the drivers of all system. For the display circuit, there are a panel module and a backlight module. The panel module consists of an OCB panel, source drivers, and gate drivers, determining the LC grey level. For a backlight module, LED and LED driver boards provide the light source and sequential driving. The block diagram is shown in Fig. 3-18. The controlled circuit is successfully implemented in FPGA and these module functions are explained in appendix.

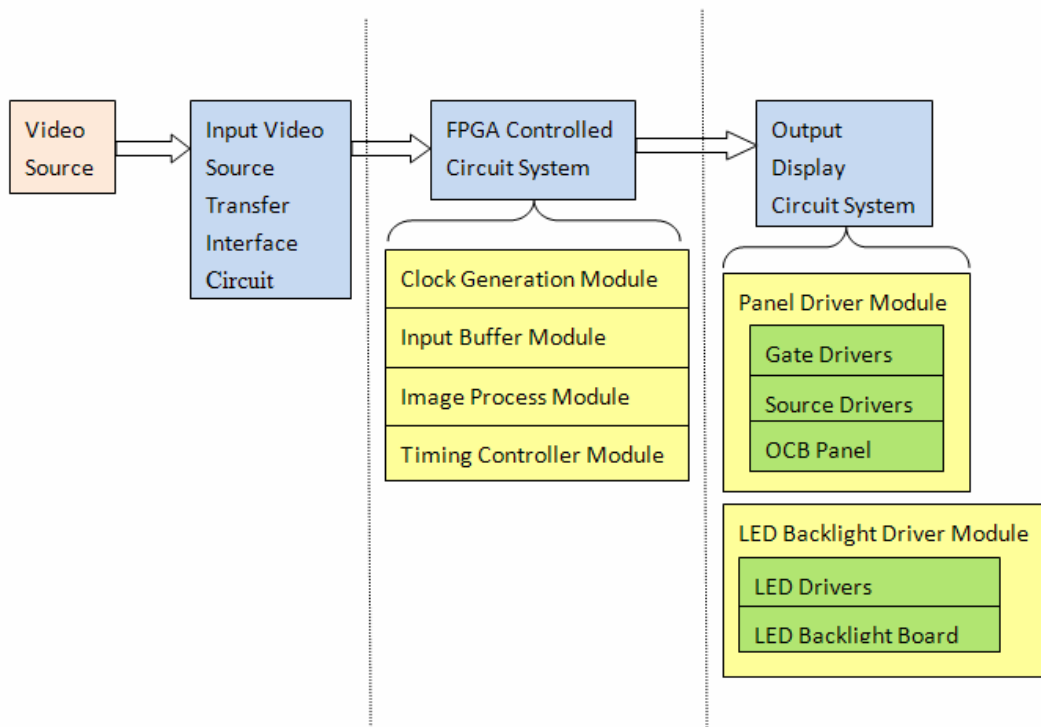


Fig. 3-18 The block diagram of system architecture.

3.4 Summary

The 4-CFA method was proposed to eliminate the CBU artifact on FSC-LCDs. The modified order of consecutive color fields results in blurred images on a retina without CBU. According to the velocity of the moving bars in test patterns, a synchronized high-speed camera was to substitute for the movement of eye tracking. The physical evaluation results of perceived image on dynamic CBU are agreed with the prediction.

In order to suppress the static CBU effectively, the RGBW method was also proposed by flashing a gray image in a white field and displaying the color residuals in remaining fields. This allows the image energy to be more focused in the initial field, thus reducing the intensities of the red, green, and blue fields thus suppressing CBU. Compared to those achieved by conventional FSC displays, perception tests have confirmed that the visibility is greatly reduced.

Further reduction in CBU visibility can be achieved by intelligently adapting the color of the individual fields, especially to incoming images with cyan, yellow, and magenta color. The exchange of RGBC/RGBY color sequence was proposed to dynamically mitigate the CBU effects in order to lighten the most sensitive green field. The redistributions of LC gray levels on the color sequence are determined by the comparison between red/green or blue/green original data. The gamma correction was also considered to maintain the white balance of image.

Chapter 4

Adaptive LC/BL Feedback Control

According to the image content, the adapted color sequence can alleviate the higher gray levels and redistribute these levels to the fourth field. With inserting a yellow or cyan field and redistributing LC signals dynamically, our results demonstrate that the proposed method is a practical way to suppress the CBU. Besides a yellow or cyan field, a dominated color-mixed field was found to minimize the color difference between the CBU and original image. Additionally, the feedback algorithm for the adaptive LC/BL signals was developed and implemented on a 32-inch optically compensated bend (OCB) mode LC panel. According to the evaluation of experiments and observations, the proposed method has been demonstrated to greatly suppress CBU in LCD applications.

4.1 The platform of FSC-LCD

The hardware of FSC-LCD consists of a display control circuit, LC panel module, and LED backlight unit. Fig. 4-1 shows the display control circuit, including an FPGA module (block 1), a LED driver module (block 2), and a power supply module (block 3). The implementation of FPGA generates the control signals to LCD drivers of LC panel module (Fig. 4-2). Meanwhile, the LED driver module operates the LED backlight unit as shown in Fig. 4-3 with the service of power supply module. The color combination of backlight can be achieved by the control of FPGA module.

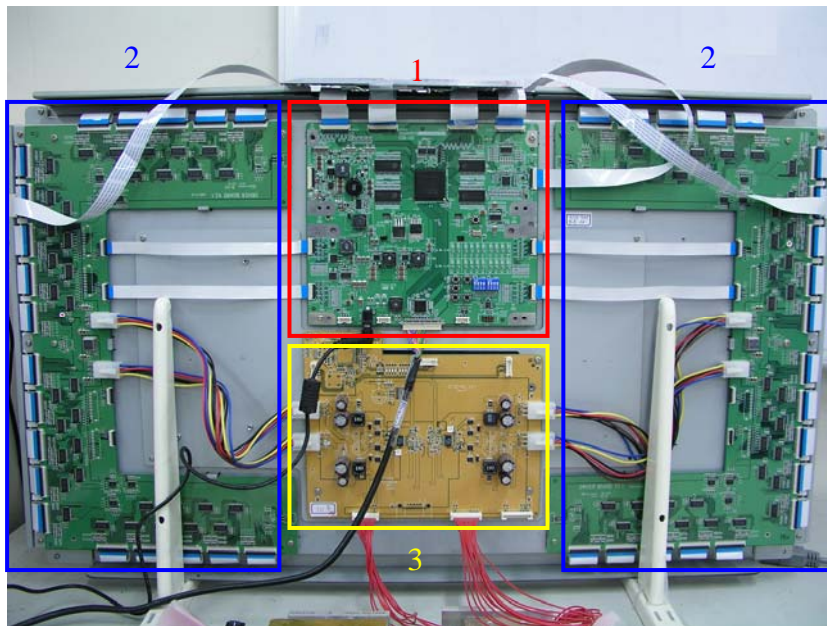


Fig. 4-1 The display circuit of FSC-LCD.

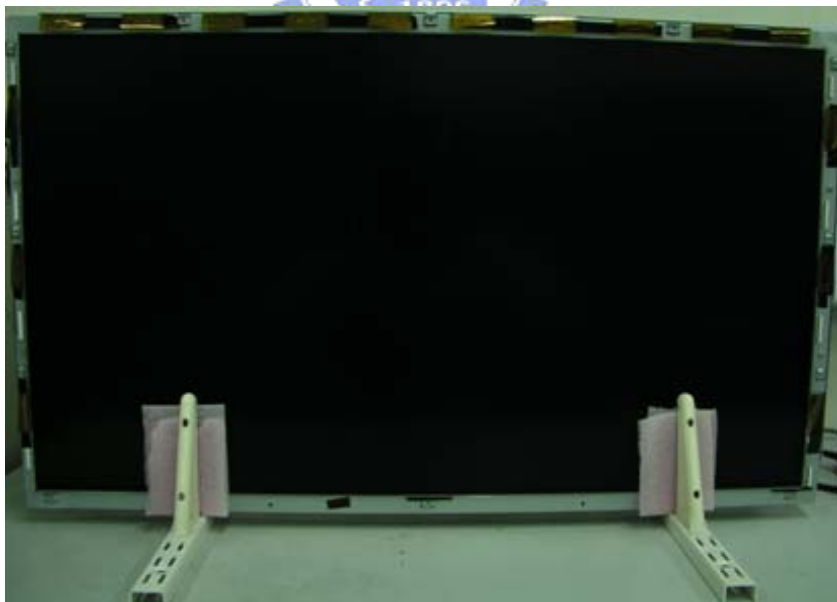


Fig. 4-2 The LC panel module of FSC-LCD.

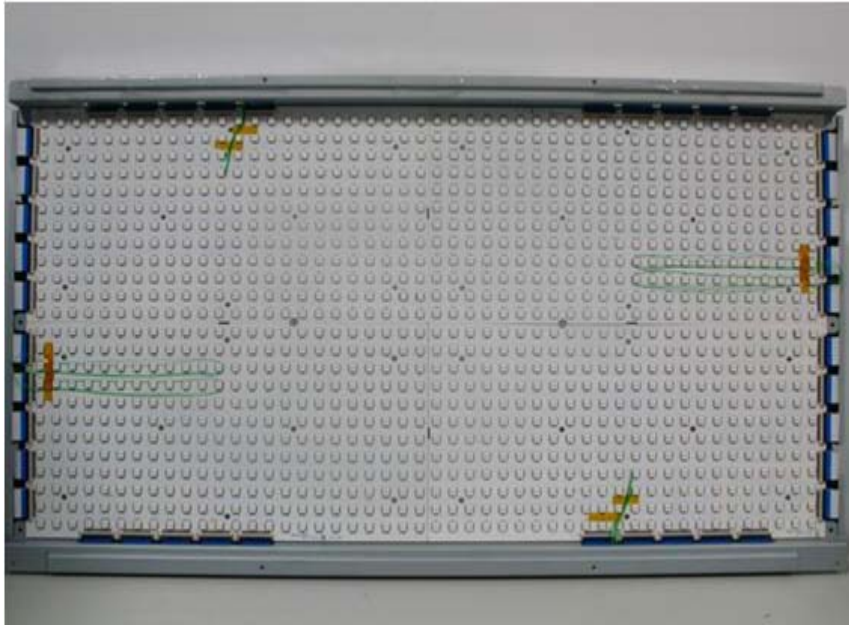


Fig. 4-3 The LED backlight of FSC-LCD.



Fig. 4-4 The demonstration of a gradual change of color board.

The demonstration was shown on a 32" OCB-LC panel of the resolution 1366x768 with the field frequency of 240Hz. The brightness of a white image can reach 400 nits at total power consumption of 50W. The specifications are shown on Tab. 4-1. The photo of this panel and the color board are shown in Fig. 4-4. Based on the measurement result of gamma function of this panel, a gradual change of color was presented smoothly.

Tab. 4-1 Specifications

Size	32" OCB
Resolution	1366x768
Brightness	400 nits at white
Power Consumption	50W
Color Gamut	105% of NTSC
Color Depth	24 bits
Field Frequency	240 Hz

4.2 RGBC/Y results

The experimental results of perceived images were agreed with the observation, as shown in Fig. 4-5. The white bar was composed of a merged yellow and a blue field that replaced three primary color fields to suppress the CBU. For the yellow or cyan bar, the CBU was eliminated because of only one observed yellow or cyan field. The specific color bars of strong red, grass green, and sky blue were also investigated. According to the experimental gamma transform function, the redistributed values of these colors' gray levels were obviously lower than those without this modification. The colors in the margins of bars (circle marks in Fig. 4-5) were discolored by the yellow or cyan field. We summed up the color difference between CBU and original image pixel by pixel as an index, ΔE_{sum} , for the evaluation of color separation.

$$\Delta E_{sum} = \sum_{total\ pixel} \sqrt{(L_{CBU} - L_0)^2 + (u'_{CBU} - u'_0)^2 + (v'_{CBU} - v'_0)^2}. \quad (\text{Eq. 4-5})$$

In Eq. 4-5, $Lu'v'_{CBU}$ and $Lu'v'_0$ are color values of CBU and original image in the $Lu'v'$ color space. The summations of color difference (ΔE_{sum}) in test images were shown in Fig. 4-6. The comparison of ΔE_{sum} between conventional and the proposed method was also presented. A lower ΔE_{sum} represents a more effective CBU

suppression [78]. In addition, the ΔE_{sum} ratio of this method to conventional one was calculated. We found the suppression ratio in specific color bars can achieve 27% to 46%. For a white bar, the value can be further improved to 56%. Consequently, the CBU effects were suppressed as the observation.

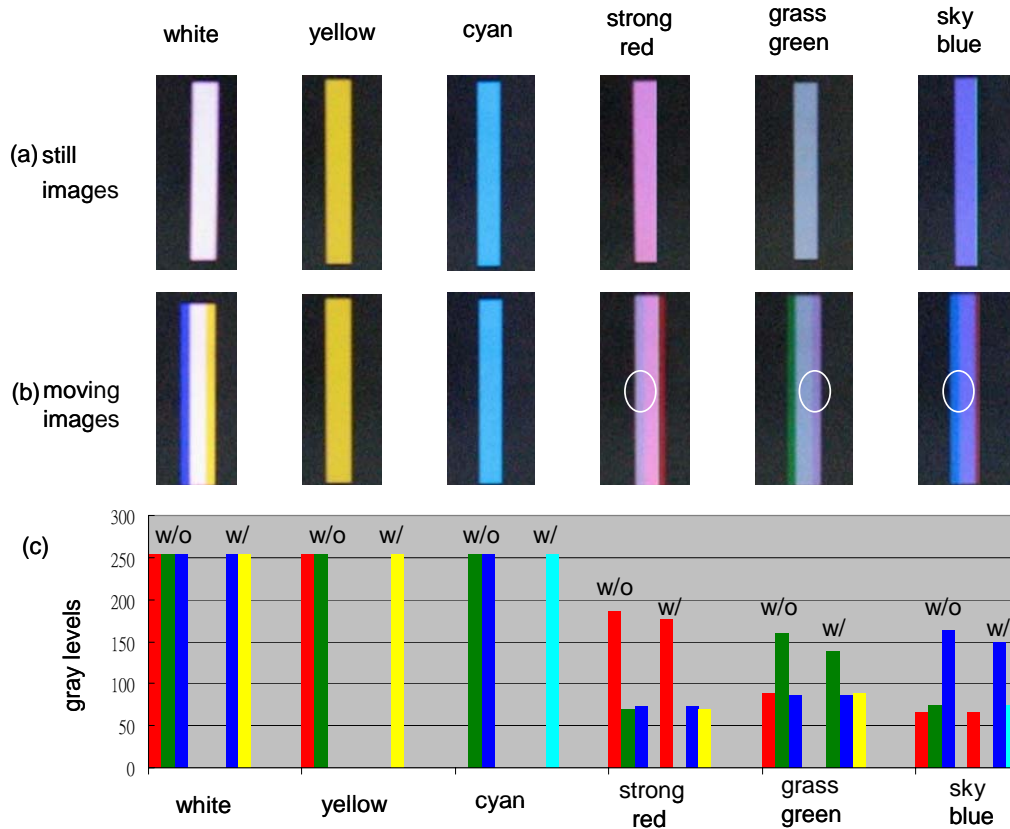


Fig. 4-5 Photos of (a) still images and (b) moving color bars taken by a tracing camera, with colors of white, yellow, cyan, and three specific colors. (c) The comparison between gray levels without and with modifications.

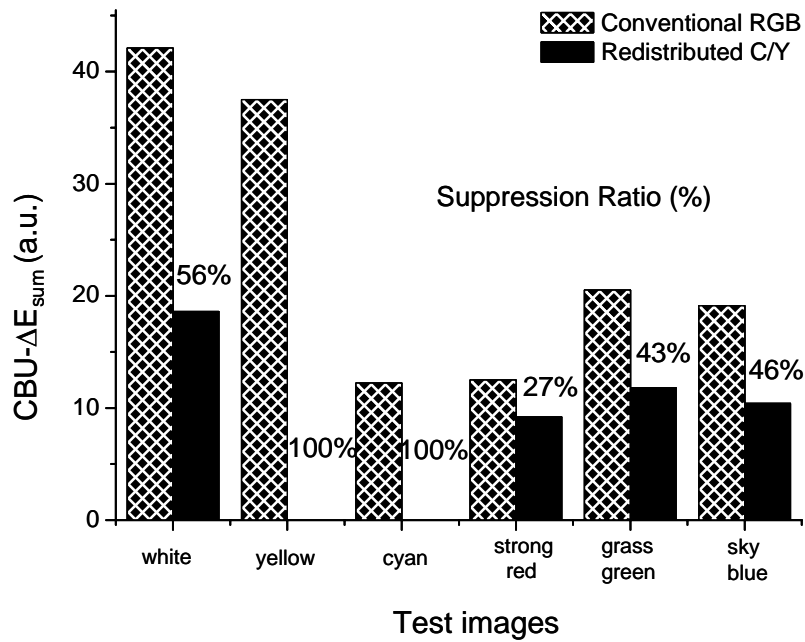


Fig. 4-6 The comparison between ΔE_{sum} with conventional and the proposed method and the suppression ratio of this method to conventional one.

4.3 Concept of adaptive backlight

We proposed to concentrate the primary color fields on the dominated color field (D-field) as shown in Fig. 4-7(b). By rearranging color fields, the intensities of primary colors are lightened and the noticeable field is condensed to a single color-mixed one. Therefore, less color separation and visibility of CBU (circle marks) as compared with that of conventional RGB 3-field one were expected. An effort was made in order to find the adaptive color of D-field according to the image content in each frame. The algorithm of feedback determination of D-field color and LC/BL signals was studied for the real time application, followed by the CBU evaluation by experiments.

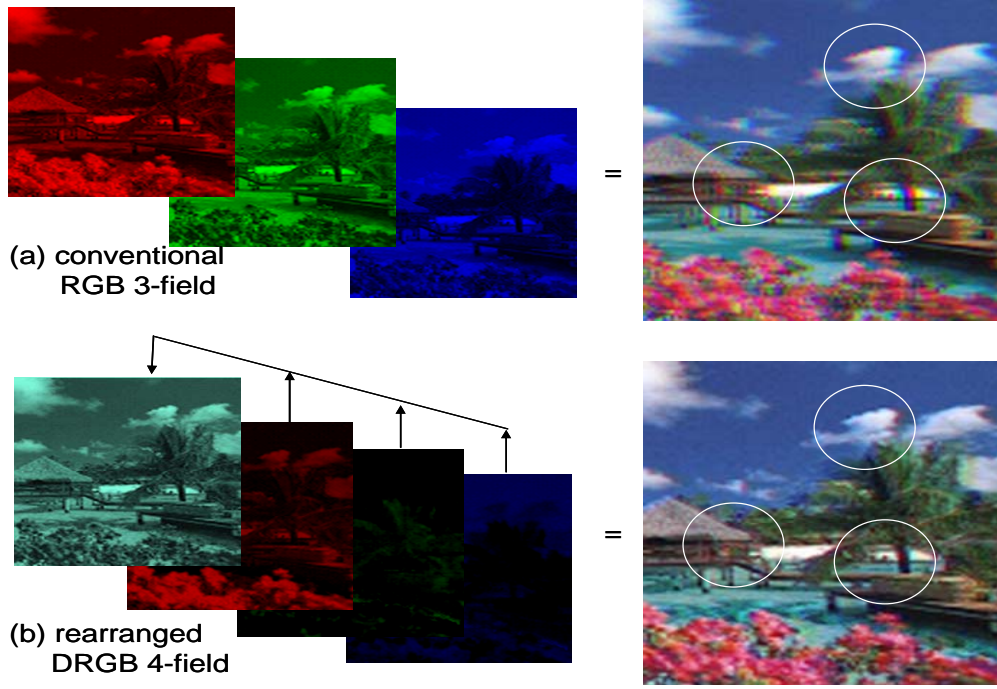


Fig. 4-7 The color field sequences and simulated CBU images on (a) conventional RGB 3-field and (b) rearranged color FSC displays.

The rearrangement of LC/BL gray levels on the DRGB color sequence are determined by the image content. In the D-field, the gray levels of three primary color backlights are set as BL_r , BL_g , and BL_b , respectively. The relation between gray levels and light intensities (gamma curve) is set as a linear proportionality. According to these backlights, the new LC gray levels r' , g' , b' and d in the red, green, blue, and D-field are represented as

$$r' = T^{-1}(T(r) - T(d) \times BL_r), \quad (\text{Eq. 4-1})$$

$$g' = T^{-1}(T(g) - T(d) \times BL_g), \quad (\text{Eq. 4-2})$$

$$b' = T^{-1}(T(b) - T(d) \times BL_b), \quad (\text{Eq. 4-3})$$

$$d = T^{-1}(\min(\frac{T(r)}{BL_r}, \frac{T(g)}{BL_g}, \frac{T(b)}{BL_b}, 1)), \quad (\text{Eq. 4-4})$$

where $T(i)$ is the transfer function from gray level i to transmittance of LC and T^{-1} is the inverse function. This gamma curve between gray levels and less than one of transmittances should be considered to maintain the white balance.

The determination of color backlights of D-field was found to be critical for color breakup reduction. Fig. 4-8 shows the simulated CBU images of test image, Lena, in three backlight gray level conditions of D-field. The simulated CBU images can be obtained by the superimposition of the shifted 4 color images as shown on top of Fig. 4-8. We utilized the computing software, MATLAB, to process these image data arrays. Fig. 4-8(a) shows the CBU image with zero RGB values of D-field (KRGB); in other words, this image represents the perceived one with a conventional RGB 3-field driving. On the contrary, the exchange RGBC/Y method was applied on the D-field in Fig. 4-8(b), thus showing the cyan or yellow color in the D-field. The color backlight determines the distribution of image brightness in color fields. When major intensity of brightness is condensed in the D-field, the primary color fields are discolored. Consequently, less color separation will be perceived. The ΔE_{sum} of DRGB was found to be lower than those of other ones as well as the least CBU in these three images. Therefore, the visibility of CBU can be reasonably minimized when the color backlight for D-field was optimized. Furthermore, the CBU effect could be determined by the index of ΔE_{sum} .

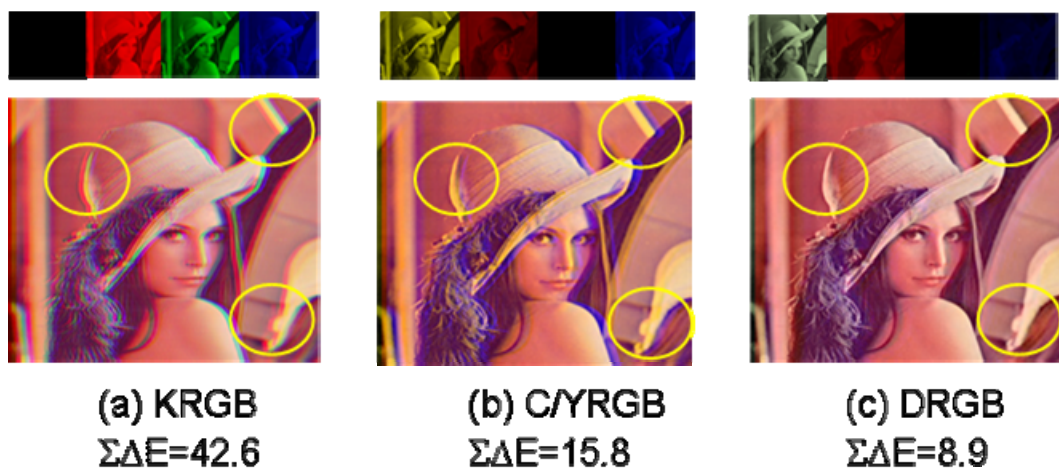


Fig. 4-8 The simulated CBU images of Lena in three conditions of (a) none, (b) c/y, and (c) proposed D-field

4.4 Feedback control for optimized BL determination method

The simplification of color backlight optimization on D-field is necessary in a real time application for the ΔE_{sum} calculation. The more bit number of backlight can obtain the minimum ΔE_{sum} with higher accuracy. However, the computation loading will increase exponentially with the increase of backlight accuracy. Fig. 4-9 shows the ΔE_{sum} of five test images are corresponding to the bit number of backlight. In comparison with 1-bit accuracy, these ΔE_{sum} were saturate while the bit number was higher than 3. Therefore, the 3-bit accuracy is set as the modified factor of RGB backlight. Moreover, the resolution of image also determines the complexity of computing. We used several sampling periods, ranging from 1x2 to 4x8 pixels, to lower the resolution of image.

For example, four sub-images with the 1/4 resolution can be obtained by the 2x2 sampling. If these four sub-images can replace the original one for the ΔE_{sum} calculation, four different backlight conditions can be examined simultaneously and shorten the step of approach for the minimum ΔE_{sum} . When the RGB backlight condition of sub-image and original image with the minimum ΔE_{sum} are unequal, this sub-image is considered as an error. Fig. 4-10 shows the relation between the error rate and sampling periods of image. The error rate is defined as the ratio of the number of error to all sub-images. The sampling periods below 2x4 pixels were found without errors in these five test images. Therefore, the 2x4 sampling period was chosen to provide 8 sets of RGB backlight simultaneously for determination of the minimum ΔE_{sum} .

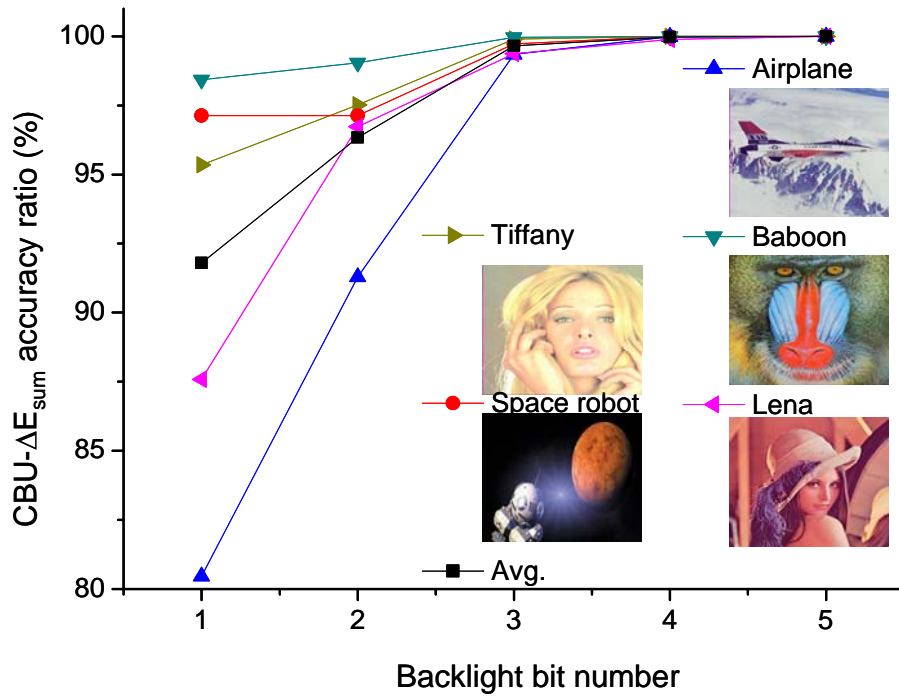


Fig. 4-9 The relation between color difference and backlight bit number.

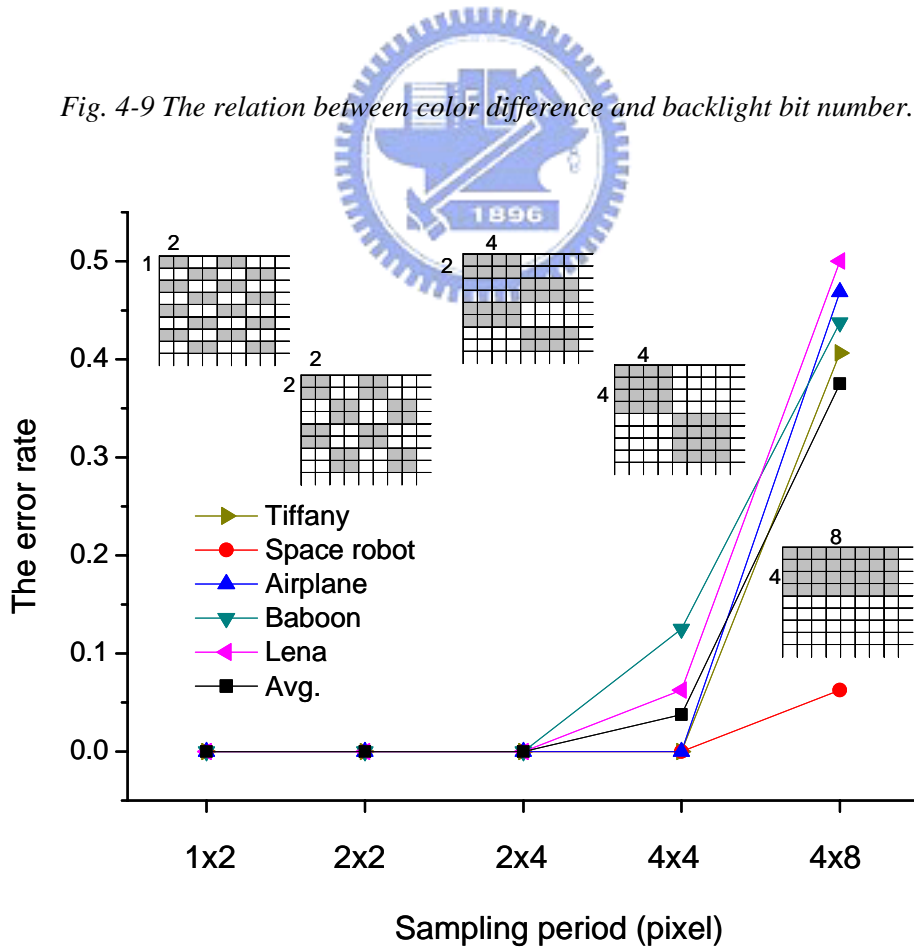


Fig. 4-10 The relation between the error rate of color difference and sampling period.

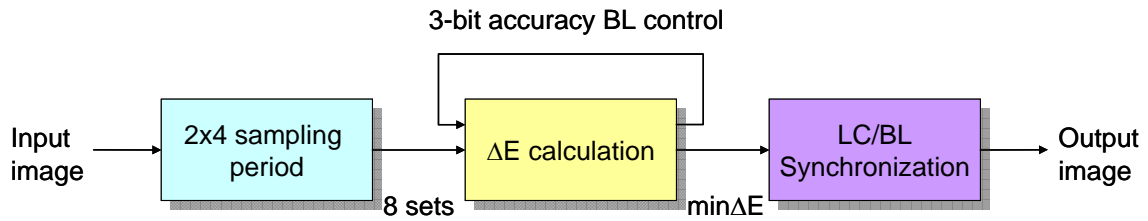


Fig. 4-11 The concept of optimized BL determination and image processing in a real time application.

The 2x4 sampling period and the 3-bit accuracy of BL determination were combined for the ΔE_{sum} calculation. The optimized BL in D-field can be obtained by the feedback control of ΔE_{sum} minimization. Fig. 4-11 presented this concept with the LC/BL synchronization. The gray levels of output image in these DRGB fields were generated according to the optimized BL.

Fig. 4-12(a) shows the detail flowchart to determinate the gray levels of LC and color backlight. First, the image of the n th frame was transferred to the Lu'v' color space as shown in Step (A1). We used 8 sets of 1-bit color backlight and sub-images sampled by 2x4 period to obtain CBU images. In comparison with the original image, 8 CBU- ΔE_{sum} were computed simultaneously in Step (A2). After sorting these ΔE_{sum} and determination of bit number for the next frame in Step (A3), 7 new 2-bit sets of color backlight near 1-bit sets with the minimum two ΔE_{sum} were considered as well as the set with the minimum ΔE_{sum} in Step (A4). The total 8 sets of color backlight will be used in Step (A2) by passing through the BL buffer, a signal register for the synchronization between LC and backlight.

In an example of Fig. 4-12(b), the solid circles at 1 and 2-bit sets represent the sets with the minimum two ΔE_{sum} (BL1 and BL2) as well as hallow circles for other sets with larger ΔE_{sum} . If any ΔE_{sum} of 2-bit sets is equal or less than those of 1-bit ones, a 3-bit approach as shown at 3-bit set will be applied in Step (A3). On the contrary, if all ΔE_{sum} of 2-bit sets are larger than those of 1-bit ones, 8 sets of 1-bit

color backlight will be computed for the $\text{CBU}-\Delta E_{\text{sum}}$ in the following frame. The bit number accuracy of color backlight is controlled by this feedback for the optimized BL determination. On the other part of flowchart, the LC signal of input image and the color backlight with the minimum $\text{CBU}-\Delta E_{\text{sum}}$ passed through the frame and BL buffer as shown in Steps (B1) and (B2). The synchronal LC and BL signals in Step (B3) were applied to generate new gray levels of LC with the lookup table (LUT) as set in Eq. 4-1 to 4-4.

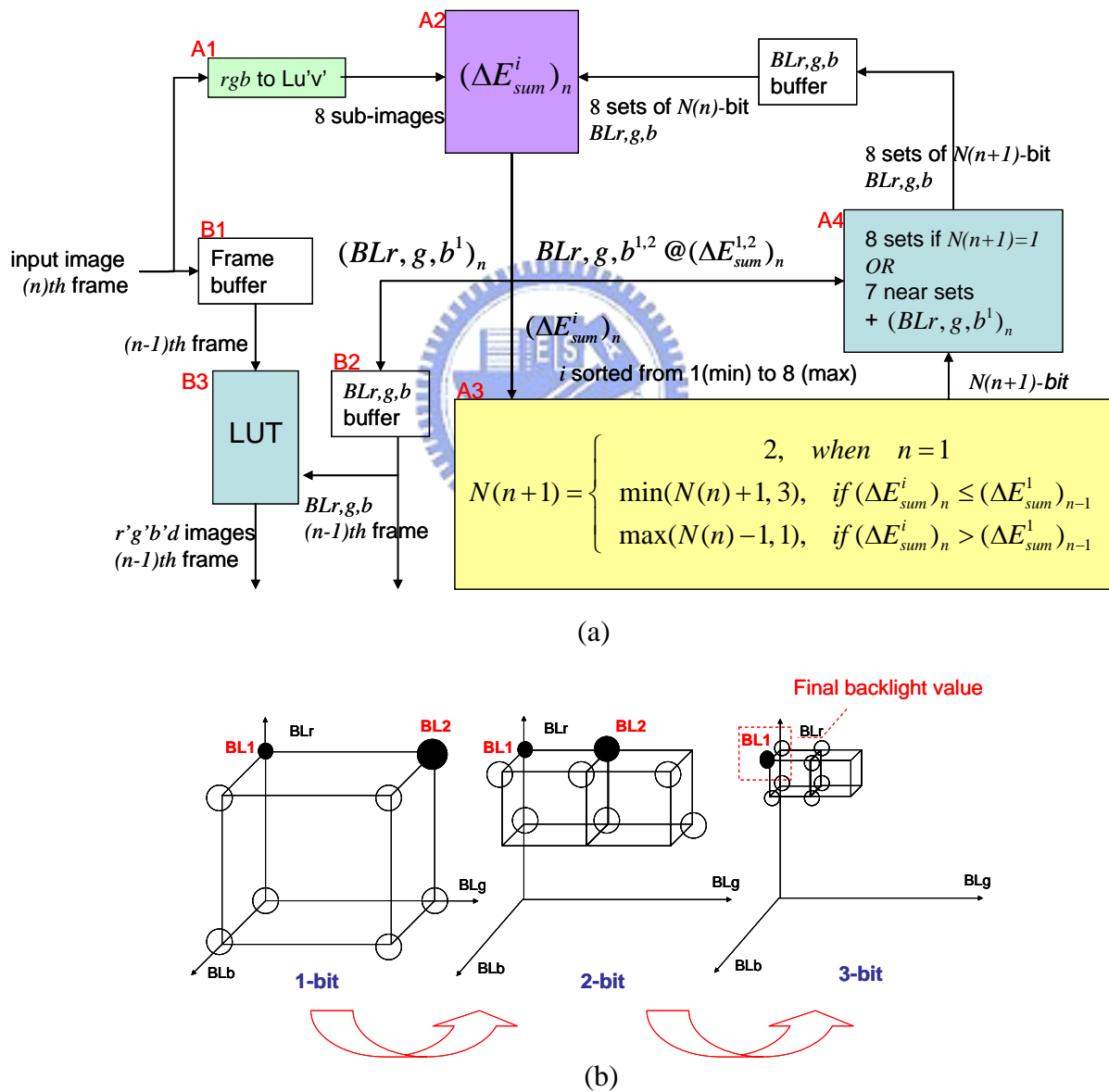


Fig. 4-12 (a) The flowchart and (b) an example of gray level determination of color backlight are according to the image content and color differences.

4.5 Results

Five images in Fig. 4-9 were scrolled with a speed of one image per second as a test video to verify this CBU reduction method. Fig. 4-13 shows the ΔE_{sum} variation with time in a frame sequence. During the first three frames of each image, the ΔE_{sum} is confirmed to be decreased and stable by the feedback control of ΔE_{sum} minimization. Thus, the feedback control technique can effectively determine optimized BL values. In addition, the ΔE_{sum} of proposed DRGB method is the lowest in comparison with those of conventional RGB and C/YRGB ones. This average CBU suppression ratio is around 70% of conventional one as shown in Fig. 4-14. According to the evaluation of observations, the CBU artifact as expected is not noticeable.

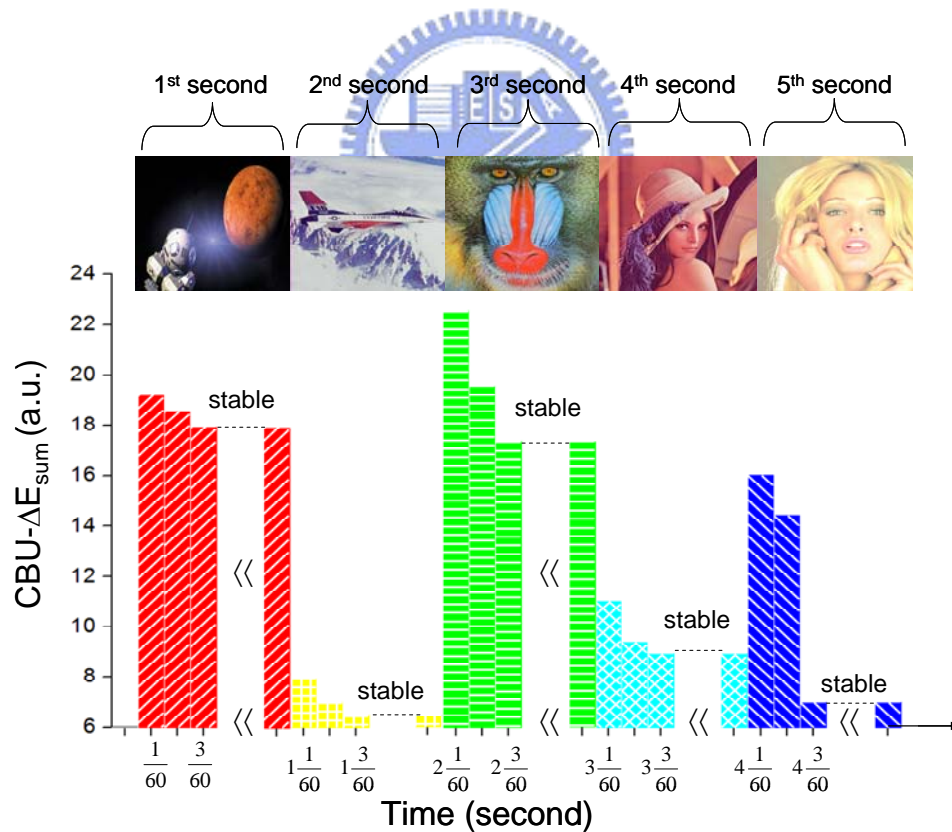


Fig. 4-13 The variation of color difference ΔE_{sum} with a scrolled speed of one image per second for these test images.

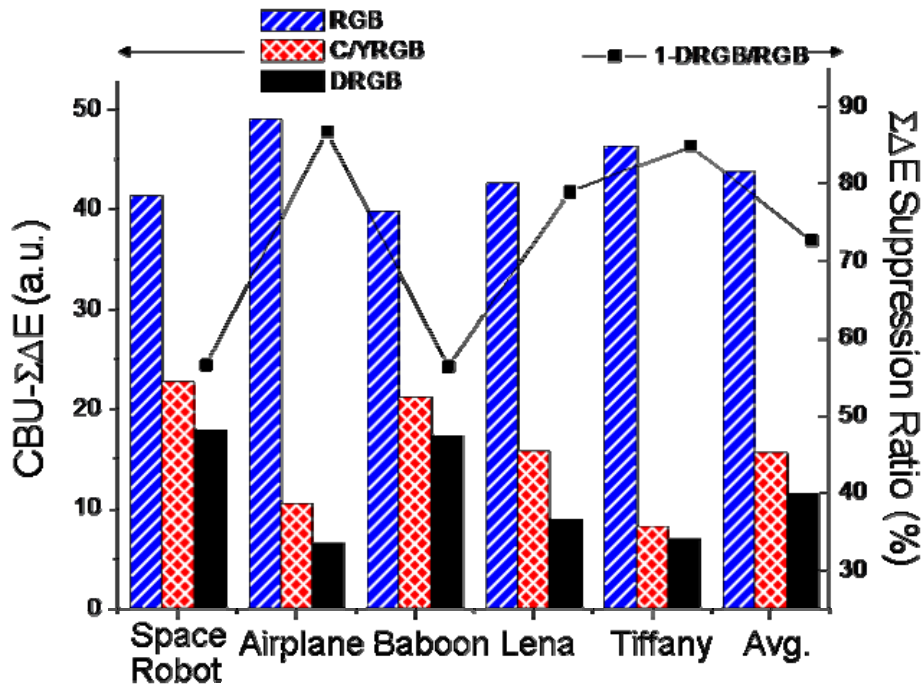


Fig. 4-14 The ΔE_{sum} comparison of test images with conventional, c/y, and dominated RGB methods and the ratio of ΔE_{sum} of DRGB to conventional one.

Fig. 4-15 shows the typical CBU and modified images by D-field with the minimum ΔE_{sum} . In the circle marks, it is obvious that the CBU artifact was greatly reduced in comparison with that of conventional RGB 3-field sequence. The color separation was greatly improved at the edges of Tiffany's face and robot's body. Similarly, the bright and dark sides of mountains in Airplane presented unnoticeable color breakup. The wing of nose in Baboon and the brim of hat in Lena also showed the reduced CBU significantly. The experiment results of perceived images were agreed with the observation. With the current platform of BL determination on D-field, the optimized value of each frame is obtained after two frame time. In order to determine this value during the same frame time, the parallel architecture of feedback loop can be designed to speed up the processing steps. A real-time CBU reduction becomes realizable for fast moving images.

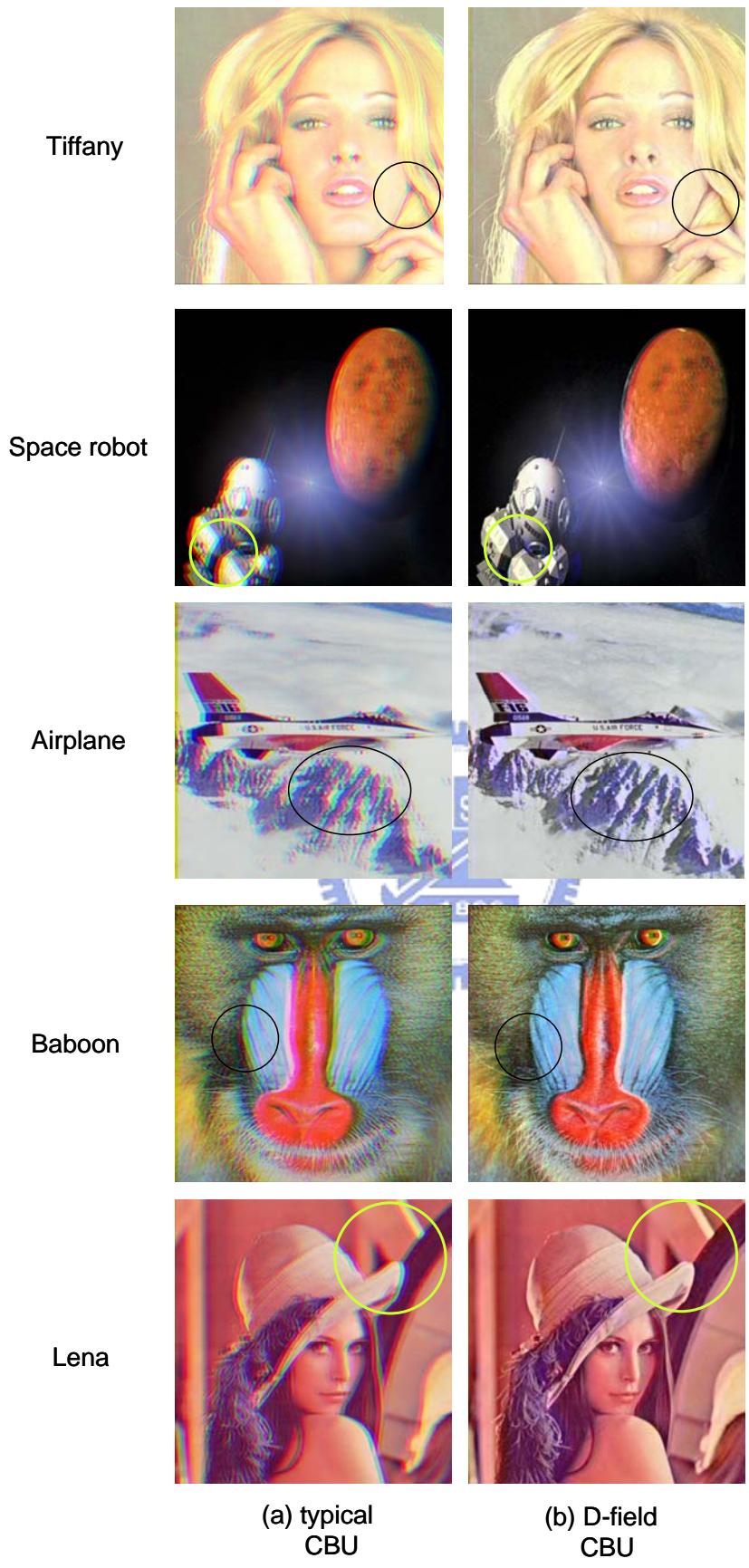


Fig. 4-15 The CBU images with (a) conventional RGB and (b) adaptive DRGB fields.

4.6 Summary

An adaptive feedback control for gray level rearrangement of LC/BL signals to reduce CBU artifact was demonstrated on a 32" FSC-LCD. The color backlight of the D-field with the minimum color difference between CBU images and original ones was proposed to suppress the CBU artifact effectively. According to the image content, the adapted color backlight can concentrate the light intensity on the dominated field and minimize the CBU effect. The 2x4 sampling period of image and 3-bit gray levels of color backlight were applied for the simplification of hardware implementation. The field frequency of 240 Hz, the brightness of 400 nits, and the total power consumption of 50W were achieved. Most importantly, the 4 fields per frame have been fulfilled compared to the other techniques for reducing CBU effect. With rearranging LC/BL signals dynamically and the proposed feedback algorithm of optimized color backlight, our results successfully demonstrate that the proposed method is a practical way to suppress the CBU in field sequence color LCD applications.

Chapter 5

Local Adaptation and Boundary Issue

So far, the color of D-field is modulated on the whole backlight, or called the global adaptation. To contain more intensity of brightness in D-field and further reduce the CBU artifact, local adaptation can be applied along horizontal and vertical segments (2D-dimming) for locally optimizing CBU on corresponding areas of image [55]. The proper light distribution in a segment is required to achieve whole backlight profile as uniform as possible when each segment switched on the same level [87][88]. On the other hand, the boundaries should not be visible while 2D dimming. In this thesis, we investigated the effects of optical profiles on the perceived image quality. The threshold of boundary-free image was found according to human contrast sensitivity function. Simultaneously, the proper light profile in each segment was derived for the design of large-sized FSC-LCDs (the third part of thesis architecture in Fig. 5-1).

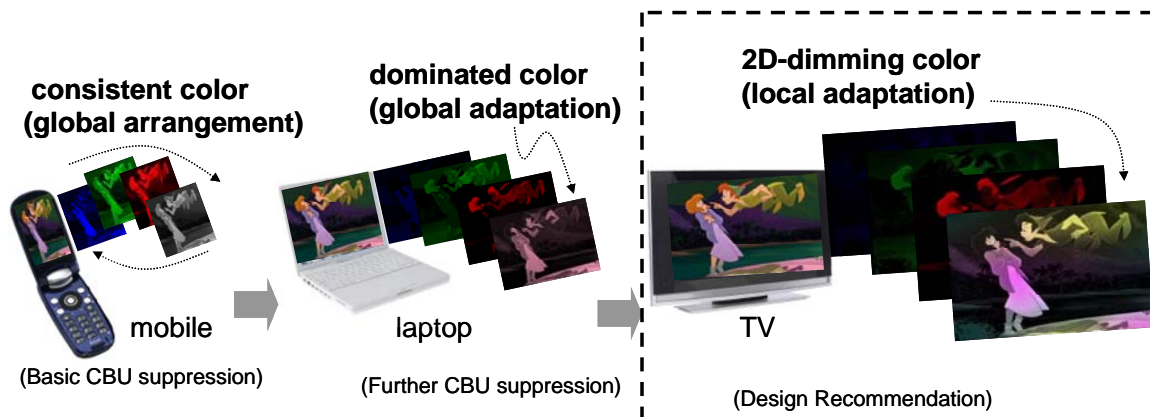


Fig. 5-1 The thesis architecture.

5.1 Contrast sensitivity function considered

The human contrast sensitivity function is analyzed in order to determine a condition for boundary-free perception in 2D-dimming backlight. From the perceptive experiment, the contrast sensitivity function determines the threshold amplitude value of sinusoidal variation to indistinguishable perception [89][90]. At one particular frequency (cycles/degree), human eyes have different ability to perceive the light intensity variation. The sensitivity is the inversion of the contrast in Fig. 5-2[89]. For an example, at 1 cycle/degree, human can not sense less than 1/100 variation. The most sensitive frequency is 5 cycles/degree, equivalent to 20 pixels on TV application according to the viewing distance and pixel size in Tab. 5-1[90]. One segment with realistic cost level on 2D-dimming backlight covers more than 20 x 20 pixels on LC panel. Therefore, we will focus on lower frequency, as shown in left part of Fig. 5-2(a), to find the relation between contrast sensitivity and threshold of boundary-free profile.

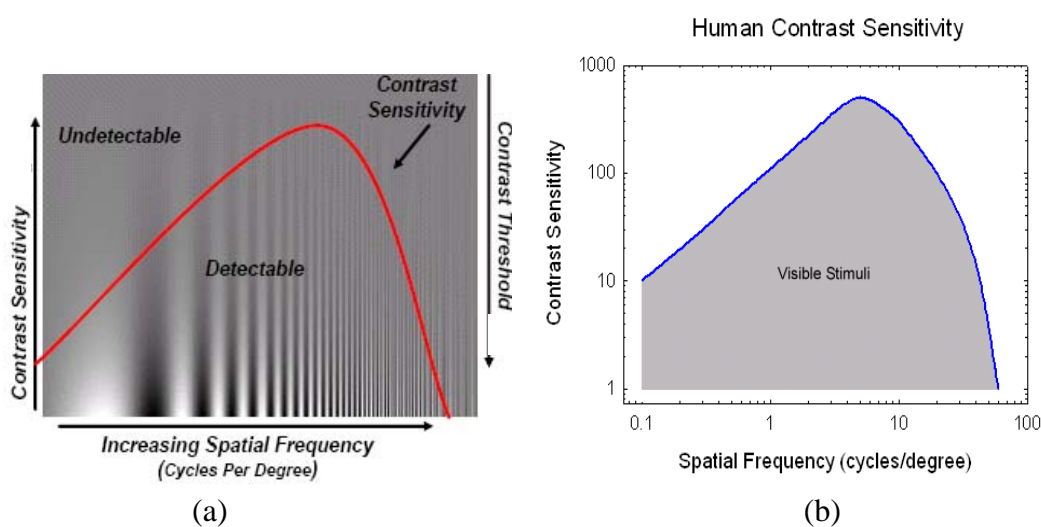


Fig. 5-2 (a) Contrast sensitivity function and (b) with experimental values

Tab. 5-1 The relation between pixel number and frequency in LCD TV and laptop

	TV	Laptop
Viewing distance (m)	3	0.5
Distance between two points on screen with 0.2 degrees (5 cycle/degree) (mm)	10.5	1.74
Pixel size (mm)	0.5	0.24
Period pixel number with 5 cycle/degree	20	8

The gradient of backlight image was analyzed to evaluate the boundary perception. We start by considering the boundary of just not noticeable that is drawn in Fig. 5-2(a).

$$P(x) = \frac{a(f)}{2} \times (\sin(2\pi fx) + 1), \quad (\text{Eq. 5-1})$$

where $P(x)$ is the sinusoidal variation of luminance at this boundary in Fig. 5-2(a), $a(f)$ is the maximum amplitude at the boundary of just not noticeable, f is frequency (cycle/degree), the distance x (unit: degree) away from origin, and an off-set value of 1 for $P(x)$ as a positive number. For an example, when f is 1 cycle/degree, $a(f)$ is 1/100 of background luminance (L_B) according to contrast sensitive function shown in Fig. 5-2(b). When the background luminance is higher than 10fL (=34.3 nits), the contrast is independent of the background luminance [91]. Then, the first derivative of $P(x)$ is,

$$P'(x) = \frac{a(f)}{2} \times 2\pi f \times \cos(2\pi fx) = K \times \cos(2\pi fx) \quad (\text{Eq. 5-2})$$

When the frequency is lower than 5 cycles/degree, the contrast sensitivity increases and the contrast decreases with the spatial frequency. The decrease in the contrast implies the decrease in the amplitude $a(f)$ of luminance variation of just not noticeable. According to Fig. 5-2(b), $a(f)$ is inversely proportional to the spatial

frequency. Therefore, the frequency factors of $a(f)$ and $2\pi f$ are cancelled out in $P'(x)$. In other words, the amplitude for the boundary of just not noticeable in Eq. 5-2 will be independent of frequency with constant K of $\pi L_B/100$ (unit: nits/degree), the maximum slope of undistinguished profile.

5.2 Verification using Lorentz distribution

The effect of backlight profiles on perceived image quality was investigated by MatlabTM to simulate 2D-dimming backlight image. A 256 x 256 resolution of an original image was divided into 8 x 8 segments as an example. The quadratic Lorentz distribution $L(r)$ in each segment was chosen for the best match with the measured profile of each segment⁵⁶. This distribution $L(r)$ can be expressed as:

$$L(r) = \frac{1}{(1 + (\frac{\Delta r}{\sigma})^2)^2}, \quad (\text{Eq. 5-3})$$

where Δr is the distance of a pixel to origin, the center of each segment, and σ determines the width of profile. The distribution decays with the distance away from the center of each segment. Moreover, the parameter of σ is used to modify the distribution $L(r)$ as the light profile of each segment. A larger σ induces a wider segment profile, resulting in more overlaps between segments. In full-on condition, the peak values in each segment were set to equal and whole backlight image was obtained by the superimposition of segment profiles. Because the Lorentz distribution has a long tail, there are overlaps with neighboring segments. The result, shown in Fig. 5-3(a), is close to a uniform profile while σ is equal to a factor of 1.2 wider than the width of segment. In 2D-dimming condition, each peak value was determined by the maximum LC signal of 32 x 32-pixel in each segment. A picture of camera man and its backlight image are shown in Figs. 5-3(b) and (c). Boundaries in the backlight

image are close to indistinguishable. Fig. 5-3(d) shows the gradient of normalized backlight image in Fig. 5-3(c). We find the gradient values on the boundary between segments are lower than $\pi/100$.

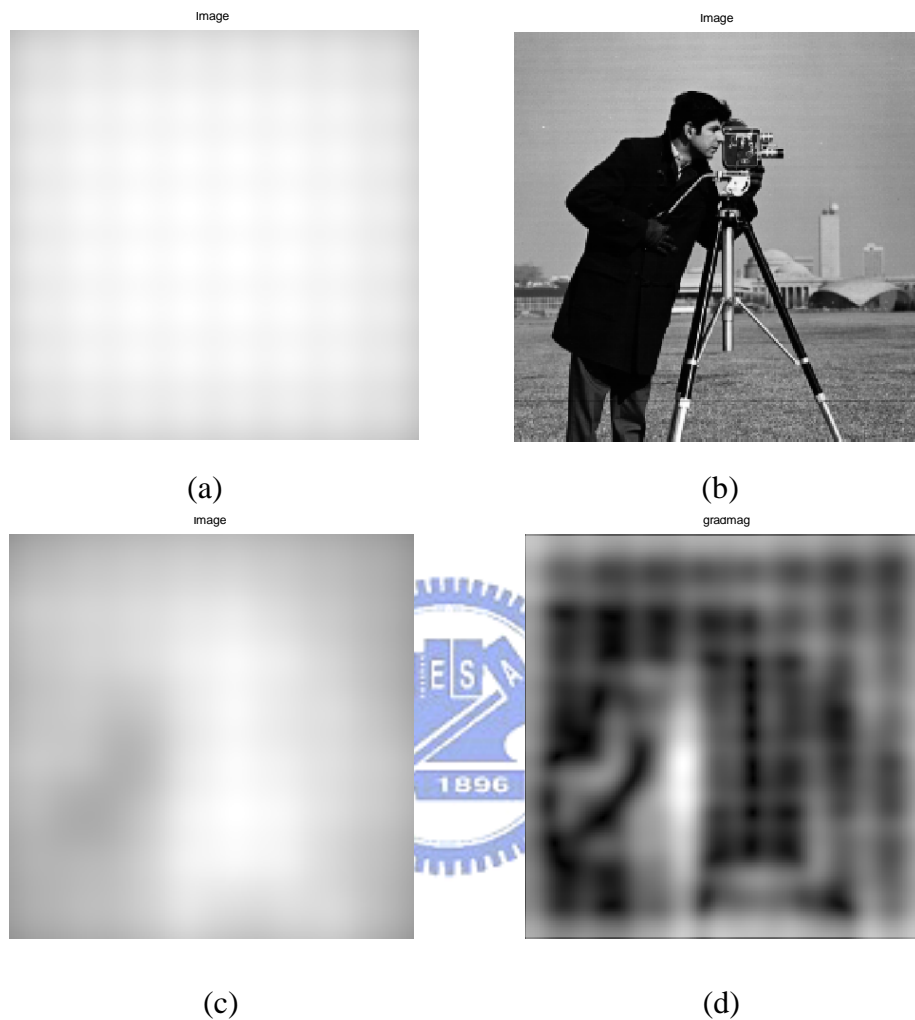
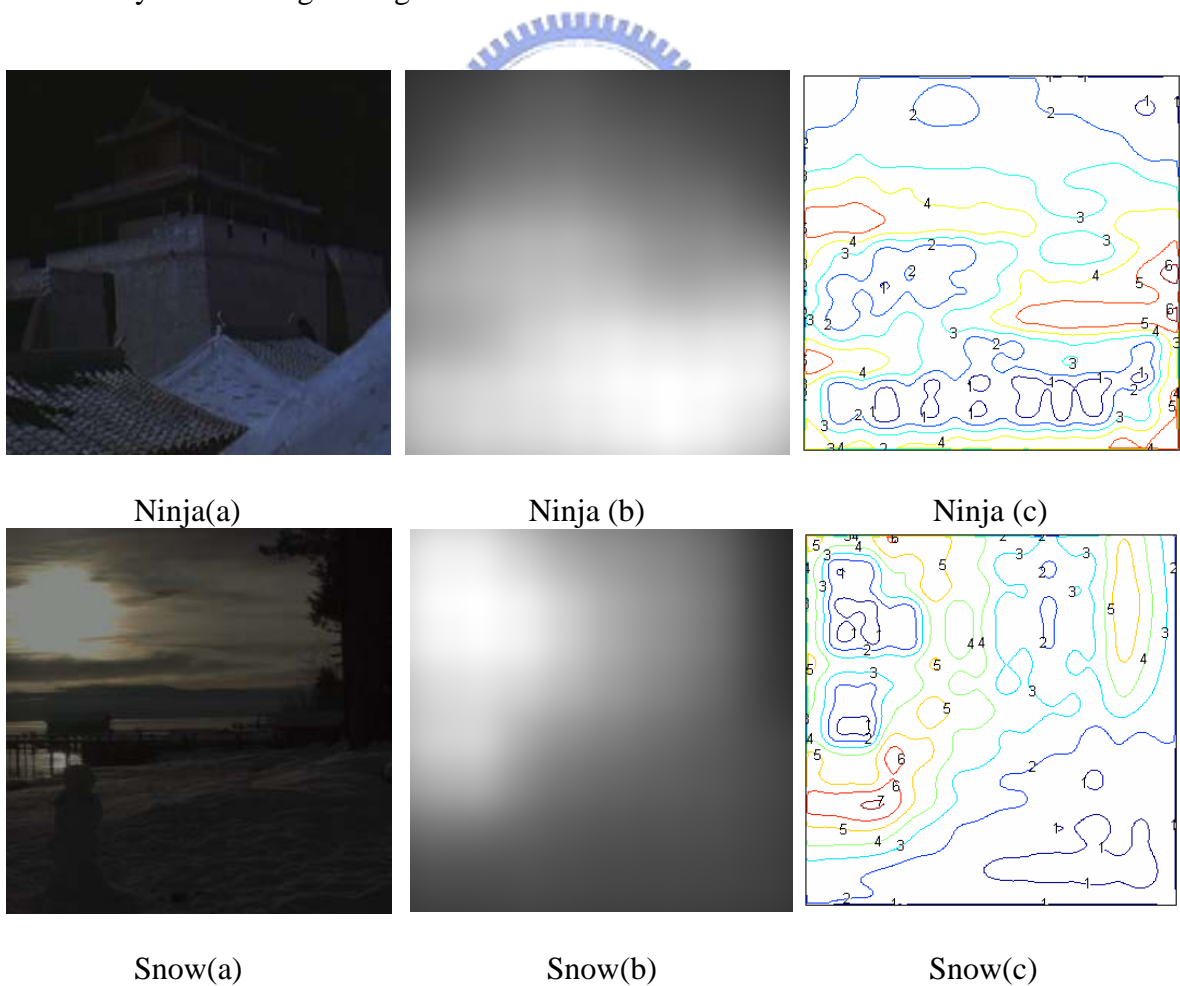
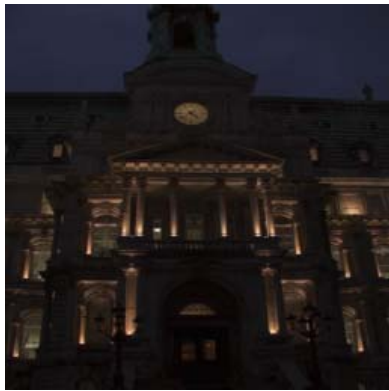


Fig. 5-3 (a) Full-on backlight, (b) original of camera man, (c) 2D-dimming backlight, and (d) the gradient of 2D-dimming backlight.

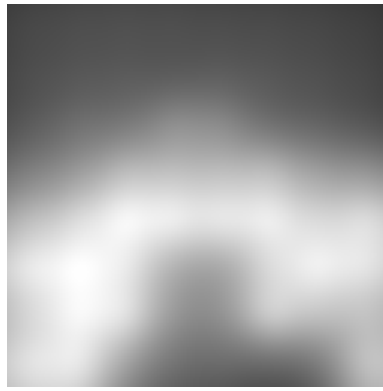
Five images, Ninja, Snow, Clockbuilding, Game, and City with different spatial scales were further investigated. Fig. 5-4 shows these original images, the results of 2D-dimming backlight images and their gradient images. The contour values of gradient are presented with 100x amplification. In images of Ninja and Snow, the spatial scale is coarse, resulting in blurring backlight images. Not only on the boundary between the segments but also on the edge of objects in these two images,

the gradient values, for the most part, are lower than 4/100 (4 on contour). However, in Clockbuilding and Game, the images with intermediate spatial scale, the edges of objects in these two images are more obvious. Even though the higher gradient values are presented, the boundary between segments is still undistinguished. We also tested the effect of backlight profile for the fine detail image. To show the detail, the segments corresponding to the buildings in City were switched on. With the superposition of profiles, the gradient values are lower in the bottom part of image. High gradient values appear on the edge between the dark sky and building in City, resulting from the switch-off segments of dark sky. Therefore, this worst case between brightest and darkest segments needs to be further investigated for boundary-free backlight image.

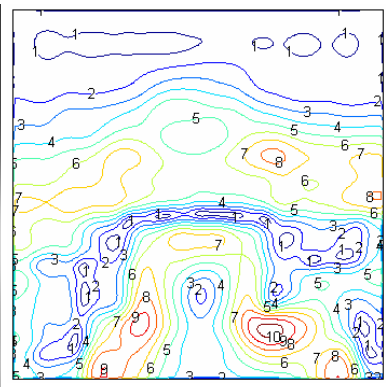




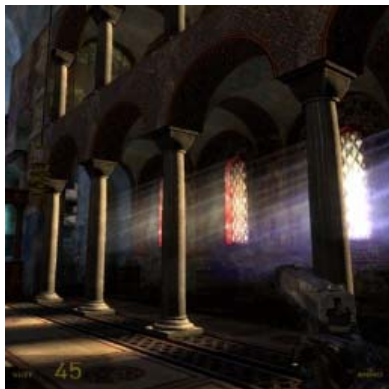
Clockbuilding(a)



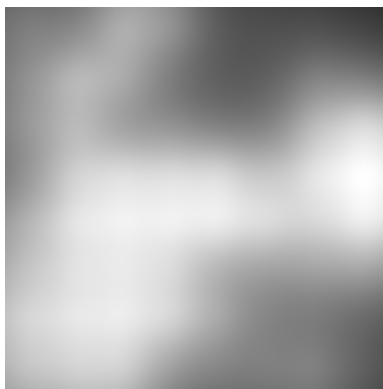
Clockbuilding(b)



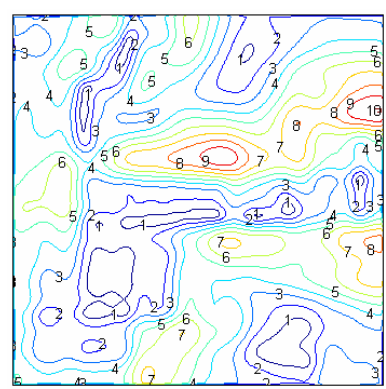
Clockbuilding(c)



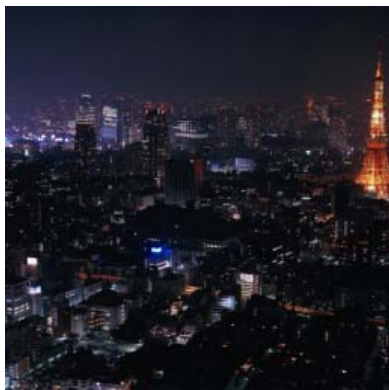
Game(a)



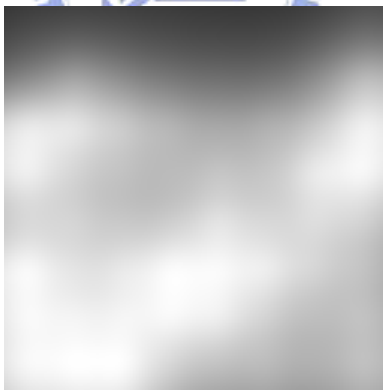
Game(b)



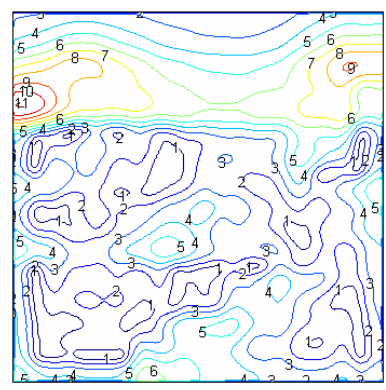
Game(c)



City(a)



City(b)



City(c)

Fig. 5-4 The selected images over different spatial scale. (a) Original image, (b) 2D-dimming backlight, and (c) the contour of gradient image (100x)

5.3 Modified profile for 2D-dimming backlight

The proper light distribution in a segment is required to achieve whole backlight profile as uniform as possible when each segment switched on the same level. On the other hand, the boundaries should not be visible while 2D dimming. Moreover, the distributions should be substantially local for maximizing contrast. Therefore, we used the contrast ratio, the maximum to minimum value of backlight images, to examine the enhancement factor. Fig. 5-5 shows the results as the segment size of 0.25 to 4 degrees. The wider size of segment lowers the contrast ratio of these five images. The average factor of these images is close to 5 at the size of 1 degree.

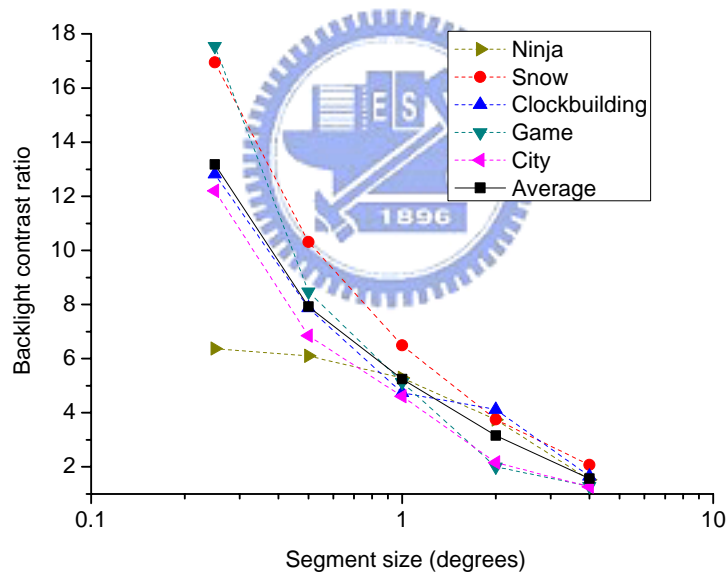


Fig. 5-5 The backlight contrast ratio per images as a function of segment size.

The solid line corresponds to the contrast ratio averaged over all the images.

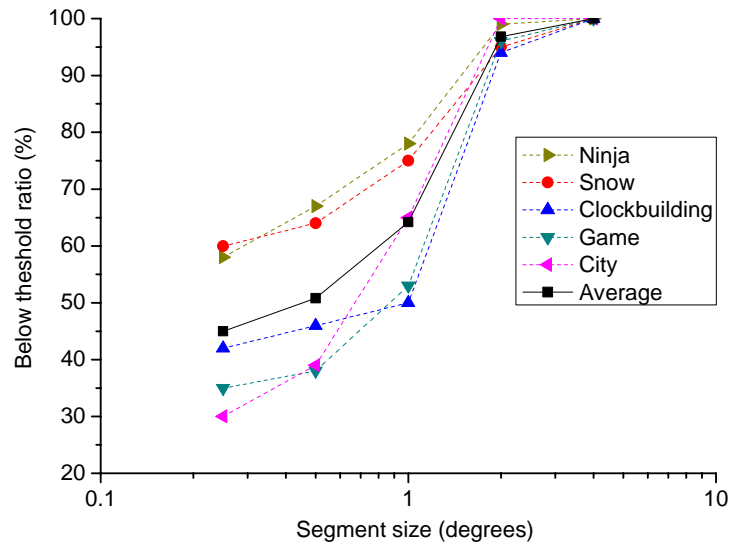


Fig. 5-6 The percentage of pixel numbers below the threshold per gradient images as a function of segment size. The solid line corresponds to the average over all the images.

Further considering the boundary perception, the percentage of pixel numbers below the threshold in a gradient image is used to evaluate the visibility of boundaries. The average value over 60% is obtained while the size of segment is wider than 1 degree as shown in Fig. 5-6. A simple recommendation is to utilize the size of 2 degrees for the balance between contrast enhancement and boundary perception. At this size, the gradient is close to 100% below the boundary-free criterion and the average contrast ratio is slightly lowered from 5 to 3.5.

To maximize the contrast ratio and minimize the boundary artifact, a spatial filter can be utilized in 2D-dimming backlight. The blurred image is simulated by convolving this filter with the backlight image. An average filter, as a low pass filter in frequency domain, is a candidate to blur the backlight image. The criterion of the size of segment to maximize the contrast ratio can be modified by the size of filter. In

a real system, to modify the size of spatial filter implies to adjust the scattering abilities of diffusers in a backlight module. Fig. 5-7 shows the percentage below the threshold and the contrast ratio with filter sizes of 0.25, 0.5, and 1 degree. Using spatial filters at the size of segment of smaller than 0.5 degree, the below threshold ratio is improved from 40% to 50% and the boundary artifact is alleviated. If this artifact is further suppressed, the maximum contrast of about 20 is achieved at the size of segment about 0.125 degree.

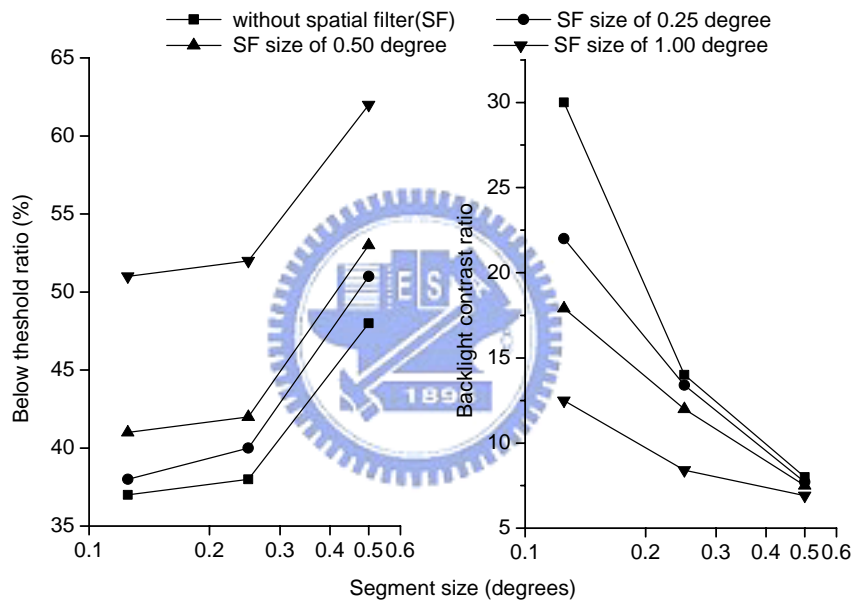


Fig. 5-7 The backlight contrast ratio and the percentage of pixel numbers below the threshold of gradient images as a function of segment and spatial filter size. The lines correspond to the average over 5 images.

Fig. 5-8 shows the relation between the segment size and number of screens, determined by viewing distances corresponding to factors of screen diagonal. At a viewing distance of a factor of 3 longer than screen diagonal, the segment size of 2 degrees results in about 10x10 as the recommended segment number. For a closer viewing distance, more segment numbers are needed. This function between viewing distances and segment numbers is useful to the screen sizes from monitor to TV-sized application.

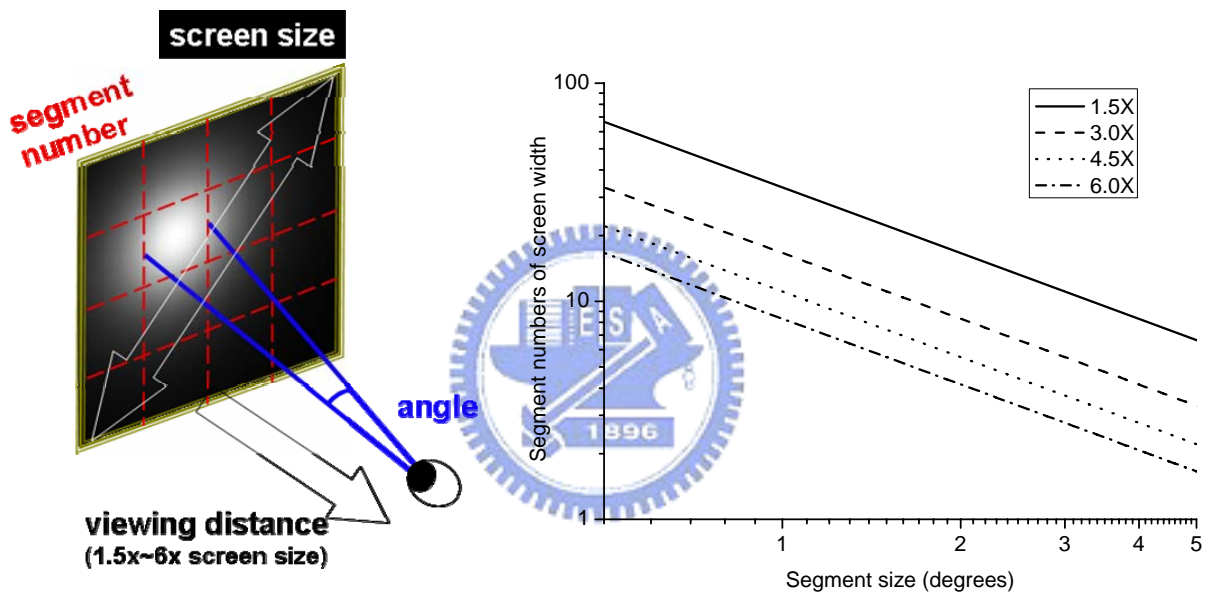


Fig. 5-8 The segment numbers of screen as a function of segment size. The lines correspond to the viewing distances of factors of 1.5 to 6 longer than screen diagonal.

5.4 Proper light distribution formula

The proper light distribution in a segment is required to achieve whole backlight profile as uniform as possible when each segment switched on the same level. On the other hand, the boundaries should not be visible while 2D dimming. Moreover, the distributions should be substantially local for maximizing contrast [92][93]. So far, the Lorentz with $\sigma=1.2$ could be a good choice. In order to find whether other light distributions are suited for 2D-dimming, a simple model is analyzed as follows.

First, the origins are set in the center of each segment, and the pitch between two origins is set to 1. We choose three points located in origin (A), middle point of segment edge (B), and crossing point of segments(C), respectively, as shown Fig. 5-9. These three points are significant for the light distribution. At point A, overlap light is contributed by four closest light sources and itself. For B, it is contributed by two closest light sources and other four sources. Similarly, four closest light sources contribute to the point C. Tab. 5-2 shows the relation between distance and number of contributed sources. Contributions from the distances larger than square root of 1.25 are cut out. Later we will show that this cut-off is justified.

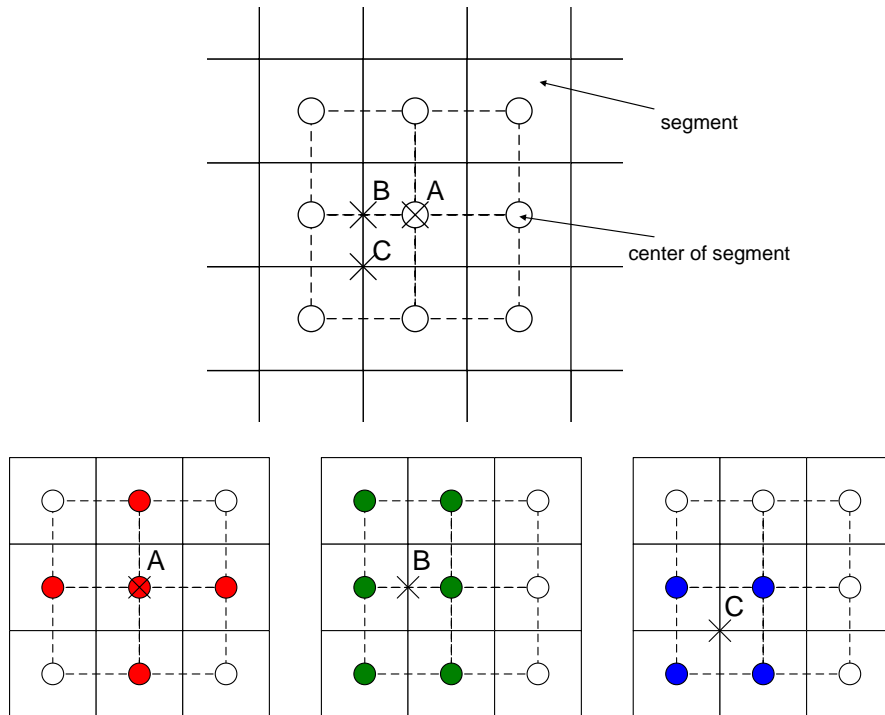


Fig. 5-9 Three points in the model for light source contribution analysis

Tab. 5-2 The relation between distance and contribution of light sources

Square Distance Δr^2	0	0.25	0.5	1	1.25
Contribution Point A #	1			4	
Contribution Point B #		2			4
Contribution Point C #			4		

In uniform condition, these three points should have the same intensity, which can be expressed as:

$$I(\sqrt{0}) + 4 \times I(\sqrt{1}) = 2 \times I(\sqrt{0.25}) + 4 \times I(\sqrt{1.25}) = 4 \times I(\sqrt{0.5}) \quad (\text{Eq. 5-4})$$

where $I(r)$ is a function of light profile. The square of distance is approximately inversion proportional to contributed number of sources in the first item on point B and C (2/0.25: 4/0.5). The possible form $I(r)$ is assumed to be

$$I(r) = \frac{1}{1 + \left(\frac{r}{k}\right)^a}, \quad (\text{Eq. 5-5})$$

where r is distance from origin, k determines the width of profile, and a is the power factor. One is added in denominator to avoid infinity at origin and normalize the contribution to one. Summation of the intensity differences between each two points is used to optimize a and k . In Fig. 5-10(a), the intensities of these three points are calculated with an extended 7×7 segments, whose cut-off distance about 3.5. While k around 0.8 to 1.2 and a around 2.5 to 2.8, these intensities are approximated. When the segments is increased to 15×15 or higher, a and k are converged on 2.2 and 1.0 as shown in Fig. 5-10(b). Convergence is achieved when the number of segments is larger than 15×15 .

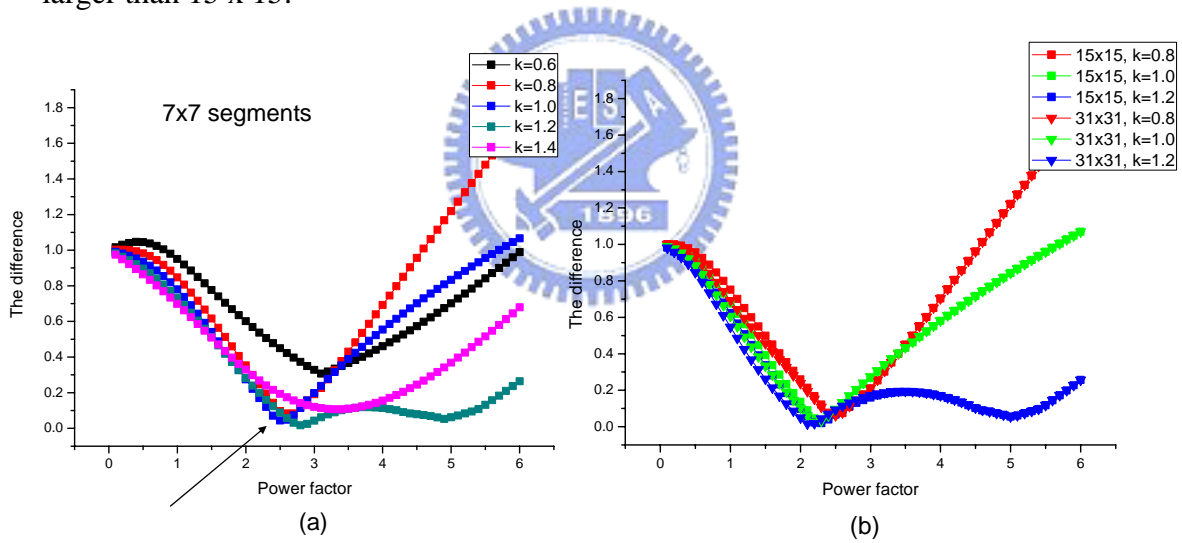


Fig. 5-10 Summation of differences and parameters in (a) 7×7 array (b) 15×15 and 31×31 array

This form of light distribution has a long tail, thus it degrades the contrast enhancement and worsens the localized ability. In order to improve contrast of backlight image, we add another power factor b as

$$I(r) = \frac{1}{\left(1 + \left(\frac{r}{k}\right)^a\right)^b}, \quad (\text{Eq. 5-6})$$

to sharpen the profile of segment. In one condition of b equal to 2, the intensity difference is converged when segment array is 7x7 or higher. The parameter (a, k) are (2.3, 1.4) as shown in Fig. 5-11(a). We further increase b to 3, and modify again the (a, k) values to (2.2, 1.5) as shown in Fig. 5-11(b). With higher b such as 4, the gradient of backlight image will exceed the boundary-free criterion. Surprisingly, the parameter (a, b, k) equal to (2.2, 3, 1.5) so matches the Gaussian distribution with width factor equal to pitch of segment as shown in Eq. 5-7 and Fig. 5-12. The full-on and 2D-dimming backlight images of camera man are shown in Fig. 5-13. Gaussian distribution has the shortest tail of these three profiles, thus the contrast enhancement is the highest. The boundary issue can be avoided because the gradient of image is less than threshold. Moreover, the most uniform backlight image of these three ones can be achieved.

$$\exp\left(-\frac{\Delta r^2}{l^2}\right) \cong \frac{1}{\left(1 + \left(\frac{\Delta r}{1.5}\right)^{2.2}\right)^3}, \quad (\text{Eq. 5-7})$$

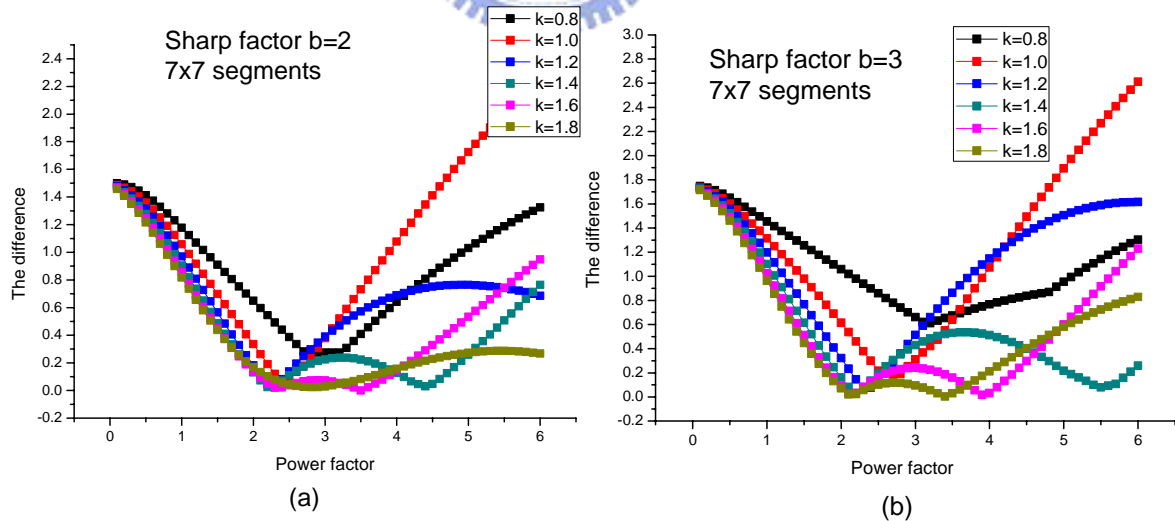


Fig. 5-11 Summation of differences and parameters with sharp factor (a) b=2 (b) b=3

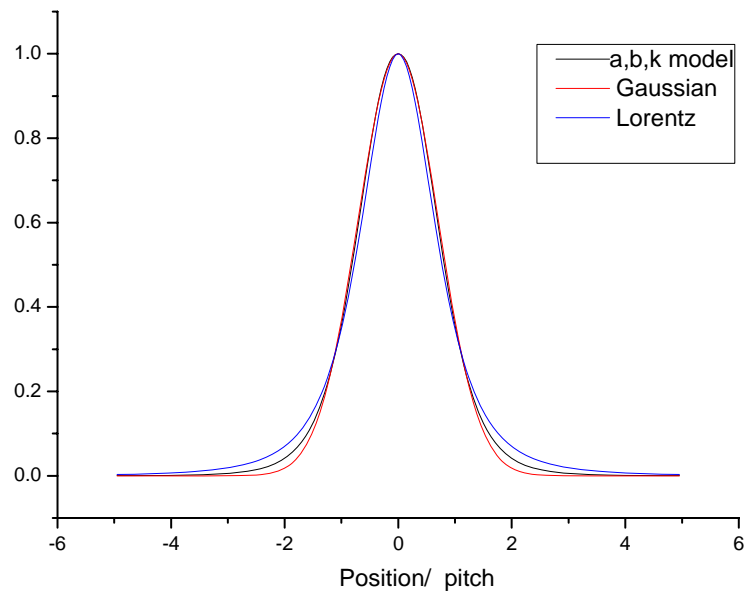


Fig. 5-12 Similarity between a, b, k model, Gaussian, and Lorentz distributions

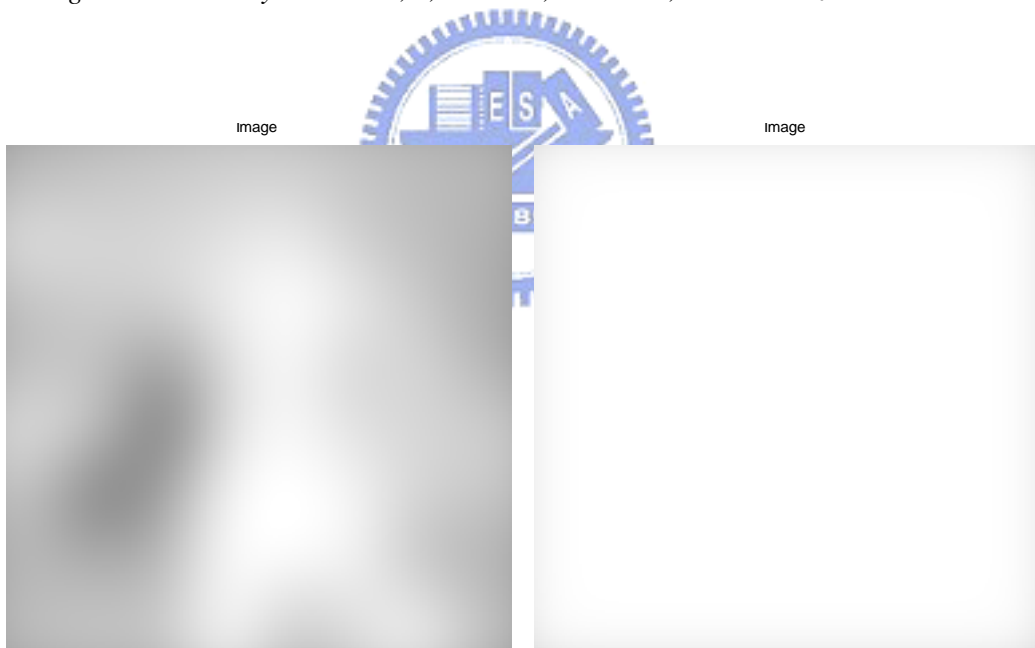


Fig. 5-13 (a) 2D-dimming (b) full-on backlight image of Gaussian distribution

5.5 Summary

The human contrast sensitivity function was analyzed to determine the threshold of boundary-free perception in 2D-dimming backlight. The gradient of backlight image was used to evaluate the visibility of boundaries. From a perception study, it was found that the gradient of backlight image should be lower $\pi/100$ of background luminance. This value appears to be the threshold for the visibility of boundaries. The Lorentz distribution of backlight profiles was examined on images over different spatial scales, ranging from coarse to fine detail. We focus on perceived image quality of dimmable backlight with an economical number of segments for 2D-dimming backlight. The effects of size and profile of segment were studied based on human visual properties. Considering the boundary perception and contrast enhancement, the size of 2 degrees was found to be the recommended profile of each segment. The gradient is close to 100% below the boundary-free criterion and the average backlight contrast is 3.5. Simultaneously, the proper light profile in each segment was derived for high uniformity of three significant points. Considering a better localized ability and high contrast enhancement, the Gaussian function was found to be the most suitable profile of each segment in 2D-dimming backlight.

Chapter 6

Conclusion and Future Work

6.1 Conclusion


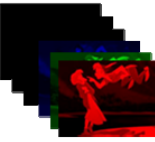



The field sequential color liquid crystal display (FSC-LCD) has emerged as a new branch of LCD application. Sequential driving LED backlight represents a potential technological breakthrough in terms of optical efficiency. Because of its needless color filter and low material cost, the FSC-LCD has become the key technology for reducing the power dissipation and the resource consumption.

FSC-LCDs rapidly flash the primaries time-sequentially such that the colors are mixed by means of temporal integration in the eye. The lacking sub-pixels and color filters result in high transitivity and large aperture ratio. The primary chromaticities are determined solely by the LEDs which enable wider gamut and scalable number of primaries. Furthermore, the impulse driving of the backlight ensures high moving image quality.

However, color breakup (CBU) is the most disturbing artifact, which occurs in FSC-LCDs. The CBU reveals itself in the appearance of multiple color images of stationary object during saccadic eye motion, or along the edges of moving objects when tracking the objects with the eye. Although increasing the frame to several thousand Hz can completely eliminate CBU [94], it is highly unlikely that affordable panels with frame rates higher than 240 Hz will be widely available in the foreseeable future.

In this thesis work, we have successfully relaxed the requirements on 240 Hz frame rate and reduced CBU significantly by modulating the backlight. The proposed methods, such as color field arrangement and gray level redistribution, were implemented in the timing controller circuit. Additionally, the index of color difference has been utilized to evaluate the CBU. Compared to the CBU perception with previously sequential driving methods, the newly developed methods have greatly improved the image performance of FSC-LCDs. Tab. 6-1 shows the dynamic control algorithm is the first sequential driving LCD in the world adapted by image contents. For LC availability, field processing loading, and power consumption, this adaptation method also presents its competitiveness.

Tab. 6-1 The comparison between normal RGB, 3 prior arts described in Chapter1, and the proposed adaptation method

FSC-LCD	Normal RGB	Double frame rate	Additional mono-color	Spatial-temporal	Dominated adaptation
Field profile	 CPT, Samsung	 Tohoku Univ.	 Genoa Color Tech	 Philips	 NCTU
CBU visibility(%)	100	62	84	70	55
Power consumption (W)	68	68	163	120	102
LC response time requirement (ms)	3	0.22	0.77	4	1.61
CF	Without	Without	Without	With	Without
Dynamic control	Without	Without	Without	Without	With
Field processing frequency (Hz)	180	360	300	120	240

* estimating criterion: 32" panel, LED full on=180W, NTSC=114%

6.1.1 The consistent color fields in mobile-sized FSC-LCDs

On a 5.6-in LCD platform, we have demonstrated the color field arrangement (CFA) method, which modifies the consecutive color order to resolve CBU issue. The integration of three consecutive frames on retina was compensated as a gray level image because of the viewpoint through the same ratio of each primary color. Blurring margins of test patterns were observed in the synchronized camera experiment for the movement of eyes tracking. Comparatively, the perceived images with the typical 3-field RGB driving strategy have obvious multicolor margins, the notable CBU phenomenon.

The 4-CFA method with consistent orders of RGBR, GRBG, and BRGB in three consecutive frames was implemented and confirmed experimentally on the CBU suppression. The physical evaluation results on dynamic CBU adhere to the prediction for the moving images. Furthermore, the field frequency of CFA method is 1.3 times faster than that of typical one, resulting in the slighter static CBU for stationary images. Generally, increasing field frequency can effectively mitigate the static CBU. However, the LC response time is still a crucial limitation to apply the sequential driving on LCDs.

We presented the 4-field RGBW method by flashing a gray image in a white field and displaying the color residuals in remaining fields. This allows the image energy to be better focused in the initial field, thus reducing the intensities of the red, green, and blue fields thus suppressing CBU within the field frequency of 240 Hz. The minimum one of the RGB gray levels per pixel is assigned as the gray level in the white field. For a pure white image, this method displays the image only in the white field, thus CBU can be totally eliminated. For other colors, at least one gray level of color fields will be zero. Perception tests have confirmed that the color separation is markedly reduced.

6.1.2 The adaptive B/L for CBU optimization in laptop-sized LCDs

The consistent color orders of field such as CFA and RGBW methods can not fulfill all kinds of image for static CBU reduction, especially in cyan, yellow, and magenta images. Remaining two primary colors result in an obvious color separation during the observation.

In order to overcome this restriction, we presented the intelligently adaptive backlight. According to the incoming video content, the exchange of RGBC/Y color sequence dynamically mitigates the CBU phenomenon to lighten the most sensitive green field. The redistribution of LC gray levels on these two color sequence is assessed by the gamma curve between gray levels and transmittances to maintain the white balance. We implemented the RGBC/Y method on a 32-in LCD platform. The brightness of a white image can reach at 400 nits at total power consumption of 50W, a half of power of typical CCFL backlight module [55]. From the CBU evaluation index, 27% to 56% of suppression ratio in the specific color pattern was obtained.

This redistributed method has been extended to determinate a suitable color in the fourth field. With RGBC/Y sequence, the fourth color is fixed as the cyan or yellow one, resulting in still one primary color with higher values of gray levels. An approach is to flash an adaptive image in a dominated field (D-field) and use the remaining fields to display the color residuals. Typical FSC displays with consistent color order like a rotating color wheel in a projector are unable to obtain an adaptive color field except the modulation of LED backlight.

The color backlight in D-field that induced the minimum color difference between CBU images and original ones was proposed for the CBU minimization. The simulation results of test images show that the 2x4 sampling period of image and 3-bit gray levels of color backlight can adequately simplify the calculation of color

difference, which is necessary in a real time application. Most importantly, an adaptive feedback control algorithm was described to locate the optimal D-field color efficiently. 8 sets of color backlight were evaluated at each frame and more accurate sets were used at following frame. Consequently, the proposed DRGB method concentrates the majority of image intensity into the D-field and owns the lowest color difference compared to those of typical RGB and RGBC/Y method. This average CBU suppression ratio around 70% of typical RGB driving is obtained. The color separation at the edges of objects in test images was essentially improved and agreed with the observation.

6.1.3 The recommended light profile for TV-sized FSC-LCDs

Adaptive dimmable backlights consisting of local addressable LEDs allow the D-field color to be optimum for each segment. For highly-colored images, the mass of image intensity in primary color fields may remain even through the entire backlight is modulated in the D-field. Nevertheless, color addressable backlights are capable to locally module the D-field along horizontal and vertical segments to resolve the issue of global adaptation, especially for large-sized LCDs. Moreover, these backlights generate only the amount of light required to correctly depict the video content while dimming underneath dark areas. The power consumption can be further reduced while simultaneously improving the black level [95]-[99].

To combine this highly-potential backlighting with FSC-LCDs, we have investigated the optical profiles on segments to influence the perceived image quality. The brightness variation at the boundary between segments should be indistinguishable in the backlight image. The gradient of backlight image was used to evaluate the visibility of boundaries. According to contrast sensitivity function, we identified $\pi/100$ of background luminance as the threshold for the boundary

perception. Below this threshold, boundary was not sensible.

Several images with different spatial scales, ranging from coarse to fine detail, were examined. Considering the boundary perception and contrast enhancement, the size of 2 degrees was found to be the optimal segment profile. The gradient is close to 100% below the boundary-free criterion. At a viewing distance of a factor of 3 longer than screen diagonal, the segment size of 2 degrees results in about 10x10 as the recommended and economical number of segments. For a closer viewing distance, more segment numbers are needed. In addition, the proper light profile in each segment was derived for high uniformity of three significant points. Considering the localized ability and contrast enhancement, the Gaussian function was the recommended profile of each segment in local adaptive backlights.

In conclusion, this dissertation explores the sequential driving and the evaluation of newly developed CBU reduction techniques. The practical circuit control and optical profile design has been examined on full-scale LCDs. In this thesis, we have demonstrated that the adaptation to image content has a great potential to attain high image quality and low power consumption, the essential capacities of FSC-LCDs.

6.2 Future work

The adaptive backlight can be viewed as a natural extension of the consistent color in the sense that the fourth field is modified instead of only white, yellow, or cyan. The adaptive field allows for a higher focusing of image energy in time, while reducing the visual saliency of individual fields. So far, the adaptive color has only been tested in combination with global LED backlights that allow fields to change color only as a whole backlight. Although this global adaptation was verified to satisfactorily reduce CBU, we anticipate that the performance will greatly improve when combined with a local color dimming LED backlight to enable a far superior

adaptation to the incoming video content. Fig. 6-1 shows the original image and individual color fields of global and local adaptive backlights. The two characters are presented by themselves color adaptation as shown in Fig. 6-1(c). Simulated results of non-adaptation (conventional RGB), global and local adaptation methods support the prediction of CBU reduction, as illustrated in Fig. 6-2. Furthermore, three or even two local color dimming fields can be applied for a slower response time with typical LCs instead of fast response ones. The algorithm for the cases of fewer color fields can be expectably reported on a normal twisted nematic (TN) mode LCD in the near future.

In the scope of whole LCD system, we have discussed and concluded that the major consuming devices in LCD embodiment are polarizers and color filters. In this thesis, the sequential driving as a feasible approach provides to leave out the color filters. Nevertheless, the polarizer still absorbs about 50% incident light, thus much lower the output light efficiency. Therefore, liquid crystal capable of having spontaneous polarization can be used for excluding the polarizer in LCD embodiment. Liquid crystalline conjugated polymers are potential candidates as inexpensive, easy to process polarized back lights for liquid crystal displays [100]. The device efficiency and brightness can be modified by the property of alignment layer. This polarized liquid crystal shall be an appealing topic to explore in the future.

In addition to enhancing the optical efficiency of components, the power consumption of light source is anticipated as low as possible. The highly efficient white LED can be introduced into the backlight besides RGB LEDs as shown in Fig. 6-3. The white LED is proposed to contribute major intensity in the color-mixed field. The efficiency of RGB mixing white of 40 lm/W is markedly lower than that of single white LED of 100 lm/W [101]. Consequently, the combination of white and RGB LEDs is viewed as a further reduction of power consumption.

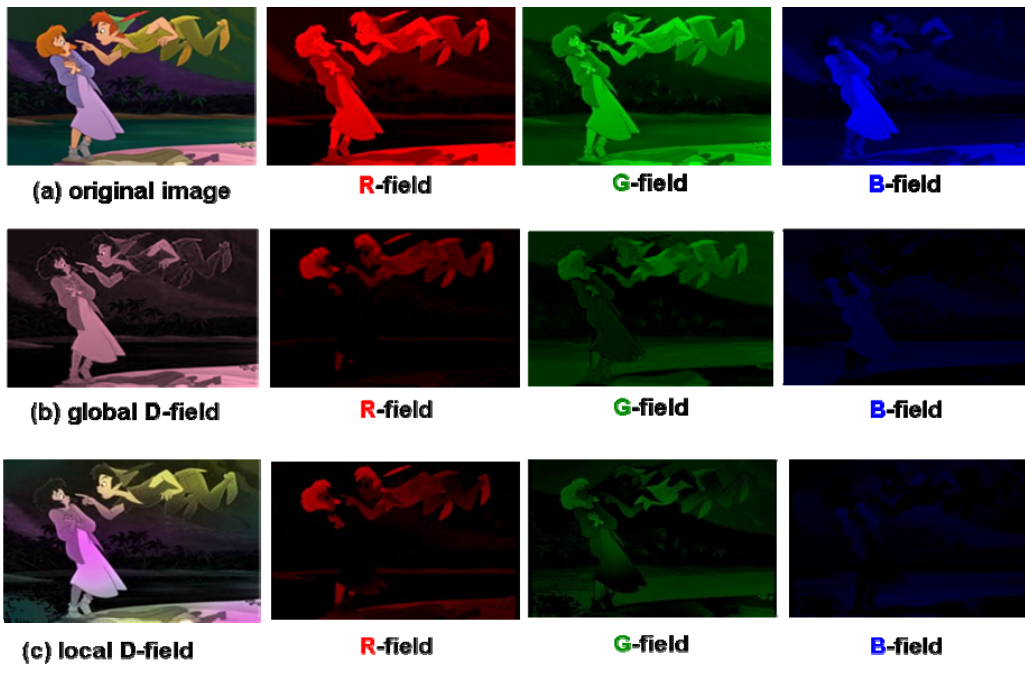


Fig. 6-1 The (a) original image and individual color fields of (b)global and (c)local adaptive backlights.



Fig. 6-2 The CBU images with (a) non-, (b) global, and (c) local adaptation.

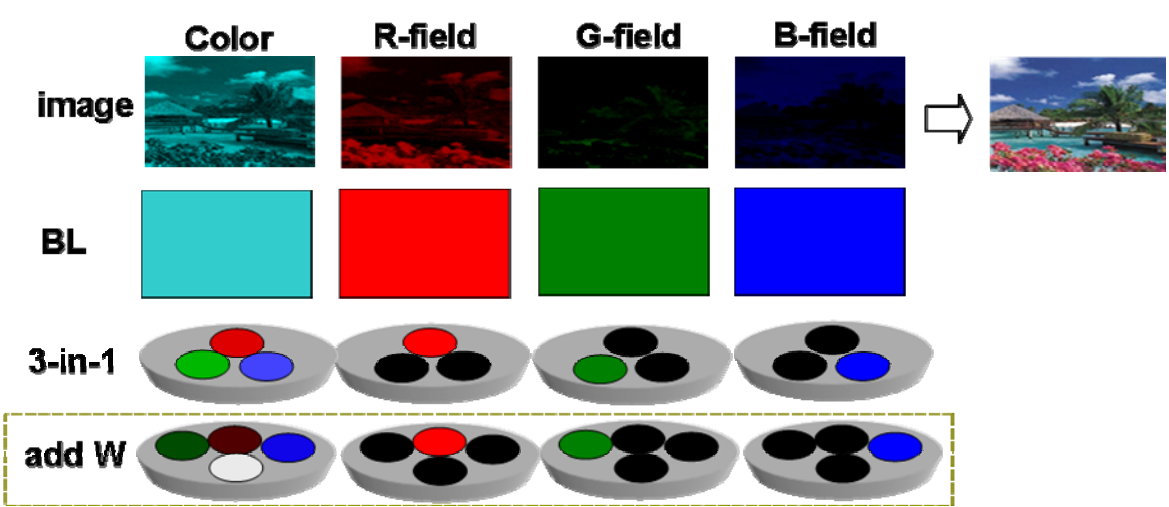


Fig. 6-3 The schematic of added white LEDs into the backlight module.

In a world that is increasingly aware of its ecological footprint and energy issue, the sequential driving technology has wide-spread acceptance to upgrade the efficiency of LCD applications. As the power-saving, or called green, technique become a common view of human beings, the sequential driving prototypes have been widely demonstrated and greatly capable of regard for both image quality and power consumption. The newly developed algorithms mitigate the effects of color breakup, and allow sequential driving LCDs to be attractive in practical scopes covering research for mobile devices, signage, monitor, and TV. Therefore, consumers can benefit from appealing multi-media; meanwhile, lower the injury that is causing to our planet.



Reference

- 1 LCD Optics 101, Retrieved August 28, 2008, from the : http://solutions.3m.com/wps/portal/3M/en_US/Vikuiti1/BrandProducts/secondary/optics101/
- 2 R. S. West, "High Brightness Direct LED Backlight for LCD-TV," SID Symposium Digest Tech Papers 34, pp. 1262-1265 (2003).
- 3 S. Sakai, "A Thin LED Backlight System with High Efficiency for Backlighting 22-in. TFT-LCDs," SID Symposium Digest Tech Papers 35, pp. 1218-1221 (2004).
- 4 Lumileds Lighting, "Luxeon Emitter Technical Data DS25 (02/13/04)"
- 5 H. Seetzen, W. Heidrich, W. Stuerzlinger, G. Ward, L. Whitehead M. Trentacoste, A. Ghosh, and A. Vorozcovs, "High Dynamic Range Display Systems," SIGGRAPH 2004, ACM Transactions on Graphics, vol. 23(3), pp. 760-768 (2004).
- 6 T. Shirai, S. Shimizukawa, T. Shiga, S. Mikoshiba, and K. Kälantär, "RGB-LED Backlights for LCD-TVs with 0D, 1D, and 2D Adaptive Dimming," SID Symposium Digest Tech Papers 37, pp. 1520-1523 (2006).
- 7 R.G. Stewart and W.R. Roach, "Field Sequential Display System Utilizing a Backlit LCD Pixel Array and Method for Forming an Image," US Patent 5337068 (1994).
- 8 T. Uchida, K. Saitoh, T. Miyasita, and M. Suzuki, "Field Sequential Full Color LCD without Color Filter for AM-LCD", Proc. 17th IDRC, pp. 37 (1997).
- 9 N. Koma, T. Miyashita, T. Uchida, and N. Mitani, "Color Field Sequential LCD Using an OCB-TFT-LCD," SID Symposium Digest Tech Papers 31, pp. 632-635 (2000).
- 10 J. C. Pan and A. Lin, "Emerging Technologies for Backlight Modules," *IDMC'07*, pp.463-466 (2007).
- 11 E. Lueder, Liquid Crystal Displays, John Wiley & Sons, pp.121 (2000).
- 12 C.-C. Kang, J.-F. Lin, M.-C. Chen, and P.-R. Wang, "An Innovative Solution for the Thinness of Backlight Units with the Implementation of Transflectors," *IDMC'07*, pp.685-688 (2007).
- 13 L. M. Seon, O. Y. Sik, P. D. Sung, K. S. Yoon, and L. J. Yeal, "Optimum Design Characteristics of a Direct Type Backlight Unit," *IDW'06*, pp.921-924 (2006)
- 14 M. Schiavoni, G. Counil, P. Gayout, J.-L. Allano and R. Marandon, "5.4: Novel Glass Diffuser Plate for Large LCD-TV," SID Symposium Digest Tech Papers 38, pp.50-53 (2007).
- 15 J.-C. Hsieh, Y.-P. Huang, C.-H. Chen, Y.-C. Lo, J.-Y. Fang, and H.-P. D. Shieh, "Multi-Performance Film (MPF) for Highly Efficient LCD Backlights," 2008

-
- Taiwan Display Conference Proceedings (TDC'08), pp. 398-401 (2008).
- 16 J.-C. Hsieh, Y.-P. Huang, C.-H. Chen, Y.-C. Lo, J.-Y. Fang, H.-P. D. Shieh, G.-S. Yu, and T. Chiang, "Multi-Performance Film (MPF) for Highly Efficient LCD Backlights," SID Symposium Digest Tech Papers 39, pp. 1606-1609 (2008)
 - 17 C.-H. Chen and H.-P. D. Shieh, "High Uniformity of Large Size Backlight System with Inclined LED Array," IDMC'05, pp. 407-409 (2005).
 - 18 C.-H. Chen and H.-P. D. Shieh, "Inclined LED Array for Large-Sized Backlight System," SID Symposium Digest Tech Papers 36, pp.558-561 (2005).
 - 19 H. Suglura, "Wide Color Gamut and High Brightness Assured by the Support of LED Backlighting in WUXGA LCD Monitor," SID Symposium Digest Tech Papers 35, pp. 1230-1233 (2004).
 - 20 M. J. Zwanenburg, "High Efficiency LEDs for LCD Backlight," SID Symposium Digest Tech Papers 35, pp. 1222-1225 (2004)
 - 21 M. Anandan, "Backlights for LCD/TV Monitors: LCD vs. CCFL," SID'06 Seminar Lecture Notes, M-2 (2006).
 - 22 J. B. Eichenlaub, "Field Sequential Color Illumination System for Liquid Crystal Display," U.S. Patent 5428366 (1995).
 - 23 F. Yamada, H. Nakamura, and Y. Sakaguchi, "Sequential-Color LCD Based on OCB with an LED Backlight," J. of Info. Display, Vol. 10, pp. 81-85 (2002).
 - 24 F. Yamada, "Color Sequential LCD Based on OCB with an LED Backlight," SID Symposium Digest Tech Papers 31, pp. 1180-1183 (2000).
 - 25 N. Koma, T. Miyashita, T. Uchida, and N. Mitani, "Color Field Sequential LCD Using an OCB-TFT-LCD," SID Symposium Digest Tech Papers 31, pp. 632-635 (2000).
 - 26 H. Yamakita, M. Sakai, Y. Taniguchi, J. Asatama, and K. Adachi, "Field-Sequential Color LCD Driven by Optimized Method for Color Breakup Reduction," IDW/AD'05, pp. 83-86, (2005).
 - 27 T. Ishinable, T. Miyashita, and T. Uchida, "High Performance OCB-mode for Field Sequential Color LCDs," SID Symposium Digest Tech Papers 38, pp. 987-990 (2007).
 - 28 K. Kälantär, T. Kishimoto, K. Sekiya, T. Miyashita, and T. Uchida, "Spatio-Temporal Scanning Backlight for Color-Field Sequential Optically Compensated Bend Liquid-Crystal Display," SID Symposium Digest Tech Papers 36, pp. 1316-1319 (2005).
 - 29 Y.-F. Chen, C.-C. Chen, and K.-H. Chen, "Mixed Color Sequential Technique for Reducing Color Breakup and Motion Blur Effects," IEEE/OSA Journal of Display Technology, Vol.3(4), pp. 377-385 (2007).
 - 30 C.-C. Chen, Y.-F. Chen, T.-T. Liu, C.-H. Chen, M.-T. Ho, K.-H. Chen, and H.-P. D. Shieh, "Spatial-temporal Division in Field Sequential Color Technique for Color

-
- Filterless LCD,” SID Symposium Digest Tech Papers 38, pp. 1806-1809 (2007).
- 31 L. Arend, J. Lubin, J. Gille, and J. Larimer, “Color Breakup in Sequential Scanned LCDs,” SID Symposium Digest Tech Papers 25, pp. 201-204, (1994).
- 32 A. Yohso and K. Ukai, “How Color Break-up Occurs in the Human-visual System: The Mechanism of the Color Break-up Phenomenon,” J. of the SID 14/12, pp. 1127-1133 (2006).
- 33 J. B. Eichenlaub, “Develop and Preliminary Evaluation of Field Sequential LCD Free of Color Breakup,” SID Symposium Digest Tech Papers 25, pp. 293-296 (1994).
- 34 D. L. Post, “Predicting Color Breakup on Field-Sequential Displays: Part 2,” SID Symposium Digest Tech Papers 29, pp. 1037–1040 (1998).
- 35 M. Mori, T. Hatada, K. Ishikawa, T. Saishouji, O. Wada, J. Nakamura, and N. Terashima, “Mechanism of Color Breakup in Field-Sequential-Color Projectors,” SID Symposium Digest Tech Papers 30, pp. 350–353 (1999).
- 36 S. Mateeff, “Saccadic Eye Movements and Localization of Visual Stimuli,” Percept Psychophys 24, pp. 215–224 (1978).
- 37 W. Hershberger, “Saccadic Eye Movements and the Perception of Visual Direction,” Percept Psychophys 41, pp. 35–44 (1987).
- 38 H. Honda, “Perceptual Localization of Visual Stimuli Flashed during Saccades,” Percept Psychophys 45, No. 2, pp. 162–174 (1989).
- 39 M. Ogata, K. Ukai, and T. Kawai, “Visual Fatigue in Congenital Nystagmus Caused by Viewing Images of Color Sequential Projectors,” IEEE/OSA Journal of Display Technology, Vol.1(2), pp. 314-320 (2005).
- 40 O. Wada, J. Nakamura, K. Ishikawa, and T. Hatada, “Analysis of Color Breakup in Field Sequential Color Projection System for Large Area Display,” IDW’99, pp. 933-996 (1999).
- 41 E. Langendijk, “A Comparison of Three Different Field Sequential Color Displays,” IDW’05, pp. 1809-1812 (2005).
- 42 E. Langendijk, “Suppression of Color Breakup in Color-Sequential Multi-Primary Projection Displays,” J. of Info. Display, Vol. 14, pp.325-329 (2006).
- 43 K. Sekiya, T. Miyashita, and T. Uchida , “A Simple and Practical Way to Cope with Color Breakup on Field Sequential Color LCDs,” SID Symposium Digest Tech Papers 37, pp. 1661-1664 (2006).
- 44 D. Eliav, E. Langendijk, S. Swinkels, and I. Baruchi, “Suppression of Color Breakup in Color Sequential Multi-Primary Projection Displays,” SID Symposium Digest Tech Papers 36, pp. 1510-1513 (2005).
- 45 F. P. Herrmann, “Color/Mono Switched Display,” US Patent 7057668 B2 (2006).
- 46 G. Cennini, O. Belik, E. Langendijk, and F. Vossen, “Spatio-Temporal Colour LCD with LED Backlight,” IDW’07, VHF 2-2 (2007).

-
- 47 Y.-T. Hsu, F.-C. Lin, C.-H. Chen, Y.-P. Huang, and H.-P. D. Shieh, "Drive and Control Circuitry of OCB Field-Sequential Color LCD with High Data Rate", IDMC'07, pp.435-438 (2007).
- 48 Y.-T. Hsu, F.-C. Lin, C.-H. Chen, Y.-P. Huang, and H.-P. D. Shieh, "A Field Sequential Color LCD Based on Color Field Arrangement for Color Breakup and Flicker Reduction," IDW'07, LCT3-3 (2007).
- 49 C.-H. Chen, F.-C. Lin, Y.-T. Hsu, Y.-P. Huang, and H.-P. D. Shieh, "A Field Sequential Color LCD Based on Color Fields Arrangement for Color Breakup and Flicker Reduction," accepted by IEEE/OSA Journal of Display Technology (JDT)
- 50 S. Shady, I. A. Macleod, and H. S. Fisher, "Adaption from Invisible Flicker," PANS'04, pp. 5170-5173 (2004).
- 51 C.-H. Chen, K.-H. Chen, Y.-P. Huang, H.-P. D. Shieh, and M.-T. Ho, "Gray Level Redistribution in Field Sequential Color LCD Technique for Color Breakup Reduction," SID Symposium Digest Tech Papers 39, pp. 1096-1099 (2008).
- 52 C.-L. Wu, C.-H. Chen, F.-C. Lin, Y.-P. Huang, and H.-P. D. Shieh, "A 5.6-inch Field Sequential Color LCD with Less Color Break-up," Optics and Photonics Taiwan'07 (OPT '07), GO-004, (2007).
- 53 C.-L. Wu, C.-H. Chen, F.-C. Lin, Y.-P. Huang, and H.-P. D. Shieh, "Demonstration of a Mobile-Sized Field Sequential Color LCD for Color Break-up Suppression," 2008 Taiwan Display Conference Proceedings (TDC'08), pp.419-422, (2008).
- 54 Y.-P. Huang, K.-H. Chen, C.-H. Chen, F.-C. Lin, and H.-P. D. Shieh, "Adaptive LC/BL Feedback Control in Field Sequential Color LCD Technique for Color Breakup Minimization," IEEE/OSA Journal of Display Technology, vol. 4(3), pp. 290-295 (2008).
- 55 F.-C. Lin, Y.-P. Huang, C.-M. Wei, and H.-P. D. Shieh, "Stencil-FSC Method for Color Break-Up Suppression and Low Power Consumption in Field-Sequential LCDs," SID Symposium Digest Tech Papers 39, pp. 1108-1111 (2008).
- 56 S. Swinkels, R. Muijs, E. Langendijk, and F. Vossen, "Effect of Backlight Complexity on Perceived Image Quality HDR Displays", IDW'06, VHF 3-4 (2006).
- 57 C.-H. Chen and H.-P. D. Shieh, "Effects of Backlight Profiles on Perceived Image Quality for High Dynamic Range LCDs," IEEE/OSA Journal of Display Technology, Vol. 4(2), pp. 153-159 (2008).
- 58 M. D. Fairchild, Color Appearance Models, 2nd Ed., Wiley-IS&T, Chichester, UK, pp.1-34 (2005).
- 59 R. W. Baloh, A. W. Sills, W. E. Kumely, and V. Honrubia, "Quantitative Measurement of Saccade Amplitude, Duration, and Velocity", NEUROLOGY, pp.1065-1070 (1975).
- 60 D. C. Burr, M. C. Morrone, and J. Ross, "Selective Suppression of the Magnocellular Visual Pathway during Saccadic Eye Movements," Nature 371, No. 6497, pp. 511-513 (1994).

-
- 61 K. Uchikawa, and M. Sato, "Saccadic Suppression of Achromatic and Chromatic responses Measured by Increment-threshold Spectral Sensitivity," *J. Opt. Soc. Am. A Opt. Image Sci. Vis.* 12, No. 4, pp. 661–666 (1995).
- 62 J. Ross, M. C. Morrone, and D. C. Burr, "Compression of Visual Space before Saccades," *Nature* 386, pp. 598–601 (1997).
- 63 J. Watanabe, "Perisaccadic Perception of Continuous Flickers," *Vision Res.* 45, pp. 413–430 (2005).
- 64 T. Jarvenpaa, "Measuring Color Breakup of Stationary Image in Field-Sequential-Color," *SID Symposium Digest Tech Papers* 35, pp. 82-85 (2004).
- 65 A. T. Bahill, M. R. Clark, and L. Stark, "The Main Sequence, a Tool for Studying Human Eye Movements," *Math. Biosci.* vol. 24, pp. 191-204 (1975).
- 66 P. C. Baron, P. Monnier, A. L. Nagy, D. L. Post, L. Christianson, J. Eicher, and R. Ewart, "Can Motion Compensation Eliminate Color Breakup of Moving Objects in Field-Sequential Color Displays?," *SID Symposium Digest Tech Papers* 27, pp. 843-846 (1996).
- 67 T. Kurita and T. Kondo, "Evaluation and Improvement of Picture Quality for Moving Images on Field-Sequential Color Displays," *IDW'00*, pp. 69-72 (2000).
- 68 T. Jarvenpaa, "Measuring Color Breakup of Stationary Image in Field-Sequential-Color," *J. of Info. Display*, Vol. 13, pp. 139-144 (2005).
- 69 T. Smith and J. Guild, "The C.I.E. Colorimetric Standards and Their Use," *Transactions of the Optical Society* 33 (3), pp. 73-134 (1931).
- 70 W. D. Wright, "A Re-determination of the Trichromatic Coefficients of the Spectral Colours," *Transactions of the Optical Society* 30, pp. 141-164 (1928).
- 71 J. Guild, "The Colorimetric Properties of the Spectrum," *Philosophical Transactions of the Royal Society of London* A230, pp. 149-187 (1931).
- 72 R. W. Hunt, *Measuring Colour*, 3rd Edition, Fountain Press, England, pp. 39-57 (1998).
- 73 A. C. Harris and I. L. Weatherall, "Objective Evaluation of Colour Variation in the Sand-burrowing Beetle *Chaerodes Trachyscelides* White by Instrumental Determination of CIELAB Values," *Journal of the Royal Society of New Zealand*, 20(3) (1990).
- 74 M. D. Fairchild, *Color Appearance Models*. Reading, MA: Addison-Wesley (1998).
- 75 D. H. Alman, R. S. Berns, G. D. Snyder, and W. A. Larson, "Performance Testing of Color Difference Metrics Using a Color-Tolerance Dataset," *Color Research and Application*, vol. 21, pp.174-188 (1989).
- 76 J. Schanda, *Colorimetry: Understanding the CIE System*, Wiley Interscience, pp. 61-64 (2007).
- 77 *Colorimetry*, 2nd edition: CIE publication 15.2. Vienna: Bureau Central CIE

-
- (1986).
- 78 J. Lee, T. Jun, J. Lee, J. Han, and J.H. Souk, "Noble Measurement Method for Color Breakup Artifact in FPDs," IMID/IDMC'06, pp. 92-97 (2006).
- 79 S.-P. Yan, Y.-K. Cheng, F.-C. Lin, C.-M. Wei, Y.-P. Huang, H.-P. D. Shieh, "A Visual Model of Color Break-Up for Design Field-Sequential LCDs," SID Symposium Digest Tech Papers 38, pp. 338-341 (2007).
- 80 S.-C. Chen, S.-P. Yan, Y.-K. Cheng, F.-C. Lin, C.-M. Wei, Y.-P. Huang, and H.-P. D. Shieh, "A Human Visual Model for Color Break-Up Artifact in Design Field Sequential Color LCDs," IDMC'07, pp. 872-875 (2007).
- 81 P. J. Bos, K.R. Koehler, and beran, "The pi-Cell: A Fast Liquid-Crystal Optical-Switching Device," Molecular Crystals and Liquid Crystals 113(1), pp. 329-339 (1984).
- 82 K. Sekiya, K. Wako, S. Nakano, T. Ishinable, T. Miyashita, and T. Uchida , "Optimized Voltage Range Selection for OCB-Mode LCD in Field Sequential Color Application," IDW'04, pp. 97-98 (2004).
- 83 T. Fukami, S. Kawaguchi, S. Araki, M. Takeoka, and A. Takimoto, "New Driving Method for Field Sequential Color LCDs Using OCB Mode," IDW'06, pp. 1617-1620 (2006).
- 84 T. Makino, T. Yoshihara, H. Shiroto, and Y. Kiyota, "Liquid crystal display," US Patent 6570554 (2003).
- 85 F. Yamada and Y. Sakaguchi, "Liquid Crystal Display," US Patent 7079162 B2 (2006).
- 86 Vision Research, Inc.: Phantom V5.1, Retrieved January 29, 2008, from the: http://www.visionresearch.com/index.cfm?sector=htm/files&page=camera_51_new
- 87 Y.-W. Wang, Y.-K. Cheng, H.-P. D. Shieh, T.-M. Wang, and H.-W. Richard Lin, "Analyses of Point Spread Function in High Dynamic Range Display System," Optics and Photonics Taiwan 2005, No. G-SA-X 4-3 (2005).
- 88 Y.-W. Wang, Y.-K. Cheng, and H.-P. D. Shieh, "Point Spread Function in High Dynamic Range Display System," TDC'06, 04-013, pp. 338-340 (2006).
- 89 The Contrast Sensitivity Function, Retrieved November 27, 2007, from the: <http://www.psych.ndsu.nodak.edu/mccourt/Psy460/Spatial%20frequency%20analysis/Spatial%20frequency%20analysis.html>
- 90 M. Fihn, "High-Resolution Displays: Path to What the Eye Demands," SID Application tutorial notes, A-4 (2006)
- 91 T.-L. Ji, M. K. Sundareshan, and H. Roehrig, "Adaptive Image Contrast Enhancement Based on Human Visual Properties," IEEE Transaction on medical imaging, Vol. 13(4), pp. 573-586 (1994).
- 92 F.-C. Lin, Y.-P. Huang, L.-Y. Liao, C.-Y. Liao, H.-P. D. Shieh, T.-M. Wang, and S.-C. Ye, "Inverse of Mapping Function (IMF) Method for Image-Quality

-
- Enhancement of High-Dynamic-Range LCD TV,” SID Symposium Digest Tech Papers 38, 39-4 (2007).
- 93 F.-C. Lin, Y.-P. Huang, L.-Y. Liao, C.-Y. Liao, H.-P. D. Shieh, T.-M. Wang, and S.-C. Ye, “Dynamic Backlight Gamma on High Dynamic Range LCD TVs,” IEEE/OSA Journal of Display Technology, vol. 4(2), pp. 139-146 (2008).
- 94 I. Miettinen, R. Nasanen, and J. Hakkinen, “Effects of Saccade Length and Target Luminance on the Refresh Frequency Threshold for the Visibility of Color Break-Up,” IEEE/OSA Journal of Display Technology, vol. 4(1), pp. 81-85, (2008).
- 95 H. Seetzen, L. A. Whitehead, and G. Ward, “A High Dynamic Range Display Using Low and High Resolution Modulators,” SID Symposium Digest Tech Papers 34, pp. 1450-1453 (2003).
- 96 E. Y. Oh, S. H. Baik, M. H. Sohn, K. D. Kim, H. J. Hong, J. Y. Bang, K. J. Kwon, M. H. Kim, H. Jang, J. K. Yoon, and I. J. Chung, “IPS-mode Dynamic LCD-TV Realization with Low Black Luminance and High Contrast by Adaptive Dynamic Image Control Technology,” J. Soc. Info. Display, vol. 13, pp. 215-219 (2005).
- 97 E.H.A. Langendijk, R. Muijs, and W. van Beek, “Quantifying Contrast Improvements and Power Savings in Displays with a 2D-Dimming Backlight,” IDW '07, pp. 311-314 (2007).
- 98 J. H. Stessen and J. G. R. van Mourik, “Algorithm for Contrast Reserve, Backlight Dimming, and Backlight Boosting on LCD,” SID Symposium Digest Tech Papers 37, pp. 1249-1252 (2006).
- 99 P. de Greef and H. Groot Hulze, “Adaptive Dimming and Boosting Backlight for LCD-TV Systems,” SID Symposium Digest Tech Papers 38, pp. 1332-1335 (2007).
- 100 K. S. Whitehead, M. Grell, D. D. C. Bradley, M. Inbasekaran, E. P. Woo, “Polarized Emission from Liquid Crystal Polymers,” Synthetic Material, vol. 111-112, 1, pp. 181-185, (2000).
- 101 Nichia Website, Retrieved August 28, 2008, from the : <http://www.nichia.com/product/led.html>

Appendix A

Implementation of FPGA

We choose XC3S2000 in Xilinx's Spartan-3 series as our platform because the gate count and I/O number in S2000 meet our requirement. The framework of FPGA controlled circuit is shown in Fig. A-1. This circuit includes clock generation, input buffer, image process, and timing controller modules. The functions of these modules will be described as follows.

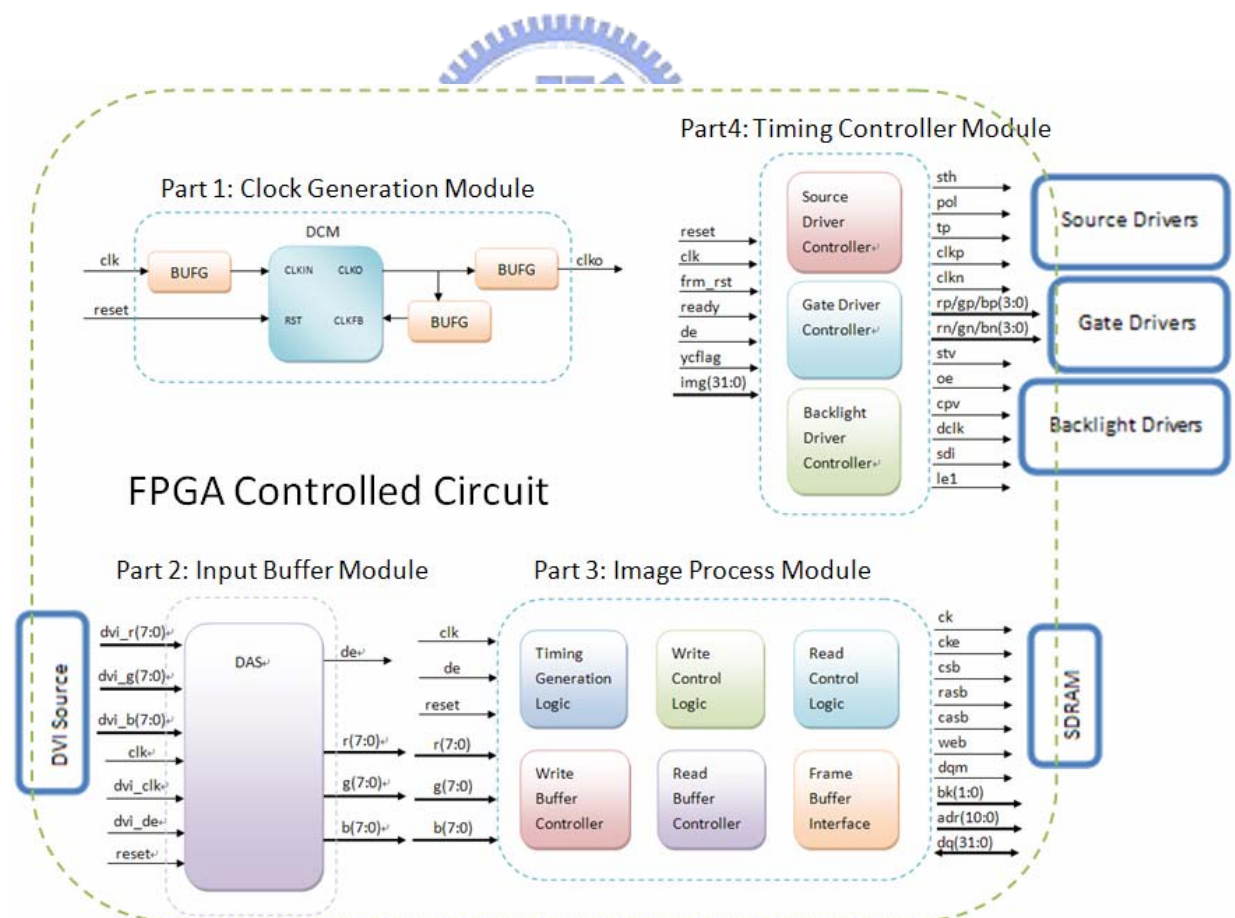


Fig. A-1 The framework of controlled circuit.

A.1 Clock generation module

The clock generation module is composed of digital clock manager (DCM) and global timing buffer (BUFG) provided by the intelligent property of Xilinx. This module is set as a time reference for other three modules in Fig. A-1. Using DCM can reduce the signal delay and clock skew to supply a robust and stable time reference. In addition, the DCM enables 2X or 0.5X frequency of original clock even an accurate phase shift signal. The BUFG provides higher fan out numbers for better driven force. Fig. A-2 and Fig. A-3 show the block diagram and the synthesis results of clock generation module. The clock signal through buffer enters the input, CLKIN of the DCM, and the feedback path is built up when the output, CLKO, is connected into CLKFB to synchronize CLKIN and CLKO.

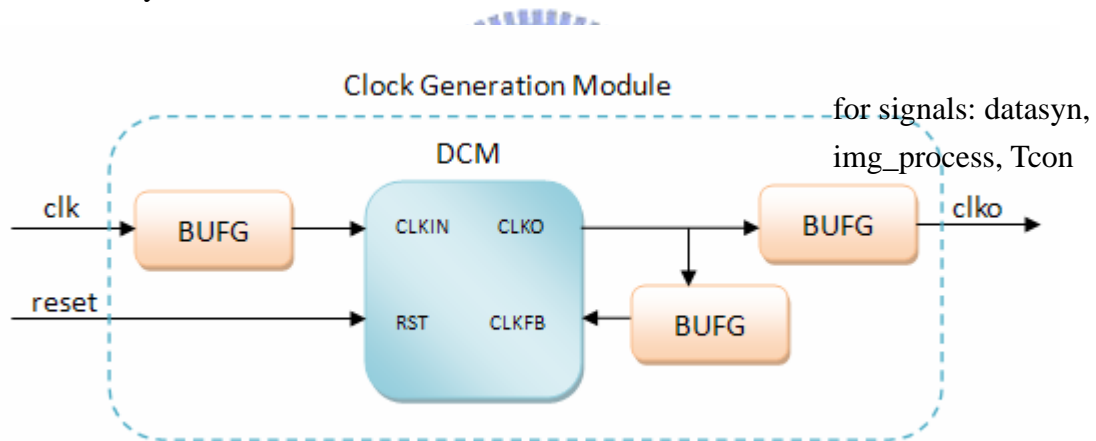


Fig. A-2 The block diagram of clock generation module.

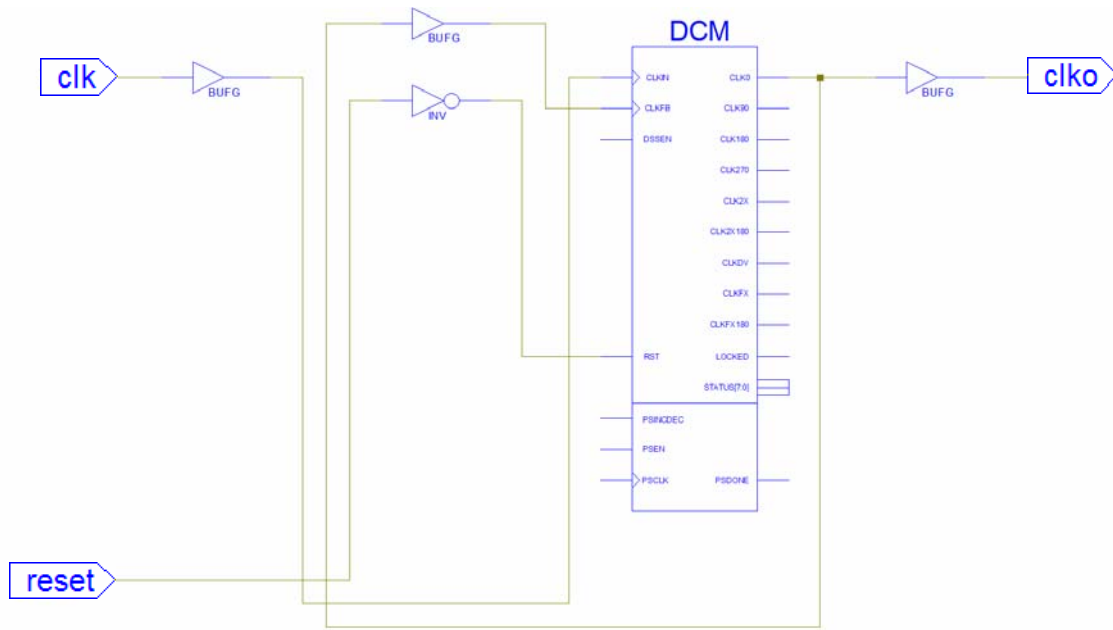


Fig. A-3 The synthesis of clock generation module.

A.2 Input Buffer module

A first-in-first-out (FIFO) in the buffer module was used to synchronize the input clock and system clock. The input clock as the write clock of FIFO saves the input image data and then the system clock as the read clock of FIFO reads out the synchronized image data. The data enable signal is also generated to define the effective image data. Fig. A-4 and Fig. A-5 show the block diagram and the synthesis results of input buffer module.

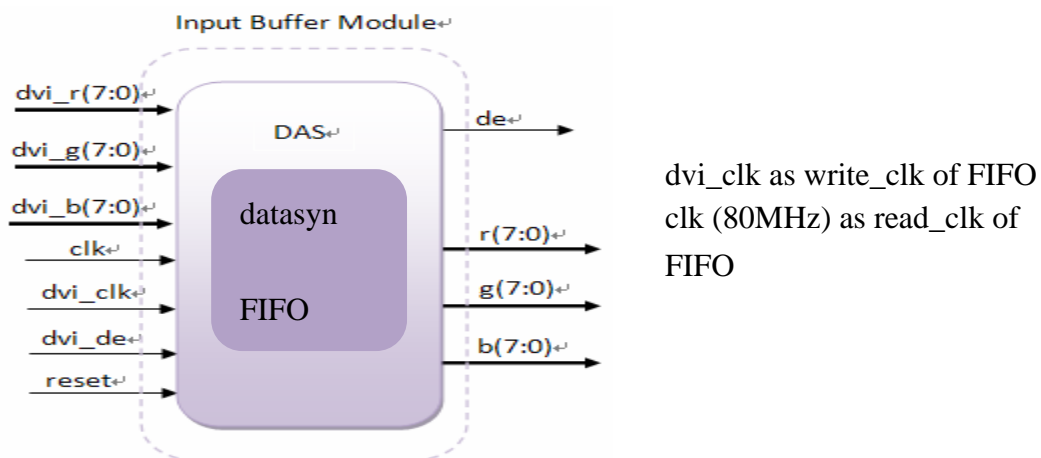


Fig. A-4 The block diagram of input buffer module.

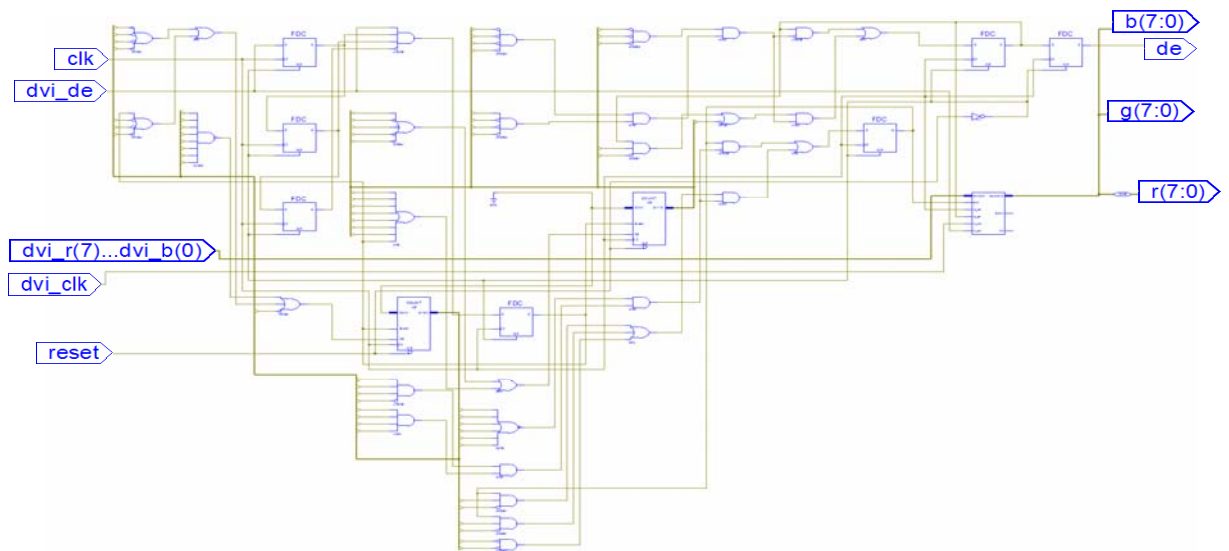


Fig. A-5 The synthesis of input buffer module.

A.3 Image process module

The main purpose of image process module is to implement the frame buffer, including data rearrangement and SDRAM access. Six blocks such as Timing Generation Logic, Write Control Logic, Read Control Logic, Write Buffer Controller, Read Buffer Controller, and Frame Buffer Interface will be described in the following.

Fig. A-6 and Fig. A-7 show the block diagram and the synthesis results of image process module.

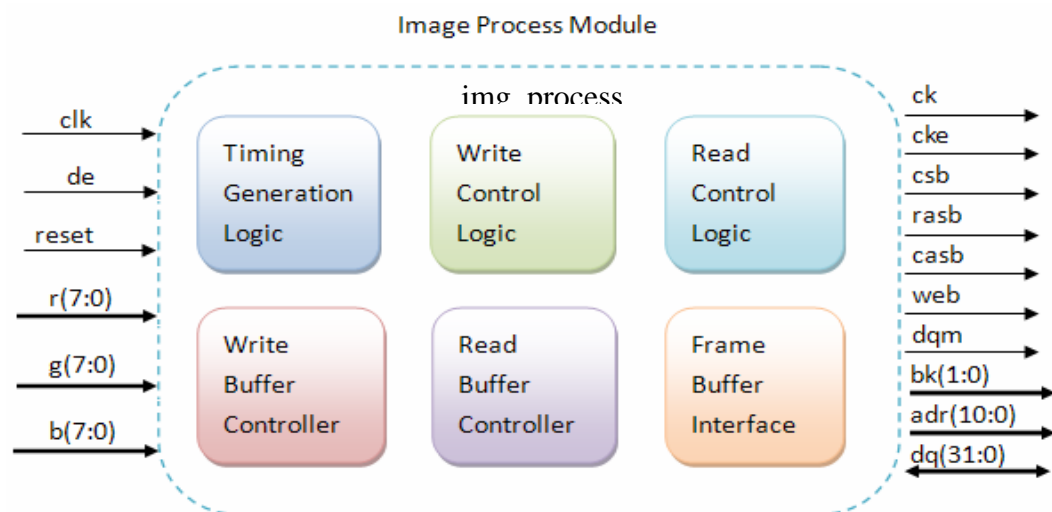


Fig. A-6 The block diagram of image process module.

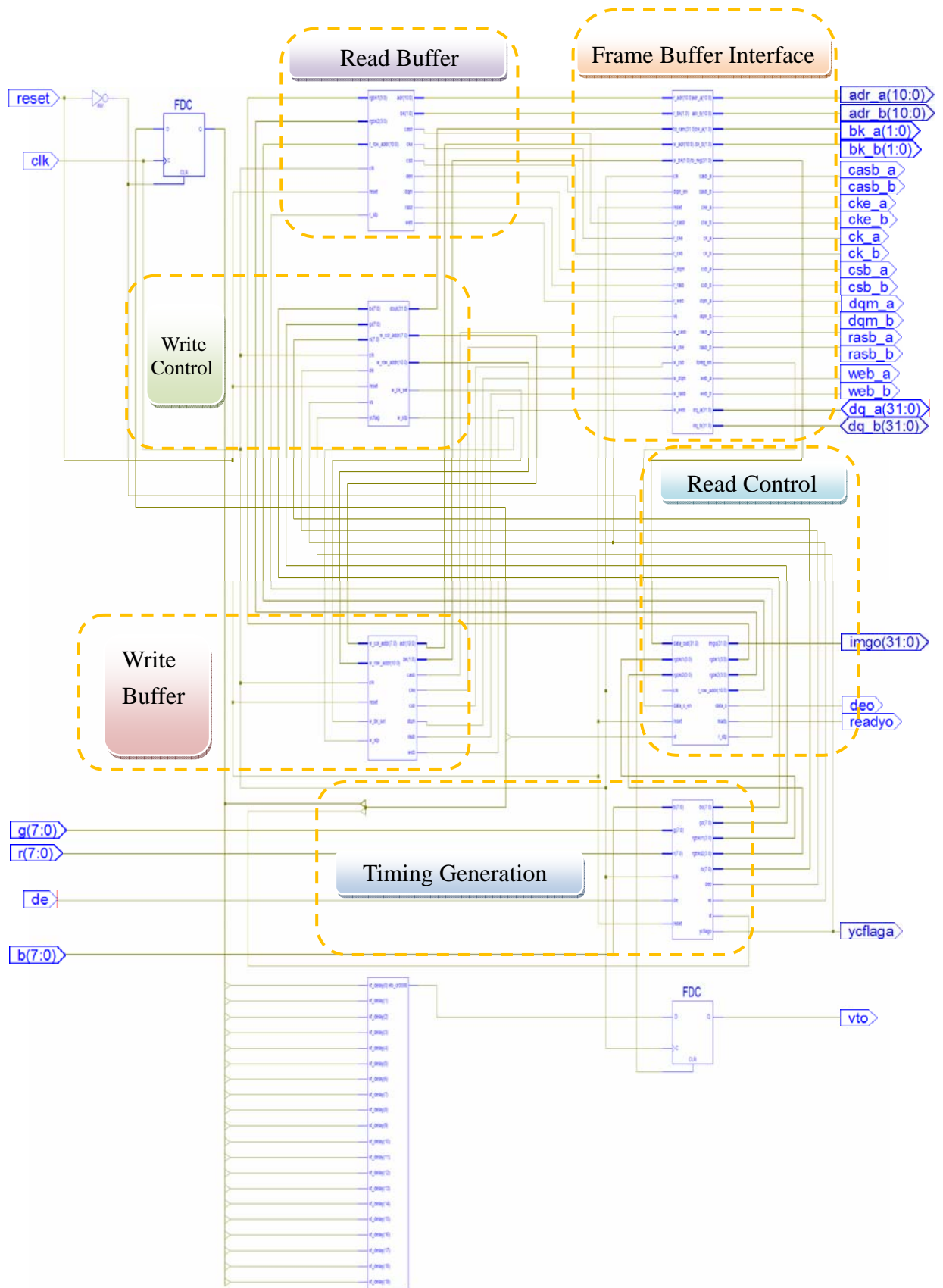


Fig. A-7 The synthesis of image process module.

A.3.1 Timing generation logic

The input signals of timing generation logic come from the data and enable signals of previous module (input buffer module). The synchronic frame signal (*vs*) and field signal (*vt*) are generated. In addition, we realized the sequence exchange index (*ycflago*) to switch between RGBY and RGBC color sequences. The blue counter adds one when the gray level of blue is equal or larger than that of green for individual pixel of image. So does the red counter when the red gray level is equal or larger than the green one. If the red counter is larger than the blue counter, RGBY will be applied in backlight sequence. Otherwise, RGBC is used in the sequence. Fig. A-8 and Fig. A-9 show the block diagram and the synthesis results of timing generation logic.

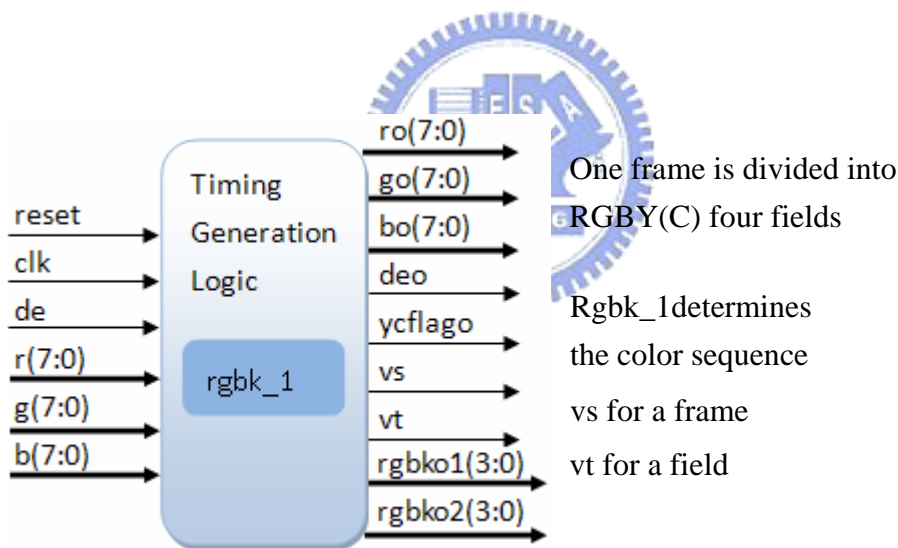


Fig. A-8 The block diagram of timing generation logic.

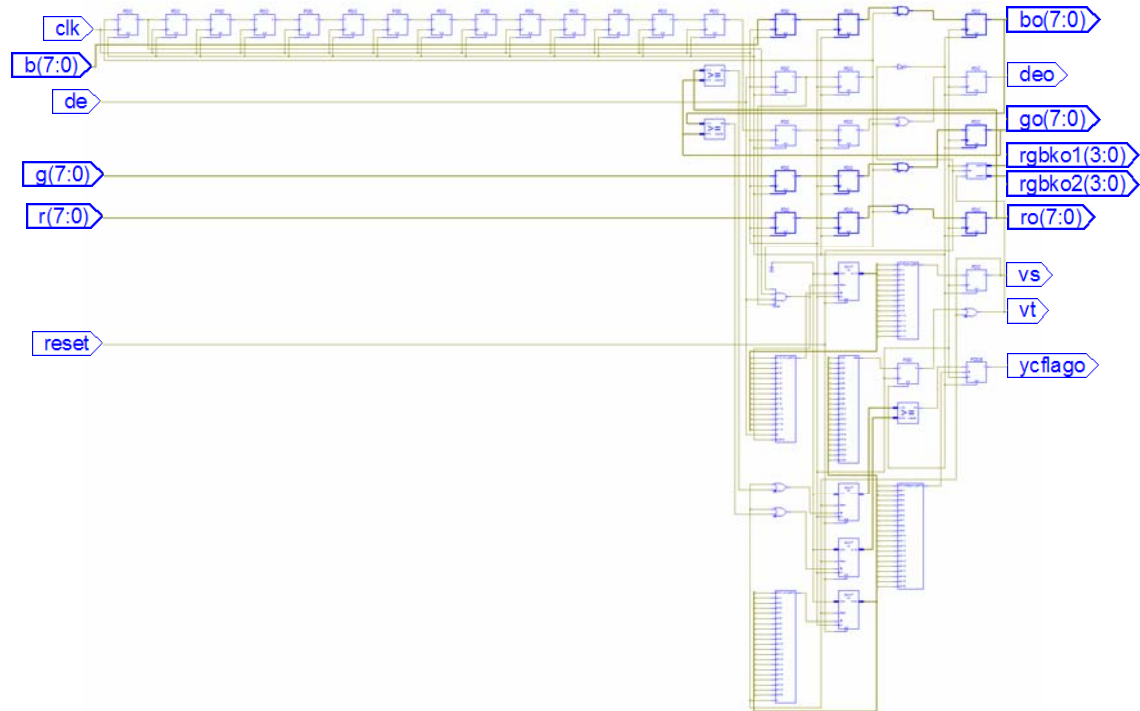


Fig. A-9 The synthesis of timing generation logic.



A.3.2 Write control logic

The write control logic, receiving control and image signals from timing generation logic, determines the new gray levels of red, green, blue, yellow, and cyan by comparing red, green, blue signals with each other. In order to cooperate with the write buffer controller, the gray levels are delivered into individual shift registers to generate the start signal (w_stp) for finite state machines in the write buffer controller. According to the address of each color field, the SDRAM access signals such as w_row_addr , w_col_addr , and w_bk_sel can be generated and sent into the write buffer controller. At the same time, this control logic forwards the sorted data ($dout$) to the frame buffer interface. Fig. A-10 and Fig. A-11 show the block diagram and the synthesis results of write control logic.

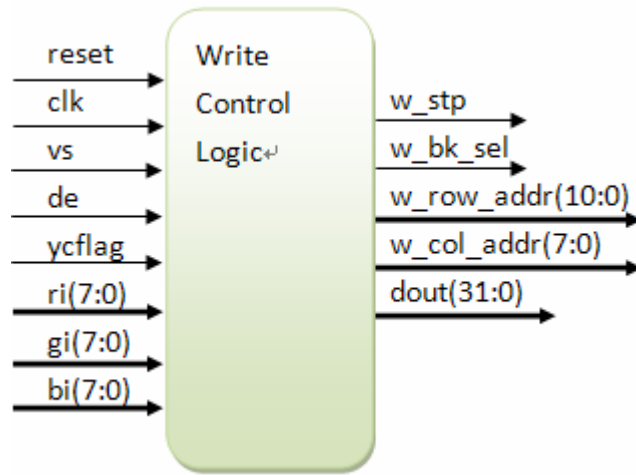


Fig. A-10 The block diagram of write control logic.

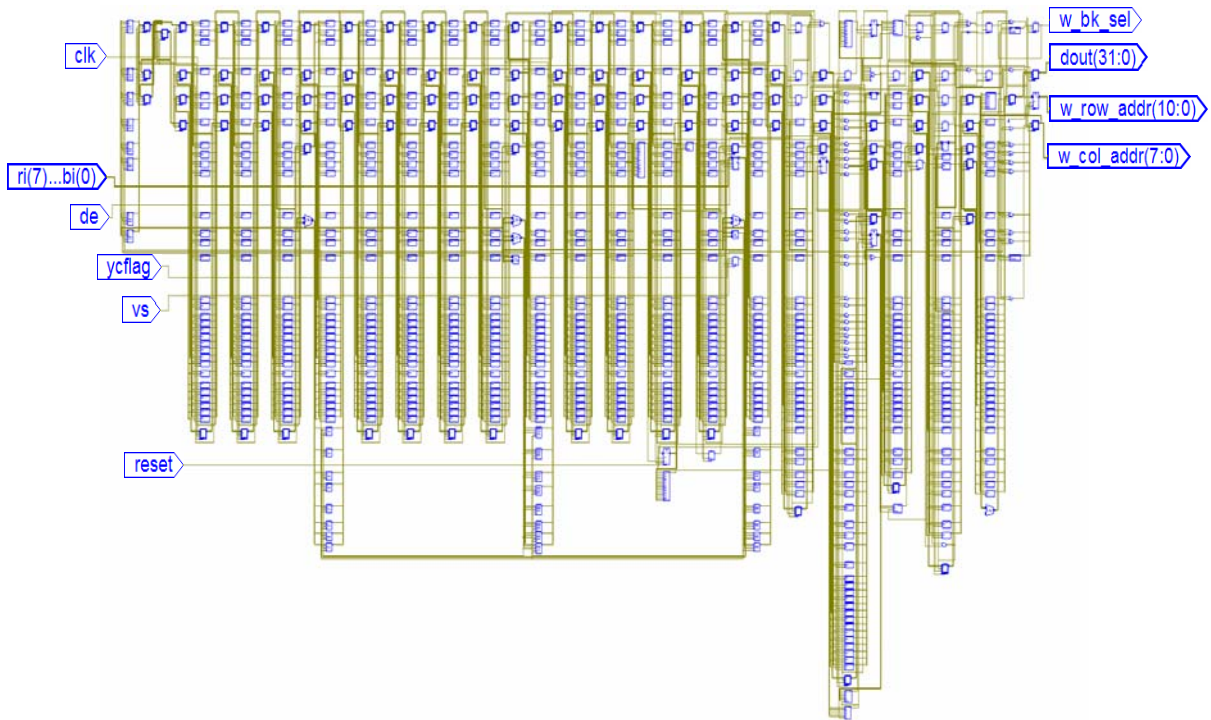


Fig. A-11 The synthesis of write control logic.

A.3.3 Write buffer controller

The SDRAM write command can be achieved by the access signals such as cke, csb, rasb, casb, web, dqm, bk, and adr, generated with finite state machines of this SDRAM write controller. After initialization of SDRAM, the state machine enters the idle mode until the coming of start signal (w_stp). In the active mode, the write commands are sent into the frame buffer interface. The mode of state machine will go back to the idle state and wait for another w_stp after writing a whole line of image data. Fig. A-12 and Fig. A-13 show the block diagram and the synthesis results of write buffer controller.

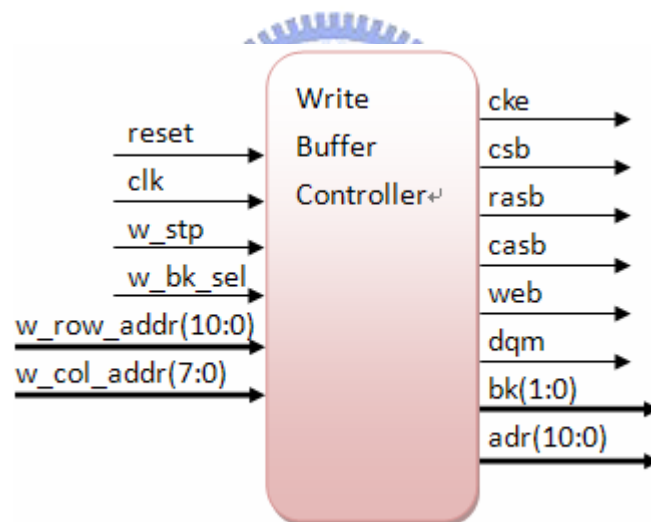


Fig. A-12 The block diagram of write buffer controller.

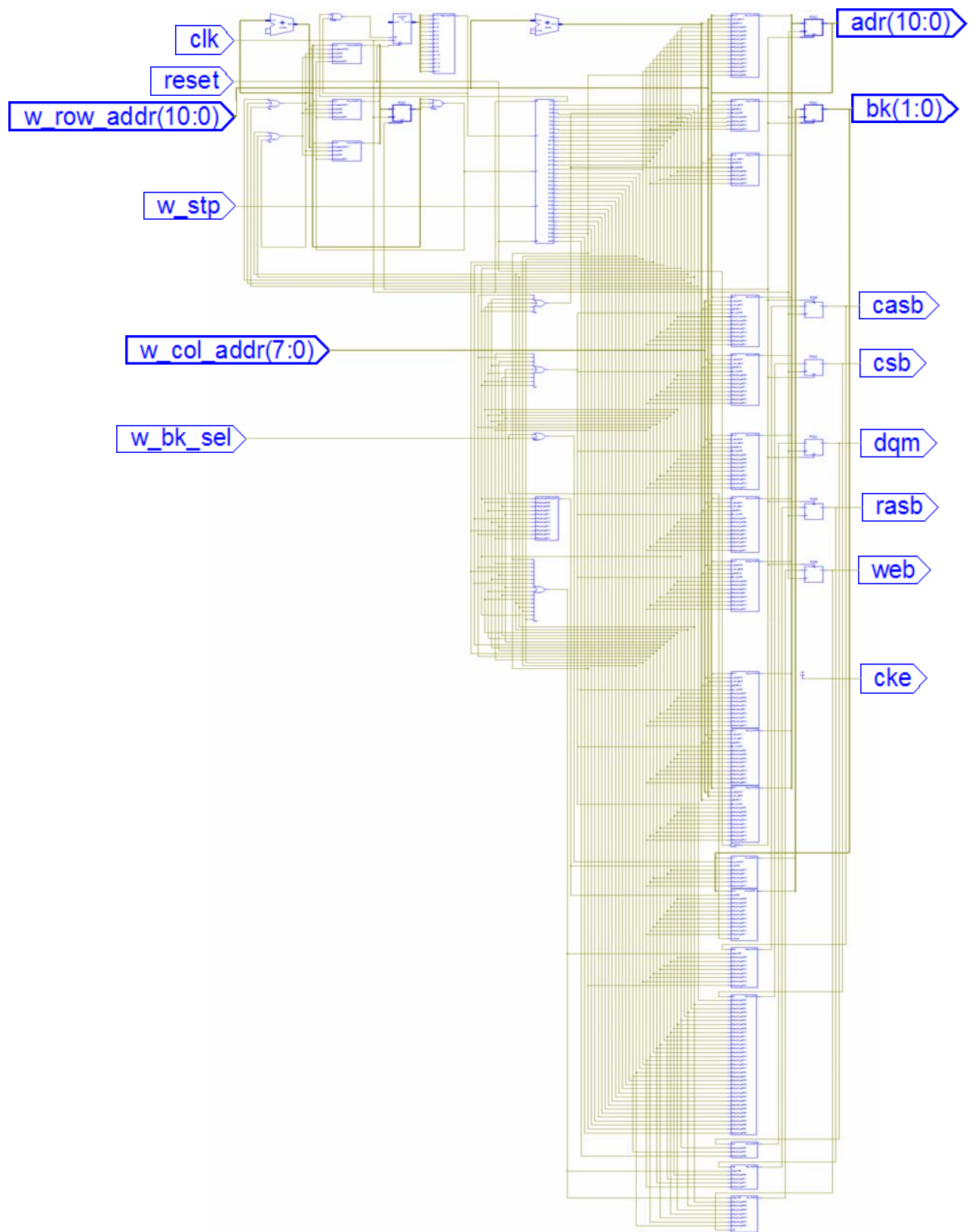


Fig. A-13 The synthesis of write buffer controller.

A.3.4 Read control logic

According to synchronic field signal (vt) and clock counter, the read control logic generates the read starting signal (r_stp), ready signal (ready), and row address (r_row_addr) to read out the four color field images. With the enable signal (data_o_en), the field data (data_out) from SDRAMs are sent into the timing control module for further processing. Fig. A-14 and Fig. A-15 show the block diagram and the synthesis results of read control logic.

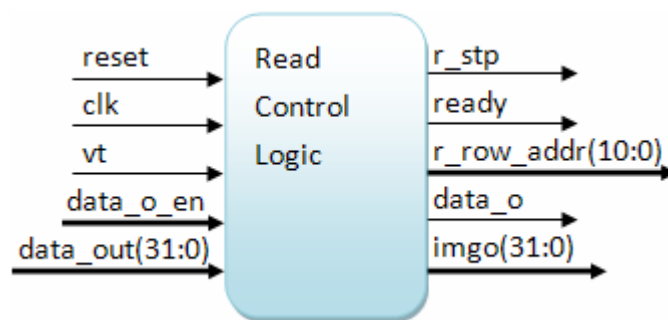


Fig. A-14 The block diagram of read control logic.

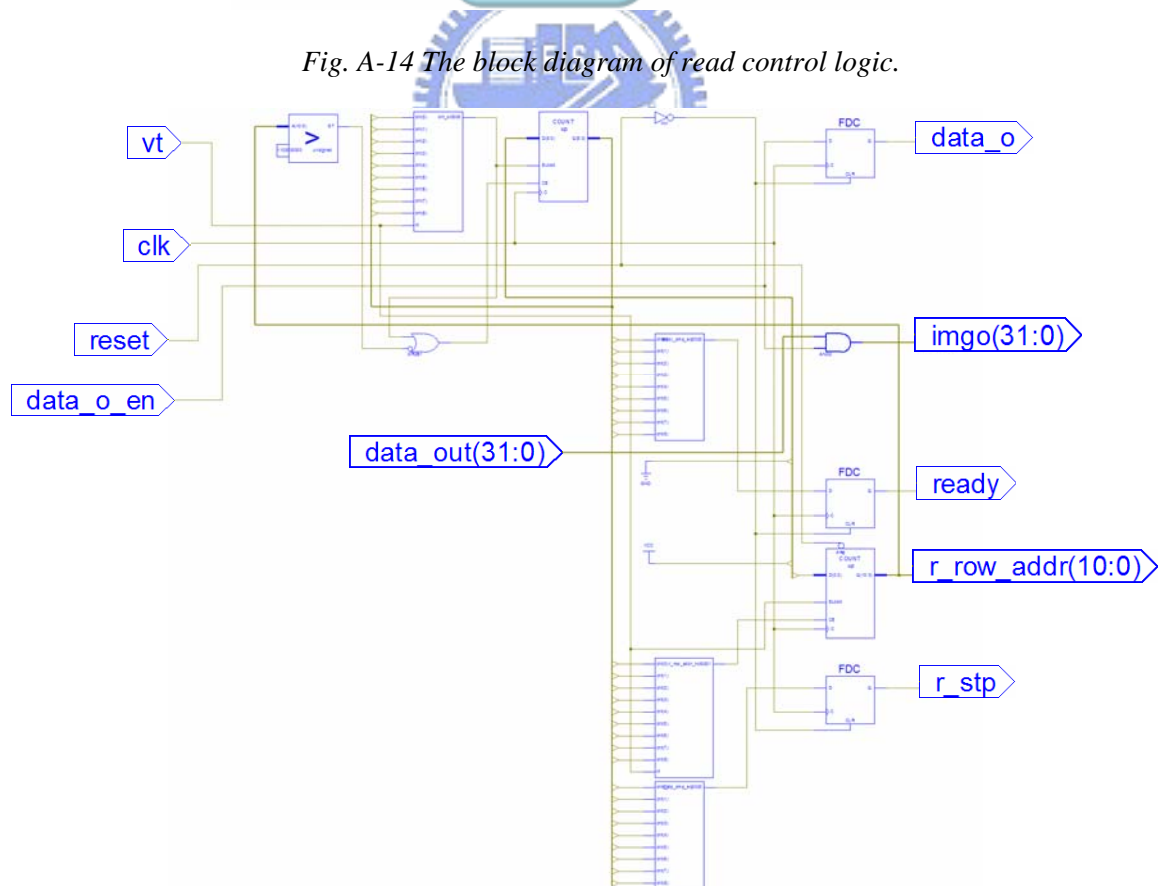


Fig. A-15 The synthesis of read control logic.

A.3.5 Read buffer controller

The SDRAM read command can be achieved by the access signals such as cke, csb, rasb, casb, web, dqm, bk, and adr, generated with finite state machines of this SDRAM read controller. After initialization of SDRAM, the state machine enters the idle mode until the coming of start signal (r_stp). In the active mode, the read commands are sent into the frame buffer interface. The rgbk_1 and rgbk_2 determine the readout of color sequence. The mode of state machine will go back to the idle state and wait for another r_stp after reading a whole line of image data. Fig. A-16 and Fig. A-17 show the block diagram and the synthesis results of read buffer controller.

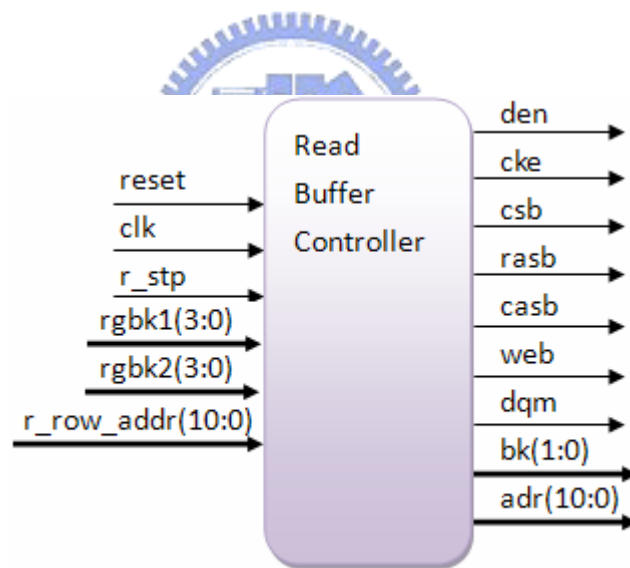


Fig. A-16 The block diagram of read buffer controller.

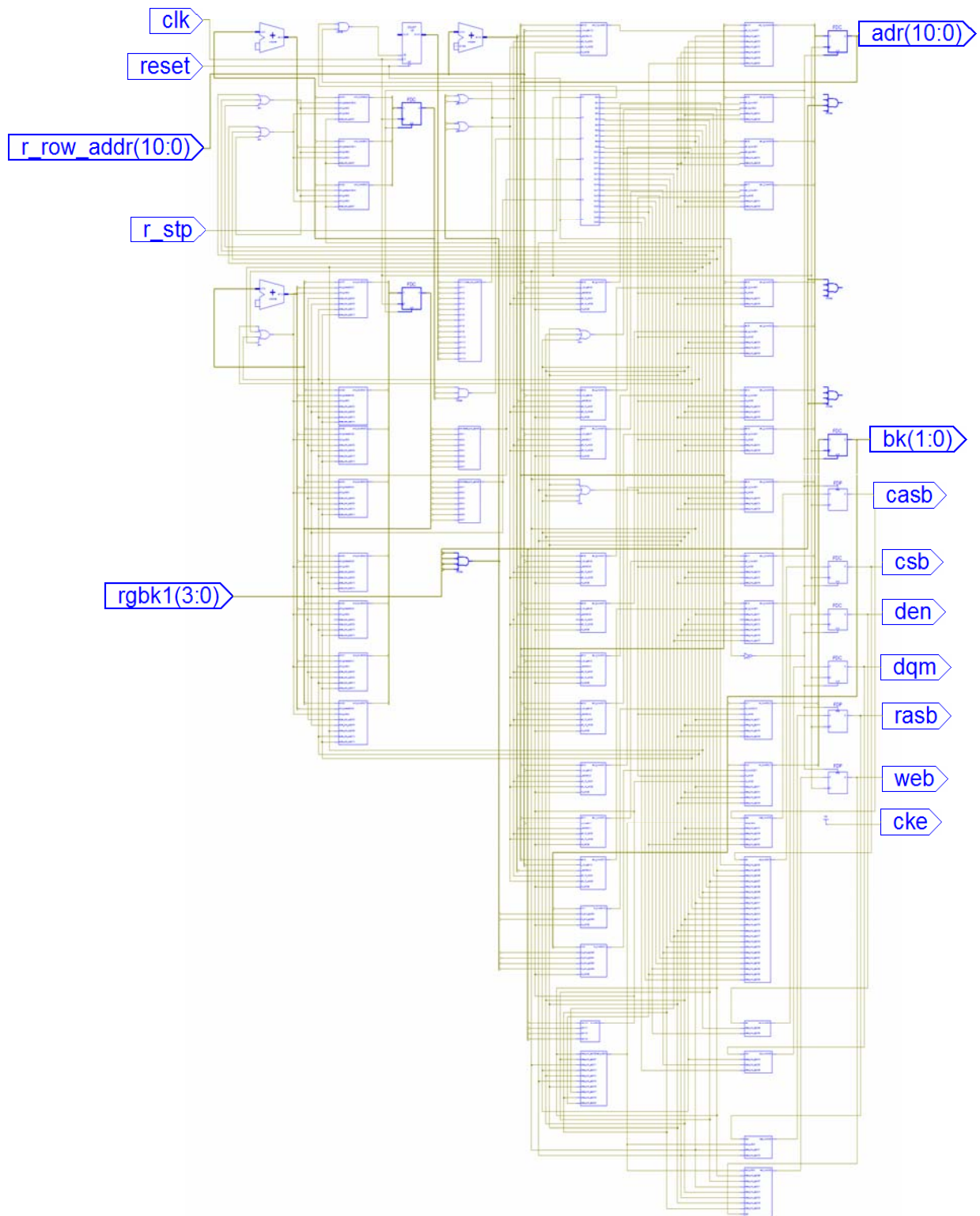


Fig. A-17 The synthesis of read buffer controller.

A.3.6 Frame buffer interface

Two SDRAMs, sdram a and b, are used as frame buffers. The read and write commands are sent to individual SDRAM and exchange on each frame of image. According to the synchronic frame signal (vs), the write enable signal (dqin_en) wrote the data (to_ram) into one frame buffer. At the same time, the signal (toreg_en) read out the image data (to_reg) from the other frame buffer. Fig. A-18 and Fig. A-19 show the block diagram and the synthesis results of frame buffer interface.

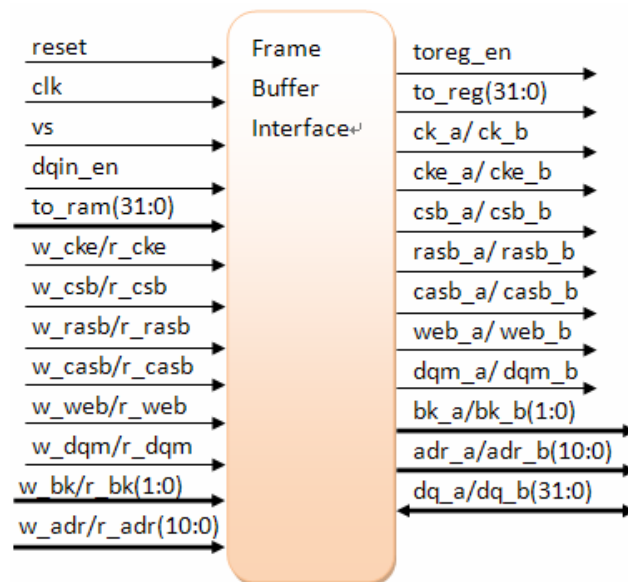


Fig. A-18 The block diagram of frame buffer interface.

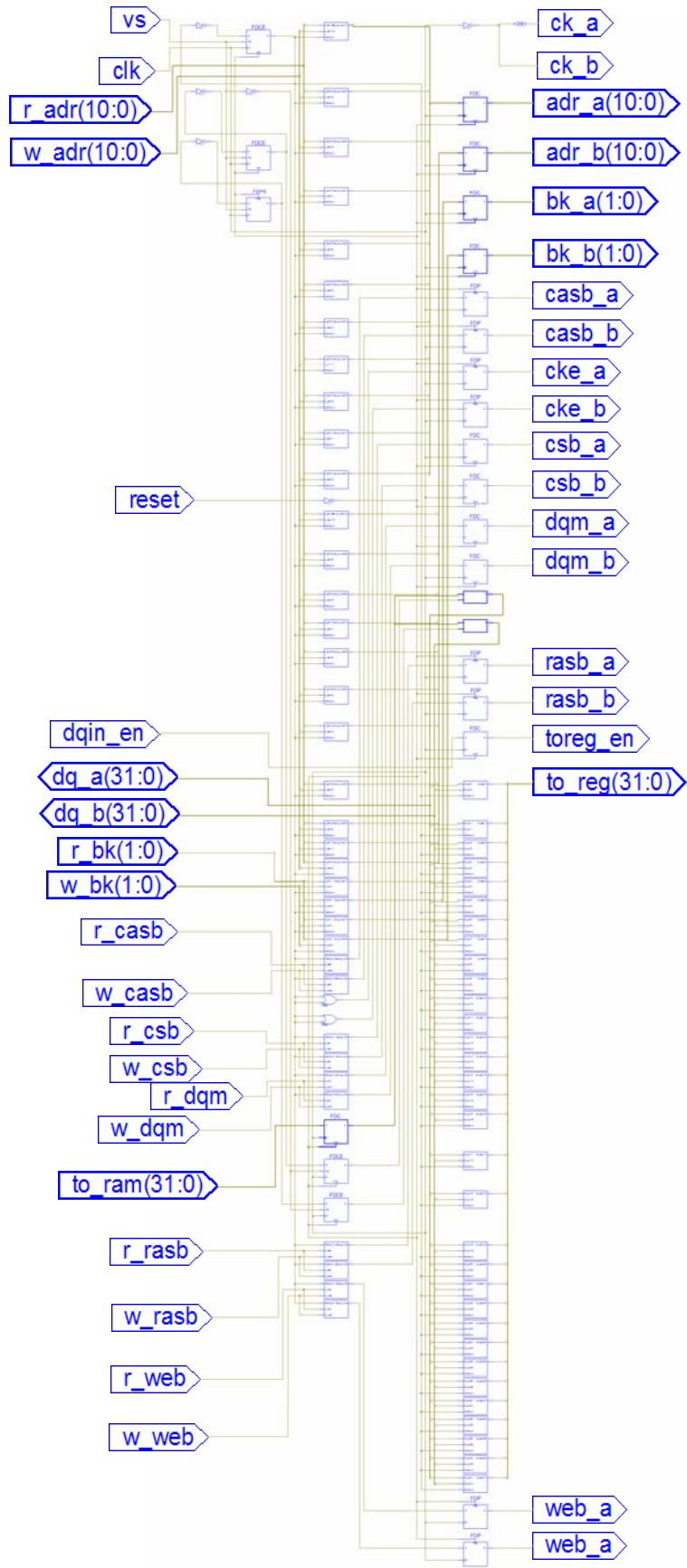


Fig. A-19 The synthesis of frame buffer interface.

A.4 Timing controller module

The main purpose of timing control module is to receive the data from image process module and generate the timing for LCD and LED drivers to display the image on the panel and backlight. This module, consisting of source, gate, and backlight driver controllers, will be described in the following. Fig. A-20 and Fig. A-21 show the block diagram and the synthesis result of timing control module.

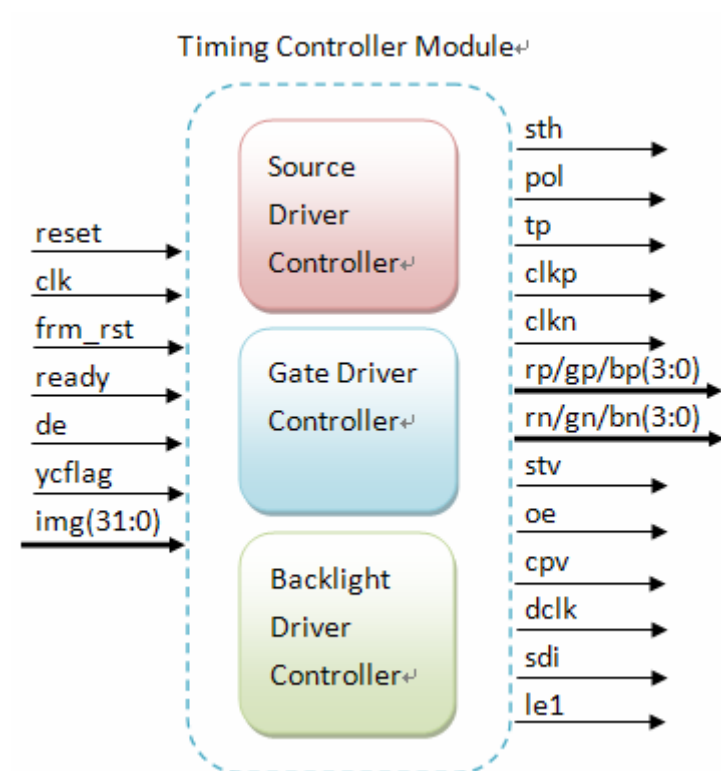


Fig. A-20 The block diagram of timing controller module.

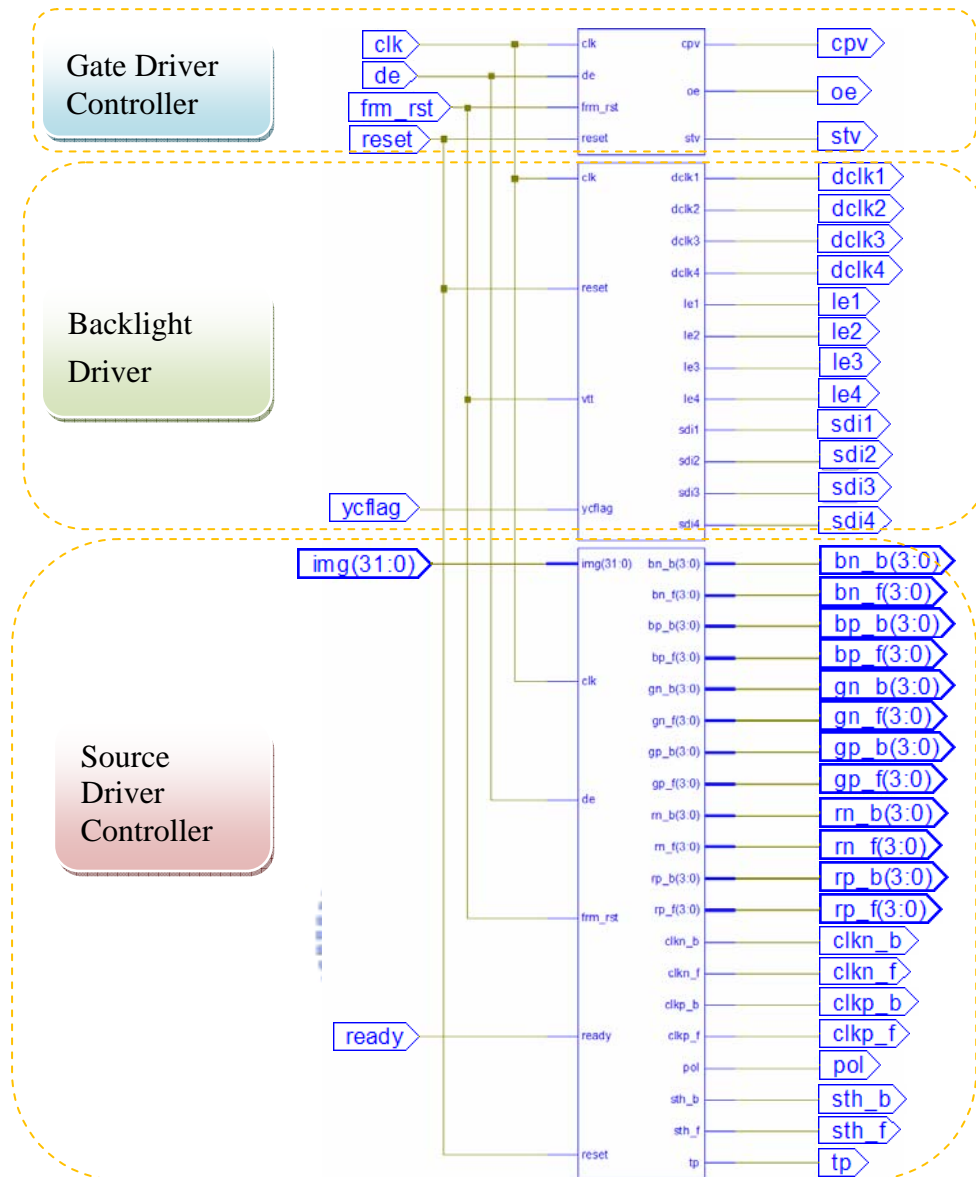


Fig. A-21 The synthesis of timing controller module.

A.4.1 Source driver controller

The source driver controller receives the image data (img) and transfers the data into RSDS mode to meet the requirement of source drivers. Fig. A-22 shows the block diagram of this controller. In order to read and write the data of one line simultaneously, one register (data1) is used as a line buffer for the data read from SDRAMs as shown in the synthesis result(Fig. A-23). The r1 and r2 are the RSDS generators. In addition, start signal (sth), polarity control (pol), and data latch (tp) are also prepared for driver inputs.

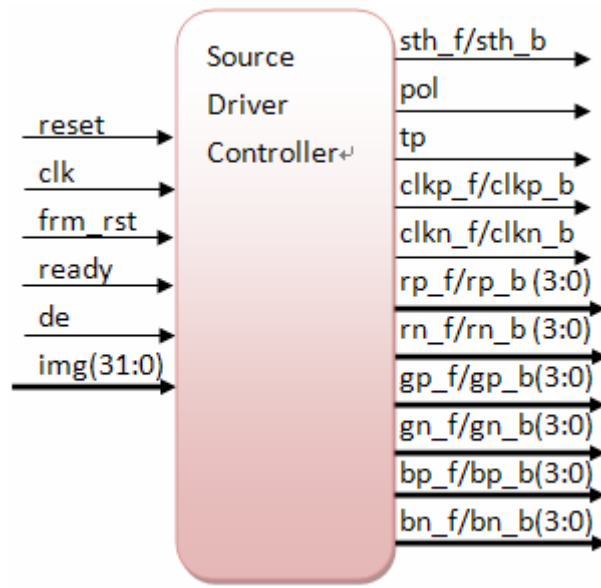


Fig. A-22 The block diagram of source driver controller.

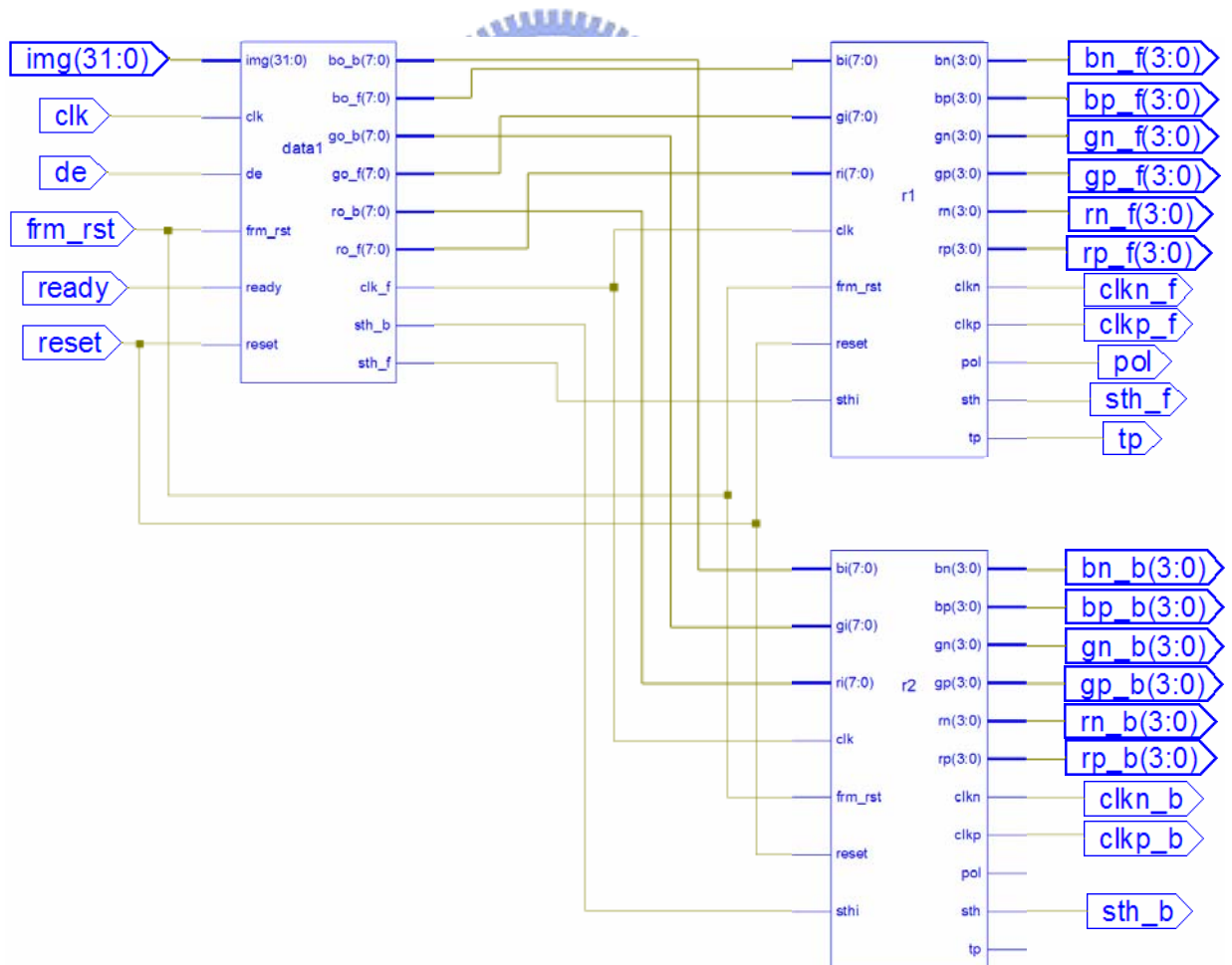


Fig. A-23 The synthesis of source driver controller.

A.4.2 Gate driver controller

Based on the frame reset signal (*frm_rst*) and data enable signal (*de*), the gate driver controller generates the start signal (*stv*) and trigger signal (*cpv*). The *cpv* enables the internal shift register of the gate driver to turn on the image row by row on LCDs. In addition, the separation enable signal (*oe*) avoids the crosstalk on adjacent rows. Fig. A-24 and Fig. A-25 show the block diagram and the synthesis result of gate driver controller.

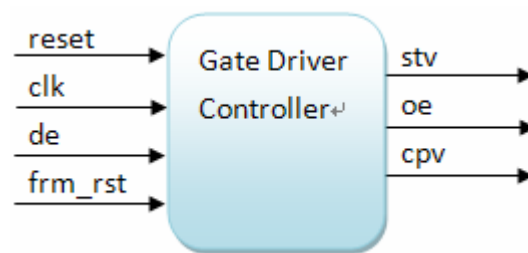


Fig. A-24 The block diagram of gate driver controller.

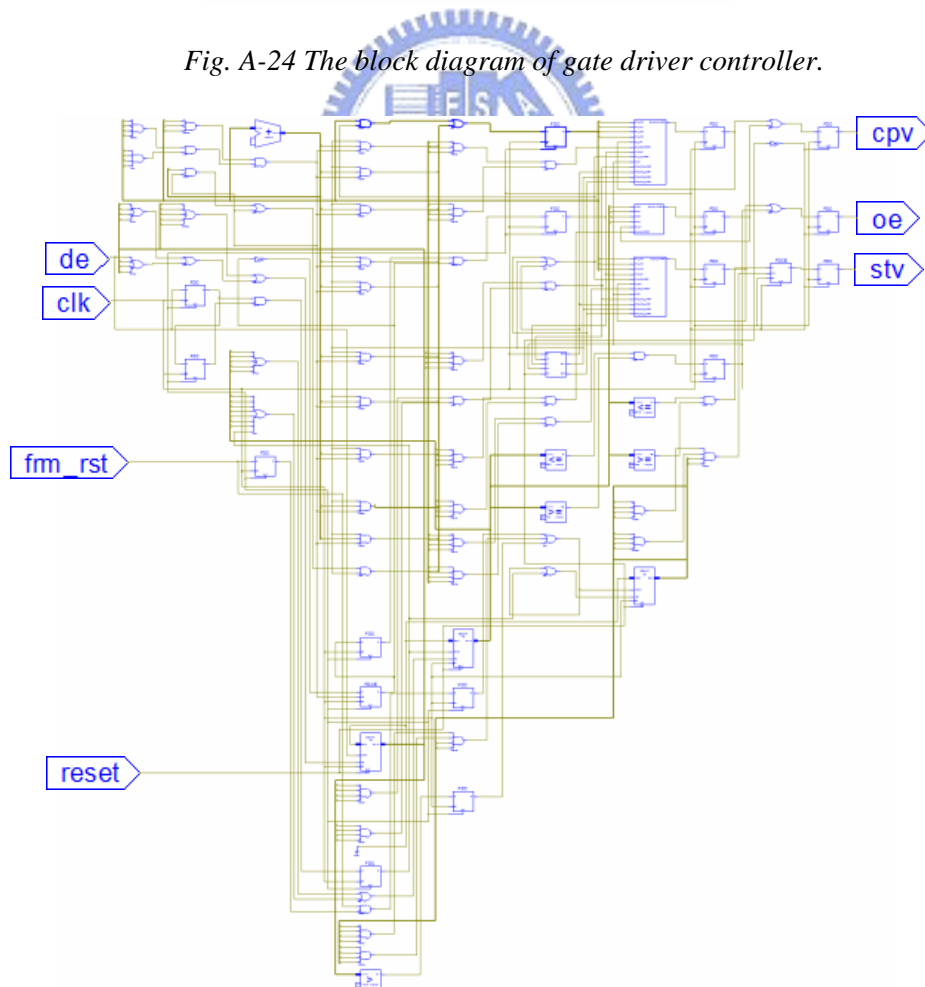


Fig. A-25 The synthesis of gate driver controller.

A.4.3 Backlight driver controller

This controller generates the input signals of backlight (LED) drivers and determines the color sequence of RGBC or RBY. The driver signals consist of timing clock (dclk), data latch (le), and serial gray level (sdi). Four sets of these control signals are designed for four groups of LED drivers in the whole backlight. According to the synchronic field signal (vtt), the backlight colors are switched and synchronized with the image data. Besides, the ycflag as an exchange index sets the fourth field is yellow or cyan. Fig. A-26 and Fig. A-27 show the block diagram and the synthesis result of backlight driver controller.

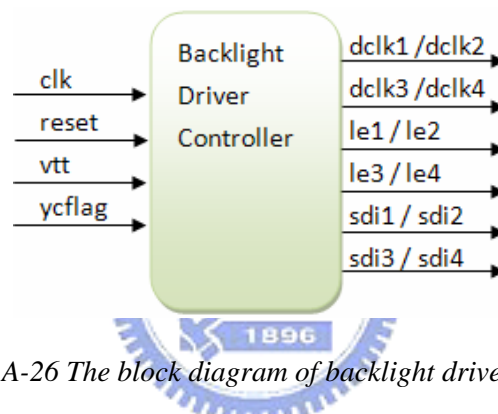


Fig. A-26 The block diagram of backlight driver controller.

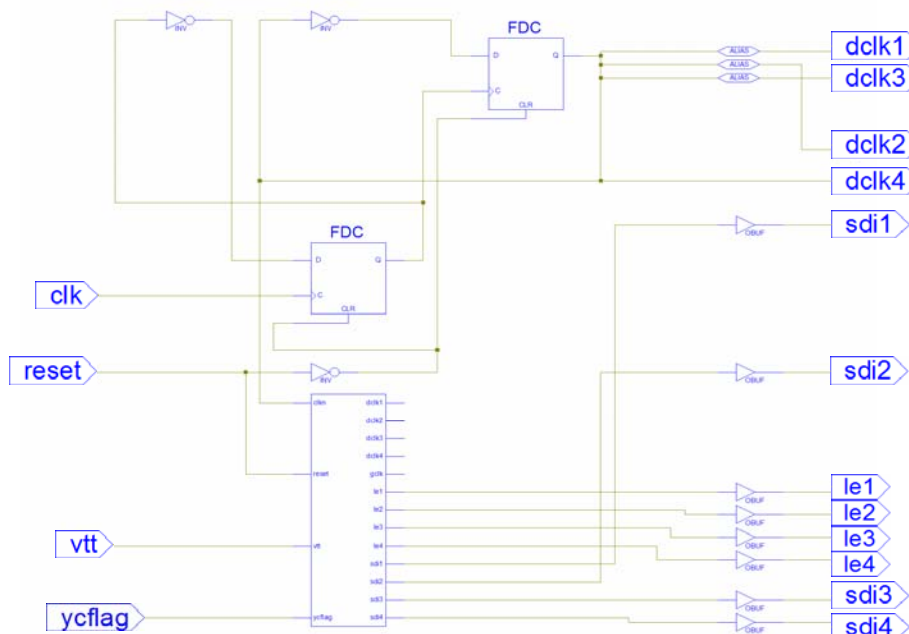
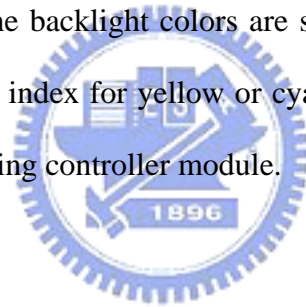


Fig. A-27 The synthesis of backlight driver controller.

A.5 Summary

In FPGA, the clock generation, input buffer, image process, and timing controller module are designed. The clock module is set as a robust and stable time reference for other three modules. In the buffer module, the input clock and system clock are synchronized. The data enable signal is also generated to define the effective image data. An implementation of frame buffer, including the data rearrangement and access of SDRAMs, is the main purpose of image process module following the input module.

Then, the timing control module receives the data from image process module and generates the timing for LCD and LED drivers to the display circuit. According to the synchronic field signal, the backlight colors are switched and synchronized with the field image. An exchange index for yellow or cyan field was also realized in the backlight controller of the timing controller module.



Publication List

Journal Papers

1. **Chun-Ho Chen**, Yao-Chung Yeh, and Han-Ping D. Shieh, “3-D Mobile Display Based on Moiré-Free Dual Directional Backlight and Driving Scheme for Image Crosstalk Reduction,” IEEE/OSA Journal of Display Technology (JDT), Vol. 4(1), pp. 92-96, 2008.
2. **Chun-Ho Chen** and Han-Ping D. Shieh, “Effects of Backlight Profiles on Perceived Image Quality for High Dynamic Range LCDs,” IEEE/OSA Journal of Display Technology (JDT), Vol. 4(2), pp. 153-159, 2008.
3. **Chun-Ho Chen**, Che-Chin Chen, Ke-Horng Chen, and Han-Ping D. Shieh, “Driving AMOLED Panel by Time-Multiplexing Clamped Inverter Circuits for Reducing Complex Control Signals,” Journal of the Society for Information Display (JSID), Vol. 16(7), pp. 787-791, 2008.
4. **Chun-Ho Chen**, Fang-Cheng Lin, Ya-Ting Hsu, Yi-Pai Huang, and Han-Ping D. Shieh, “A Field Sequential Color LCD Based on Color Fields Arrangement for Color Breakup and Flicker Reduction,” accepted by IEEE/OSA Journal of Display Technology (JDT).
5. Yi-Pai Huang, Ke-Horng Chen, **Chun-Ho Chen**, Fang-Cheng Lin, and Han-Ping D. Shieh, “Adaptive LC/BL Feedback Control in Field Sequential Color LCD Technique for Color Breakup Minimization,” IEEE/OSA Journal of Display Technology (JDT), Vol. 4(3), pp. 290-295, 2008.

International Conference Papers

1. **Chun-Ho Chen** and Han-Ping D. Shieh, “High Uniformity of Large Size Backlight System with Inclined LED Array,” IDMC2005, pp. 407-409.
2. **Chun-Ho Chen** and Han-Ping D. Shieh, “Inclined LED Array for Large-Sized Backlight System,” Society for Information Display 2005 (SID’05), pp. 558-561.
3. **Chun-Ho Chen**, Yao-Chung Yeh, and Han-Ping D. Shieh, “Morie Pattern and Image Crosstalk Reduction in 3D Mobile Display,” Society for Information Display 2006 (SID’06), pp. 1154-1157.

4. Chun-Hung Lai, **Chun-Ho Chen**, and Han-Ping D. Shieh, "A Novel 3D Double Screens Display," International Display Workshop 2006 (IDW'06), pp. 1913-1916.
5. Che-Chin Chen, Yi-Fu Chen, Ti-Ti Liu, **Chun-Ho Chen**, Ming-Tsung Ho, Ke-Horng Chen, and Han-Ping D. Shieh, "Spatial-temporal Division in Field Sequential Color Technique for Color Filterless LCD," Society for Information Display 2007 (SID'07), pp. 1806-1809.
6. Ya-Ting Hsu, Fang-Cheng Lin, **Chun-Ho Chen**, Yi-Pai Huang, and Han-Ping D. Shieh, "Drive and Control Circuitry of OCB Field-Sequential Color LCD with High Data Rate," IDMC 2007, pp.435-438.
7. Ya-Ting Hsu, Fang-Cheng Lin, **Chun-Ho Chen**, Yi-Pai Huang, and Han-Ping D. Shieh, "A Field Sequential Color LCD Based on Color Field Arrangement for Color Breakup and Flicker Reduction," International Display Workshop 2007 (IDW'07), LCT 3-3.
8. **Chun-Ho Chen**, Ke-Horng Chen, Yi-Pai Huang, Han-Ping D. Shieh, and Ming-Tsung Ho, "Gray Level Redistribution in Field Sequential Color LCD Technique for Color Breakup Reduction," Society for Information Display 2008 (SID'08), pp. 1096-1099.
9. Jen-Chieh Hsieh, Yi-Pai Huang, **Chun-Ho Chen**, Yu-Chun Lo, Jen-Yu Fang, Han-Ping D. Shieh, Gu-Sheng Yu, and Tien Chiang, "Multi-Performance Film (MPF) for Highly Efficient LCD Backlights," Society for Information Display 2008 (SID'08), pp. 1606-1609.

Domestic Conference Papers

1. Yao-Chung Yeh, **Chun-Ho Chen**, and Han-Ping D. Shieh, "Moire-free Directional Backlight System For 3D Mobile Display," Optics and Photonics Taiwan '05 (OPT '05), G-SA-X-6-2
2. Shiou-Fong Liu, **Chun-Ho Chen**, and Han-Ping D. Shieh, "Optical Modeling of LED Backlight for Evaluation of Uniformity," 2006 Taiwan Display Conference Proceedings (TDC'06), pp.396-399
3. Chien-Liang Wu, **Chun-Ho Chen**, Fang-Cheng Lin, Yi-Pai Huang, and Han-Ping D. Shieh, "A 5.6-inch Field Sequential Color LCD with Less Color Break-up," Optics and Photonics Taiwan '07 (OPT '07), GO-004

4. Jen-Chieh Hsieh, Yi-Pai Huang, **Chun-Ho Chen**, Yu-Chun Lo, Jen-Yu Fang, and Han-Ping D. Shieh, "Multi-Performance Film (MPF) for Highly Efficient LCD Backlights," 2008 Taiwan Display Conference Proceedings (TDC'08), pp.398-401.
5. Chien-Liang Wu, **Chun-Ho Chen**, Fang-Cheng Lin, Yi-Pai Huang, and Han-Ping D. Shieh, "Demonstration of a Mobile-Sized Field Sequential Color LCD for Color Break-up Suppression," 2008 Taiwan Display Conference Proceedings (TDC'08), pp.419-422.

Patents

1. Ke-Horng Chen, **Chun-Ho Chen**, Hsien-Chun Chiu, Han-Ping D. Shieh, and Ti-Ti Liu, "Spatial-temporal Division Filed Sequential Color LCD display," (ROC Taiwan Patent pending)
2. **Chun-Ho Chen**, Hugo Cornelissen, Pijlman Fetze, and Han-Ping D. Shieh, "Illumination system for illuminating a display device, and display device," (US and ROC Taiwan Patent pending)
3. **Chun-Ho Chen**, Yi-Pai Huang, Ke-Horng Chen, Fang-Cheng Lin, and Han-Ping D. Shieh, "Adaptive Feedback Control in Field Sequential Color Display," (ROC Taiwan Patent pending)



Awards

- 2005 1st AUO Award in High Efficiency LCD, sponsored by AU Optronics.**
- 2005 GSSAP scholarship by National Science Council (NSC).**
- 2004 Student fellowship, Institute of Electro-Optical Engineering, NCTU.**

Vita

Name: Chun-Ho Chen 陳均合

Day of birth: June 13, 1979

Address: 彰化縣秀水鄉花秀路 122 號

Education:

Sep. '03 – Present : National Chiao Tung University, Hsinchu, Taiwan.
Ph. D. in Institute of Electro-Optical Engineering.

Sep. '01 – Jan. '03 : National Chiao Tung University, Hsinchu, Taiwan.
Master in Institute of Electronics.

Sep. '97 – Jun. '01 : National Chiao Tung University, Hsinchu, Taiwan.
Bachelor in Department of Electronics Engineering.



Experience:

Sep, '06-Mar, '07 Internship student at Philips Research Lab.,
Eindhoven, Netherland

Sep. '05- Oct. '05 Project members of AUO, FPD05' Exhibition,
Yokohama, Japan.

Feb. '05- Jun. '05 TA of Display Technology Experiment, Display
Institute, NCTU.

Jul. '04- Sep. '04 Short-term internship at Chunghwa Picture Tubes,
LTD.